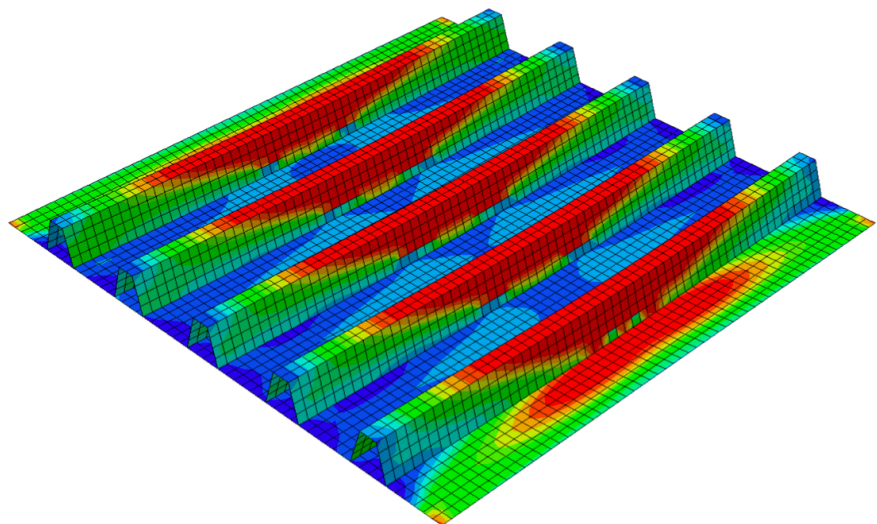Abulfazl Masumi
Kristian Thor Gendron

Uniaxially Stiffened Steel Plates

In-plane and Out-of-plane Loads

Master's thesis in MTBYGG
Supervisor: Arne Aalberg
Co-supervisor: Svein Rune Kleppe

June 2022

Master's thesis

NTNU
Norwegian University of Science and Technology
Faculty of Engineering
Department of Structural Engineering

NTNU
Kunnskap for en bedre verden

Abulfazl Masumi
Kristian Thor Gendron

Uniaxially Stiffened Steel Plates

In-plane and Out-of-plane Loads

NTNU
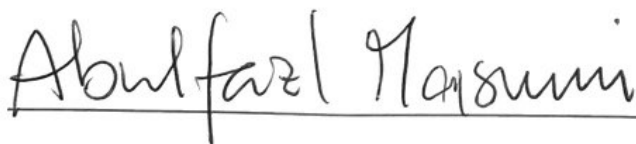Norwegian University of
Science and Technology

Foreword

This report is the final thesis and marks the end of the five-year master's engineering program at the Norwegian University of Science and Technology, NTNU. The thesis has been prepared in a collaboration by Abulfazl Masumi and Kristian Thor Gendron in the spring of 2022. Supervisors in this thesis were Professor Arne Aalberg and Dr. ing. Svein-Rune Kleppe.

The report addresses, among other things, the various rules for calculating buckling loads according to Eurocode EN 1993-1-5 and EN 1993-1-1. The buckling load is calculated for longitudinal and transverse axial loads, as well as biaxial in combination with out of plane loads. Calculation examples are performed and the resulting buckling loads are compared with the buckling loads calculated using the softwares Abaqus and EBPlate.

The thesis has been very interesting and educational. The authors of the thesis would like to thank the supervisor Arne Aalberg and Svein-Rune Kleppe for alle the help and assistance during this report's preparation.

Trondheim 25. Juni 2022

Abulfazl Masumi

Kristian Thor Gendron

Sammendrag

Denne masteroppgaven omhandler oppførsel av avstivede platefelt av stål. Den består av et litteraturstudium, utregninger for hånd og analyse via elementmetoden. Eurocodene 1993-1-1 og 1993-1-5 utgjør grunnlaget for utregningene av aksialkapasitet på langs og tvers. Metodene herfra er ikke nødvendivis er ikke nødvendigvis særlig treffsikker, da de reduserer som regel kapasiteten av hensyn til global knekking i tilfeller der det er lokal og ikke globalknekk som er kritisk. Dette er spesielt relevant da disse plategeometriene er ikke særlig utsatt for globalknekk i utgangspunktet. Totalt er det 30 geometrier (10 lengder per valgt tverrsnitt).

Lineær knekkanalyse og kapasitetsanalyse med imperfeksjon ble utført med hjelp av FEM-analyse programvaren Abaqus.

Øvrig teori tas av boka "Dimensjonering av stålkonstruksjoner" av Per Kristian Larsen, og denne brukes til å tilpasse Eurocodemetoden for kapasitetsutregning i lastsituasjoner på tvers. En hybridmetode brukes også i kapasitetsanalyse med langsetter last for å ta høyde for forskjellen på kritiskknekklast regnet ut fra henholdsvis Abaqus og Eurocoden, som ikke tar høyde for torsjonsstivheten til lukkede stivertverrsnitt.

En viss likhet i oppførsel identifiseres for avstivede plater med store, lignende stivere, nemlig fordi disse har et lignende forhold mellom stiver- og platestivhet i bøyning.

I tillegg utførtes et studium på oppførselen til avstivede plater med last ut av planet, både for trykk og sug. Tre forskjellige aksiallastkombinasjoner ble sett på for å utforske hvordan kapasiteten påvirkes av aksiallast. Her ble FEM-analysen sammenlignet med en metode fra Eurocode 1999-1-1, og denne ble vurdert til å være ufullstendig.

For aksiallast på langs, Eurocodemetodene var betraklig konservative, med et avvik fra FEM-analysekapasiteten på rundt 40% på de lengste platene. Hybridmetoden var også betraktlig konservativ. For tverrlast, den tilpassede metoden ga rimlige resultater for 2 av 3 tverrsnitt, med et avvik på 7-10%, men var utrygg for den tredje geometrien som hadde mindre stivere. Materialfaktorer ble ekskludert for å kunne sammenligne metodene.

Abstract

This master's thesis consists of a literature study, hand-calculations and finite element analysis modeling for longitudinally stiffened plates. The Eurocodes 1993-1-1 and 1993-1-5 provide the basis for hand calculations of the axial capacity of the plate when uniaxially loaded in either the longitudinal or transverse direction. These methods are not necessarily perfectly accurate, as they primarily focus on global buckling and provide capacity reduction even in cases where global buckling is not critical. There are 30 different geometries (10 lengths per cross-section).

Linear buckling analyses and capacity analyses with imperfections were performed in the FEM software Abaqus.

Additional material comes from the textbook "Dimensjonering av stålkonstruksjoner" by Per Kristian Larsen, providing the theory through which one can adapt the Eurocode guidelines in the case of loading in the transverse direction. A hybrid method is also used in the case of loading in the longitudinal direction to account for different critical buckling loads determined by the FEM software Abaqus and the Eurocode, which does not account for torsional stiffness of closed-section stiffeners.

A similarity is found between the behaviors of plates with large similar stiffeners, as these have a similar relationship between the stiffener and plate bending stiffnesses.

An additional study was performed on one length per cross section regarding out-of-plane pressure and suction load. Three different axial load combinations per geometry were studied to examine how axial load affects the capacity for out-of-plane load. Here the finite element analysis is compared to a method retrieved from EC 1999-1-1, Design of Aluminum Structures.

For axial loads in the longitudinal direction, the Eurocode methods were found to be very conservative, with a deviation of around 40% in the longest plates. The hybrid method was also excessively conservative. For transverse loading, the Eurocode provided decent results for two of the three cross-sections (7-10% deviation) after adaptation, but was nonconservative in the case of the third geometry, which had smaller stiffeners. Material safety factors were excluded for the sake of comparison between methods.

Contents

Figures

Tables

1. Introduction

Stiffened plates are suitable for use in several types of load-bearing structures. Such plates are often used in bridge constructions such as bridge beams and boxes. Other uses include ship hulls and offshore structures, as well as containers and vehicles. Stiffened plates are especially attractive for use in constructions due to their high axial and moment resistance capacities relative to their weight and slenderness.

This thesis covers steel plates designed with closed-section longitudinal stiffeners. The Eurocode 1993-1-1 and 1993-1-5 provide means of dimensioning by analytical means, but its methods and resulting capacities differ somewhat from the true ones, which can be approximated more closely by analysis using the Finite Element Method. Different geometrical combinations result in significant capacity differences, and the Eurocode is not equally equipped to deal with them all. Specifically in this thesis, we have chosen stiffeners that have relatively high resistance to global buckling, though the individual plate members may be slender. That is, the critical elastic buckling loads are close to or larger than the nonreduced axial capacity of the relevant cross section. In chapters 4 and 5 we examine the behavior of stiffened plates when uniaxially loaded, and in chapters 7 and 8 we examine their response to out-of-plane loading with different load combinations, and compare them to a relevant method for Aluminum plates from 1999-1-1(3).

The buckling loads were calculated using the calculation rules in EN 1993-1-5 and EN 1993-1-1 (1, 2). These are compared to buckling analyzes that were produced by the element method software Abaqus and the plate program EBPlate in chapter 5 .

2. Theory of Stiffened Steel Plates

2.1 Design Process

2.1.1 General

EN 1993-1-5 covers three approaches to the analysis of the plated structures, effective width method, reduced stress method and finite element analysis (FEA). The effective width method is divided into three parts, these parts consist of:

- Effective width - shear lag effects

- Effective width - local buckling of plates

- Effective width - interaction of shear lag and local buckling

The effective width method and the reduced stress method are covered much more than the design applying finite element method. The standard has very detailed design procedures for the two first mentioned methods, while only the general principles of FEA are described. The reason behind this is that the design of plated structures is mostly performed via the effective width and reduced stress method. FEA is often used to calculate the elastic critical stresses which is needed in calculation of effective width.

2.1.2 Effective Width Method

The effective width method is used in the warm-up example in chapter 3. The effective width method and reduced stress method produce the same results when analyzing a uniaxially loaded plate with longitudinal stiffeners. Effective width method comes in use when a thin plate which is loaded by in-plane compressive stresses has buckled. The stress distribution after buckling is non-linear for a simply supported plate as shown in figure 2.1, for a simply supported plate. Since the stress distribution varies along the edge of the plate, which makes it difficult to analyze, the effective width method transforms the plate into a "fictitious plate" with an effective width of b_{eff} and makes the stress distribution uniform and equal to the yield stress, as shown in figure 2.2.
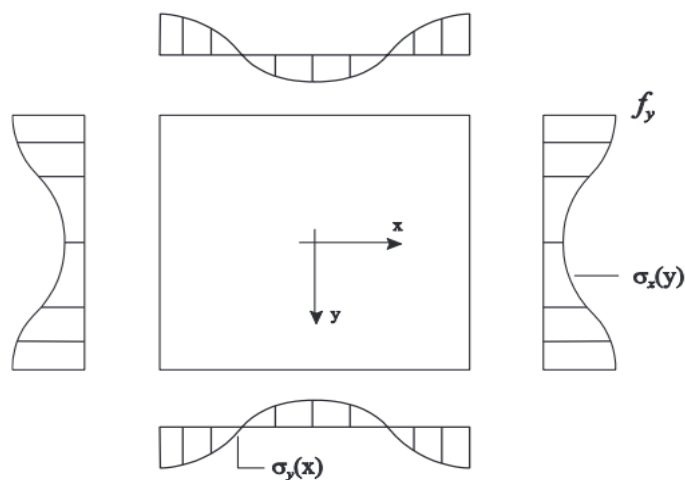
Figure 2.1: Effective width method

2.1.3 Reduced Stress Method

Section 10 of the EN 1993-1-5 provides the reduced stress method, which aids in finding the critical stresses for both stiffened and unstiffened plates. This method applies both for standard steel cross sections and non-parallel flanges and webs with openings and non-orthogonal stiffeners. In contrast to the effective width method, this method assumes a linear stress distribution instead of reducing the cross section area due to buckling, as shown in figure 2.2. This assumption is valid up to the stress limit of the first plate element which buckles first, and up to this point the cross section is fully effective. This method assumes class 3 properties.
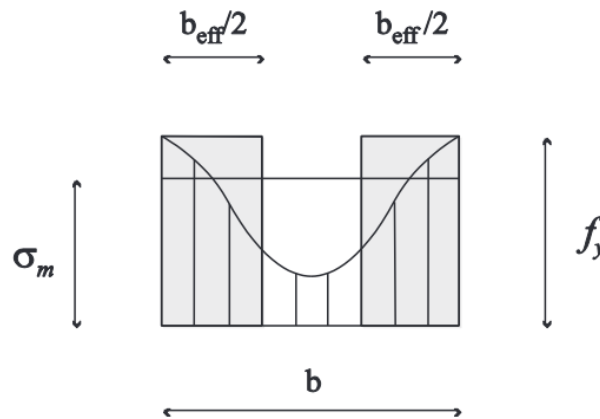
Figure 2.2: Reduces stress method

The benefits of the reduced stress method is that it is more applicable to non-standard plate constructions (standard being I girder and box cross sections) than the reduced width method. It is applicable to all geometries, including those with non orthogonal stiffeners or flanges that are not parallel. Load shedding from members with high stress to members with low stress is not considered in the reduced stress method as it is in the effective width method, and this makes the method more conservative over all. Additionally, the reduced width method is not applicable to situations of loading from multiple directions.

In cases where the cross section of a plate consists of several plate parts, then the difference between the effective width method and the reduced stress method is very easy to identify. But in cases where the cross section is made of a single plate there will be no difference and therefore the reduced method will give the same results as the effective width method.

In his master's thesis on the reduced stress method, Derik (8) performed analyses on several different loading scenarios in order to analyze the differences of the methods, under three categories. Unstiffened uniaxially loaded plates, unstiffened biaxially loaded plates and stiffened uniaxially loaded plates. In our project we will be looking at stiffened uniaxially and biaxially loaded plates.

The findings show that for uniaxial loading of unstiffened plates, effective width method and reduced stress method produced the same results, and these closely match the FEM analysis performed in Abaqus. Meanwhile for biaxially loaded plates, there was a significant difference in

the calculated buckling strength for Abaqus and the reduced stress method when the plate had an aspect ratio larger than one, demonstrating that the RSM fails to account for the aspect ratio.

For stiffened plates uniaxially loaded, effective width and RSM produce, again, the same critical buckling strength, which was 10-15% off from the calculated values in Abaqus, demonstrating that the hand calculations are conservative.

In uniaxial loading conditions, Derik found that effective width method was more appropriate when it came to strength capacity, but the reduced strength method can be quickly and efficiently used as the parameter $a_{ult,k}$ can be easily retrieved from the FEM software Abaqus, EBplate or similar FE tools. The reduced stress method is also the only one that can be used in loading situations in which the load comes from multiple directions.

2.1.4 Design Procedure of Effective Width and Reduced Stress Method

The effective width is determined by multiplying the mean value of the stresses and the maximum stress by the original width of the plate

$$\rho = \frac{\sigma_m}{f_y} = \frac{b_{eff}}{b} \qquad (2.1)$$

where ρ is the reduction factor for the plate buckling resistance.

The mentioned reduction factor is in EN 1993-1-5 calculates by the following rules:

$$\rho = 1 \qquad \text{for } \overline{\lambda}_p \leq 0.5 + \sqrt{0.085 - 0.055\psi} \qquad (2.2)$$

$$\rho = \frac{\overline{\lambda}_p - 0.055(3+\psi)}{\overline{\lambda}_p^2} \qquad \text{for } \overline{\lambda}_p > 0.5 + \sqrt{0.085 - 0.055\psi} \qquad (2.3)$$

where ψ represents the stress ratio along the loaded edge, and $\overline{\lambda}_p$ represents the slenderness of a four-edge supported plate, which is given by the following:

$$\overline{\lambda}_p = \frac{b/t}{28.4\varepsilon\sqrt{k_\sigma}} \qquad (2.4)$$

being k_σ the buckling coefficient and $\varepsilon=\sqrt{\frac{235}{f_y}}$ with f_y in MPa.

The reduction factor for outstand elements loaded by compression is given by:

$$\begin{array}{ll} \rho = 1 & \text{for } \overline{\lambda}_p \le 0.748 \\ \rho = \frac{\overline{\lambda}_p - 0.188}{\overline{\lambda}_p{}^2} & \text{for } \overline{\lambda}_p > 0.748 \end{array} \qquad (2.5)$$

The reduced stress method solves the interaction between different stress types by using von Mises criterion.

2.2 Pourostad´s Suggestions

In Pourostad's presentation, he identifies problems with the current EC procedures and has two suggestions for improvement (10). This is specifically relevant to panels in uniaxial or biaxial compression. His suggestions for improvements to the design process of plates with in-plane moments is not included here.

Firstly, Pourostad notes that in the reduced stressed method (referred to hereafter as RSM) according to the Eurocode, torsional stiffness is not taken into account for plates with closed stiffeners.

Neglecting torsional stiffness means that a part of the resistance to buckling is neglected and that the strength/stiffness analyses are overly conservative, and leads therefore to designs with unnecessarily thick plates. He identifies several possible solutions:

- Use $\rho_{p,x}$ according to Annex B of Eurocode 1993-1-5 and considering torsional stiffness in calculation of α_{cr}

- Modification of interpolation function for column-like and plate-like buckling to ensure safety of results when torsional stiffness is considered.

The interpolation function as it stands in the Eurocode today is:

$$\xi := \frac{\sigma_{cr.p}}{\sigma_{cr.c}} - 1 \tag{2.6}$$

$$\rho_c := \chi_c + (\rho - \chi_c) \, f \tag{2.7}$$

$$f := \xi \cdot (2 - \xi) \tag{2.8}$$

Pourostad's suggestion is to replace the function f with a new function with more conservative interpolation. Namely:

$$f := V \cdot \left(\ln(\xi + 1)\right)^P \tag{2.9}$$

Local buckling	Global buckling
V=1	$V := \dfrac{1}{\left(\lambda_p - 1\right)^{\frac{2}{3}}}$
P = 0.5 for long. loads	
P = 1.5 for transv. loads	P = 1.5
Table 2.1: Parameter values in Pourostad's interpolation formula	

This suggestion improved the results of the reduced stress method, and was considerably "safer" than the current Eurocode method would be if torsional stiffness were to be included in calculation of critical buckling stress.

Figure 2.3: Comparison of Eurocode values and Pourostad's proposal values (10)
RM X2 = Eurocode, RM X3 = Pourostad
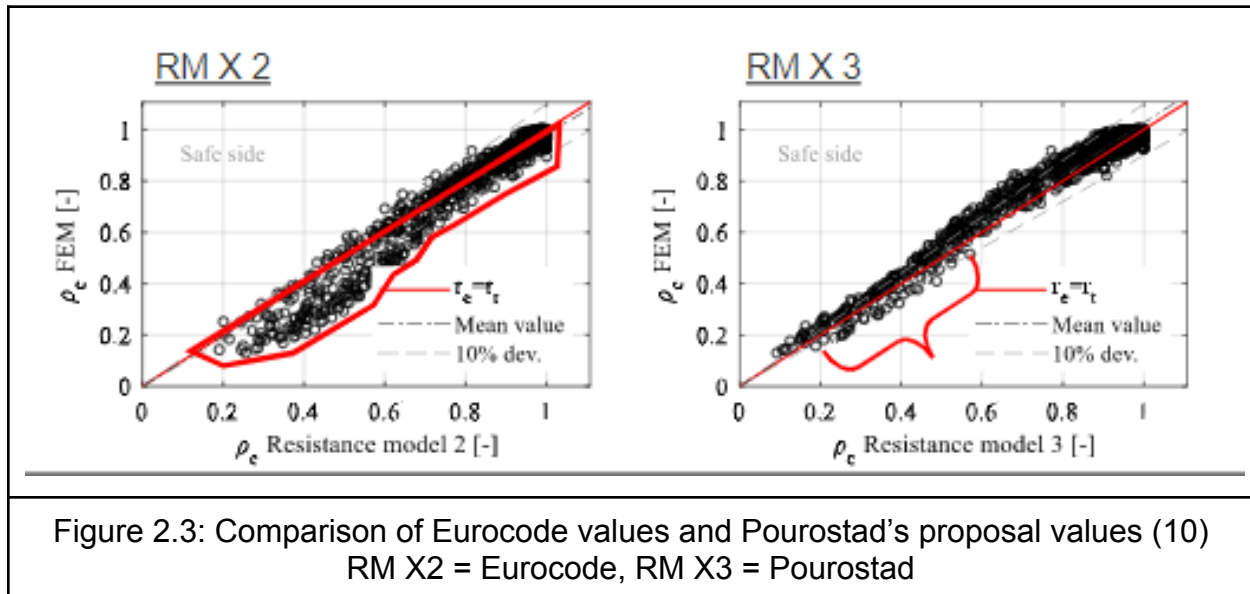
The second suggestion Pourostad had was to ignore plate-like buckling behavior for panels loaded transversely to the stiffener direction., and to assume that column-like behavior would dominate. This produces good results and simplifies the buckling verification process, since it is unnecessary to then check against a second order analysis.

Compared to the FEM analysis, the method with these two corrections does reasonably well, but for stocky panels under biaxial stress, there is a region of instability, which Pourostad recommends fixing by performing verifications individually in the transverse and longitudinal direction.

2.3 EN 1999-1-1, Design of Aluminum Constructions (3)

In the new (coming) aluminum standard EN 1999-1-1, the combined loading of axial forces, expressed through η_N and bending moments due to out-of-plane loading which is expressed by η_m, the resistances of the most exposed areas of the cross-section should satisfy the following interaction formula which shows the utilization grade,

$$U = \sqrt{\eta_N^2 + 0,9\eta_m^2 - k_{Nm}\eta_N\eta_m} \qquad (2.10)$$

where k_{Nm}=1 if the bending moment gives compression in the studied layer, and k_{Nm}=-1 if the bending moment gives tension in the layer of interest, which is the plate in this case. The contribution from the axial forces η_N is found by the following formula,

$$\eta_N = \sqrt{\left(\frac{N_{x,Ed}}{N_{x,b,Rd}}\right)^2 + \left(\frac{N_{y,Ed}}{N_{y,b,Rd}}\right)^2 - k_{xy}\left(\frac{N_{x,Ed}}{N_{x,b,Rd}}\right)\left(\frac{N_{y,Ed}}{N_{y,b,Rd}}\right)} \qquad (2.11)$$

where $k_{xy} = 2\chi_x\chi_y - 1$ when both $N_{x,Ed}$ and $N_{y,Ed}$ are both compressive, which is the case in the following study. The contribution from the out-of-plane load is accounted for by the formula below:

$$\eta_m = \sqrt{\left(\frac{m_{x,Ed}}{m_{x,Rd}}\right)^2 + \left(\frac{m_{y,Ed}}{m_{y,Rd}}\right)^2 - \left(\frac{m_{x,Ed}}{m_{x,Rd}}\right)\left(\frac{m_{y,Ed}}{m_{y,Rd}}\right)} \qquad (2.12)$$

where the moments $m_{x,Ed}$ and $m_{y,Ed}$ can be calculated using either numerical methods or the following formulas for cases where the plate is simply supported,

$$m_{x,Ed} = B_x \frac{16q_{Ed}}{\pi^6} \sum_{m=1,3,5}^{\infty}\sum_{n=1,3,5}^{\infty} \left(\frac{\left(\frac{m\pi}{L}\right)^2 \cdot \sin\left(\frac{m\pi x}{L}\right)\sin\left(\frac{n\pi y}{b}\right)}{mn\left(\frac{m^4}{L^4}B_x + \frac{2m^2n^2}{L^2b^2}H + \frac{n^4}{b^4}B_y\right)} \right) \qquad (2.13)$$

$$m_{y,Ed} = B_y \frac{16q_{Ed}}{\pi^6} \sum_{m=1,3,5}^{\infty}\sum_{n=1,3,5}^{\infty} \left(\frac{\left(\frac{n\pi}{b}\right)^2 \cdot \sin\left(\frac{m\pi x}{L}\right)\sin\left(\frac{n\pi y}{b}\right)}{mn\left(\frac{m^4}{L^4}B_x + \frac{2m^2n^2}{L^2b^2}H + \frac{n^4}{b^4}B_y\right)} \right) \qquad (2.14)$$

where B_x, B_y and H are for a cross section as shown in figure 2.3 given by the following formulas,

$$B_x = \frac{EI_L}{2a} \qquad (2.15)$$

I_L is the second moment of area of the cross section given in figure 2.3, and $2a$ is the width of a stiffener plus the adjacent plating.

$$B_y = \frac{2Ba}{2a_4 + \dfrac{2a_1 a_3 t_1^3 (4a_2 t_3^3 + a_3 t_2^3)}{a_3 t_1^3 (4a_2 t_3^3 + a_3 t_2^3) + a_1 t_3^3 (12a_2 t_3^3 + 4a_3 t_2^3)}} \qquad (2.16)$$

here a_1, a_2 and a_3 are the length of the different parts of a stiffener, as shown in figure 2.3. T This formula is only used when the cross-section is as shown in figure 2.4. B is given by the formula below,

$$B = \frac{E t_1^3}{12(1 - v^2)} \qquad (2.17)$$

$$H = 2B + \frac{GI_t}{2a} \cdot \frac{1}{2 + \dfrac{8GI_t}{Lab}\left[\varphi_{plt} + \varphi_{dis}\right]} \qquad (2.18)$$

where I_t is the torsional constant of the cross section shown in figure 2.3. Here ϕ_{plt} and ϕ_{dis} is determined by,

$$\varphi_{plt} = \frac{2a_4^2}{aEt_1^3}\left[a_4 + \frac{a_1(3\alpha_3 + 4\alpha_2)}{3\alpha_3 + 4\alpha_2 + 4\alpha_1 + 4\alpha_1\alpha_2 / \alpha_3}\right] \qquad (2.19)$$

$$\varphi_{dis} = \frac{ha_2\left(3\alpha_3^2 + 4\alpha_1\alpha_2 + 4\alpha_1\alpha_3 + 4\alpha_2\alpha_3\right)}{2a_2\alpha_2 + f2a_1\alpha_1 + (2 + f)a_2\alpha_3 + (1 + 2f)a_1\alpha_3} \qquad (2.20)$$

and the values of α_1, α_2, α_3 and f is found by these:

$$\alpha_1 = \frac{2a_1}{Et_1^3}, \; \alpha_2 = \frac{2a_2}{Et_2^3}, \; \alpha_3 = \frac{a^3}{Et_3^3} \qquad (2.21)$$

$$f = 1 + \frac{(a_1 - a_2)a_3}{ha_2} \qquad (2.22)$$

All of these steps have to be done in order to find the bending moments in x and y direction. These moments are given as moments per unit width, and therefore the moment resistances in both directions have to be calculated accordingly.
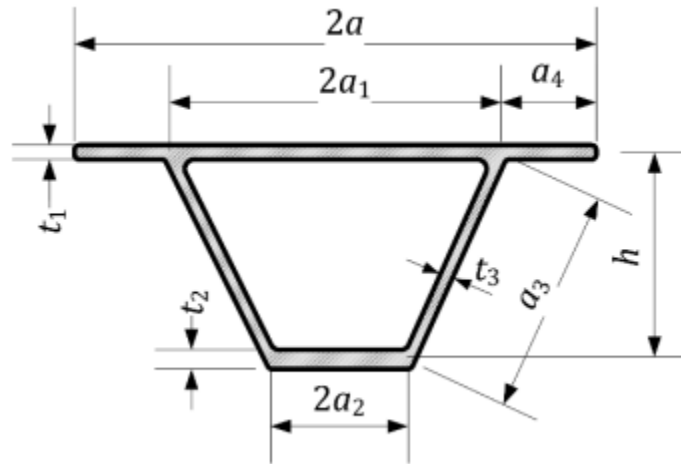
Figure 2.4: Cross section notations

2.4 EBPlate

EBPlate is a freely available software that provides accurate values of elastic critical stresses for rectangular plates subjected to in-plane loading. The rectangular plates can be unstiffened or stiffened by either longitudinal or transverse stiffeners. Numerical eigenvalues for buckling can be solved by using the Rayleigh-Ritz *Method.* This software is used as an alternative to find the buckling load of the plates that are presented. Buckling load analysis in EBPlate includes not only the bending of the stiffeners and of the plate in the longitudinal and transversal direction, but also torsion.

By using the Rayleigh-ritz method and a series expression for the buckling displacement, EBPlate is able to calculate a factor ϕ_{cr} , known as a_{cr} in the reduced stress method of capacity calculation. Rayleigh-ritz method is an energy method and furthermore the principle of stationary potential energy is used to set up a formula for energy balance in case of instability

$$\Delta U - \Delta W_{int} = 0 \qquad (2.10)$$

where ΔU represents the total energy and ΔW_{int} represents the total inner work of the critical stress $S_{cr} = \phi_{cr} S.$

The eigenvalue problem can now be solved by the help of the aforementioned formulas

$$det[R_0 TY - \phi_{cr} R_G(S) = 0 \qquad (2.11)$$

where R_0 represents material stiffness and R_G represents the geometrical stiffness.

3. Warm-up Example

On page 181 of the commentary to the current steel eurocode there is a worked example of a longitudinally stiffened plate where the plate is loaded in-plane (11). The plate has dimensions as shown below
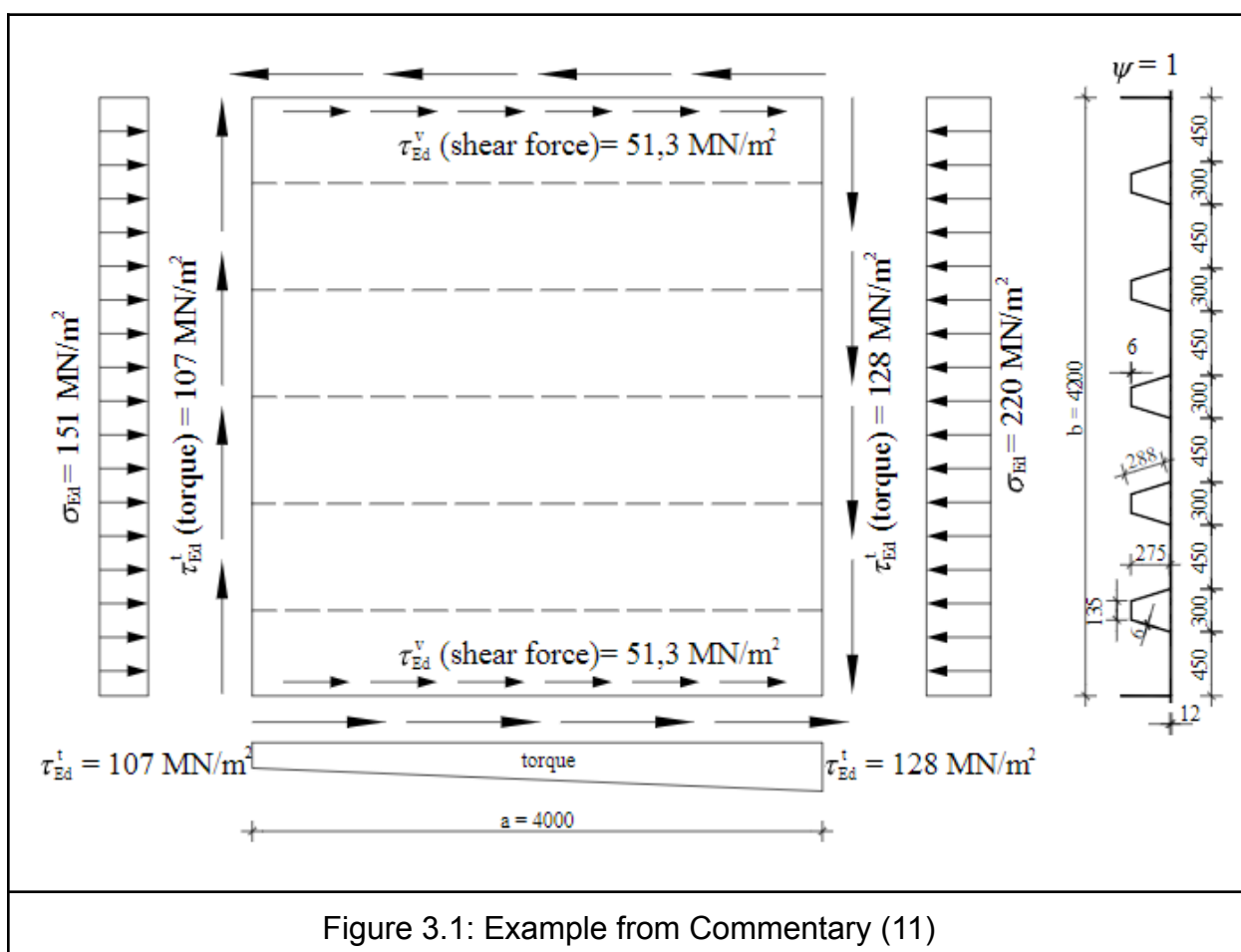
Figure 3.1: Example from Commentary (11)

The example in the commentary included strength verification for a specific loading situation, but we used it as the basis of calculating the buckling load for the plate, making sure to follow the commentary closely.

In addition to hand calculations, we performed a FEM analysis with the software Abaqus in order to compare the results.

Figure 3.2: Local buckling mode
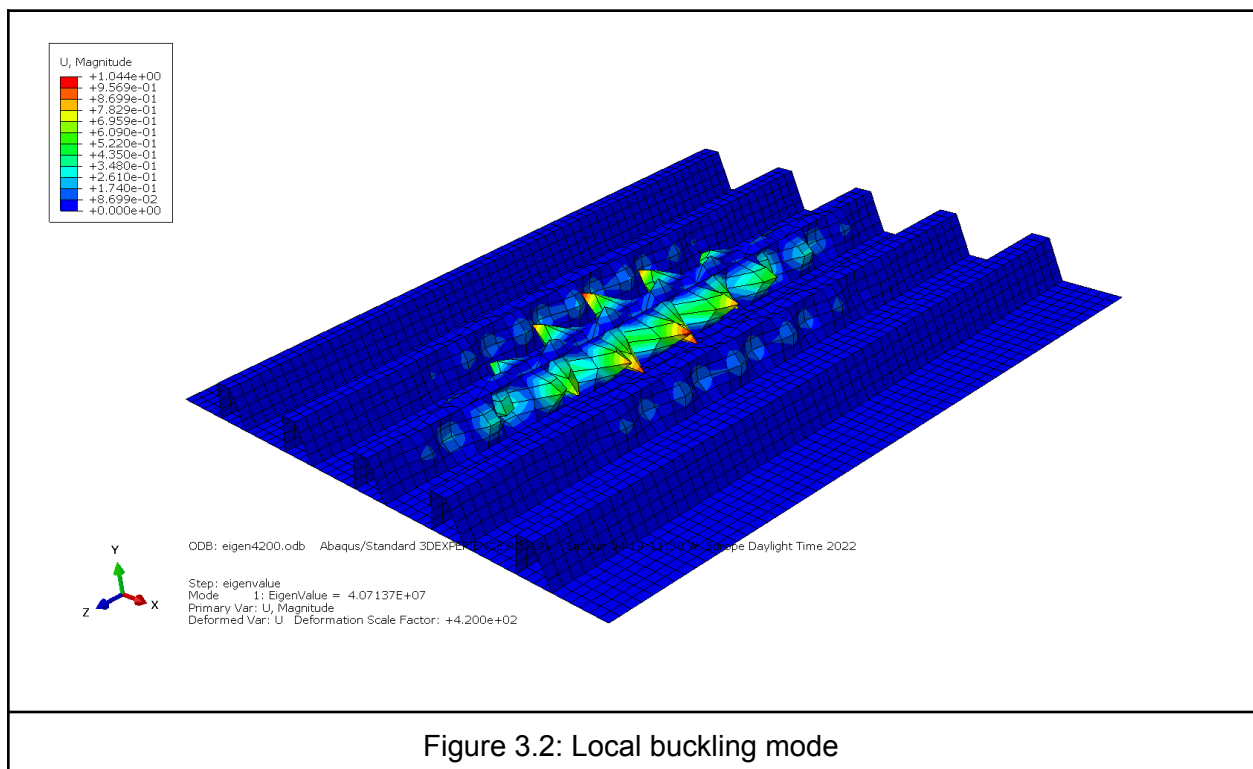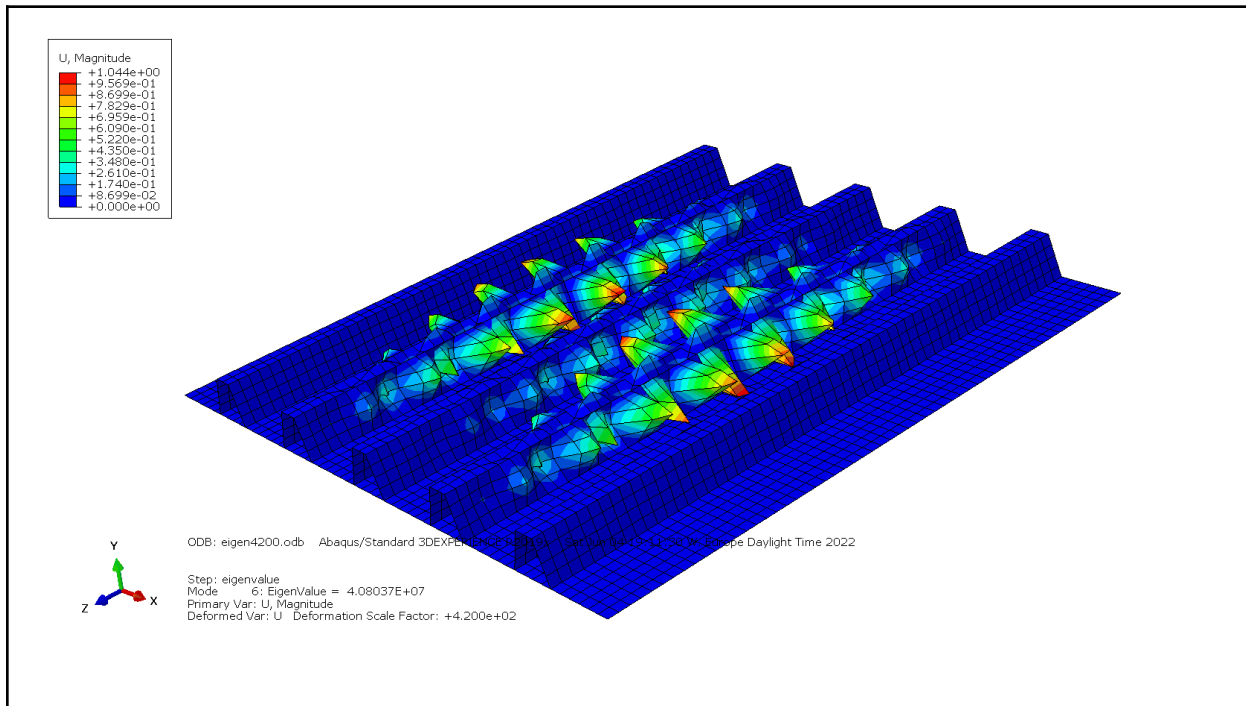
Figure 3.3: Local buckling mode
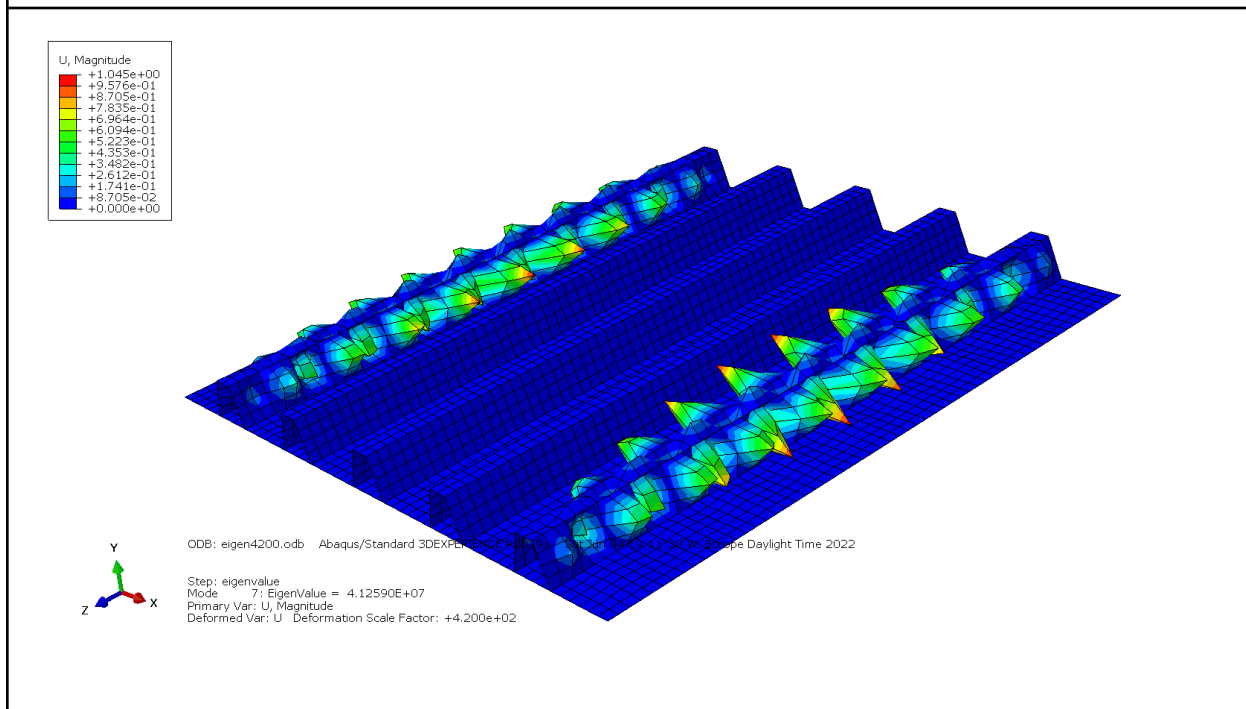
Figure 3.4: Local buckling mode
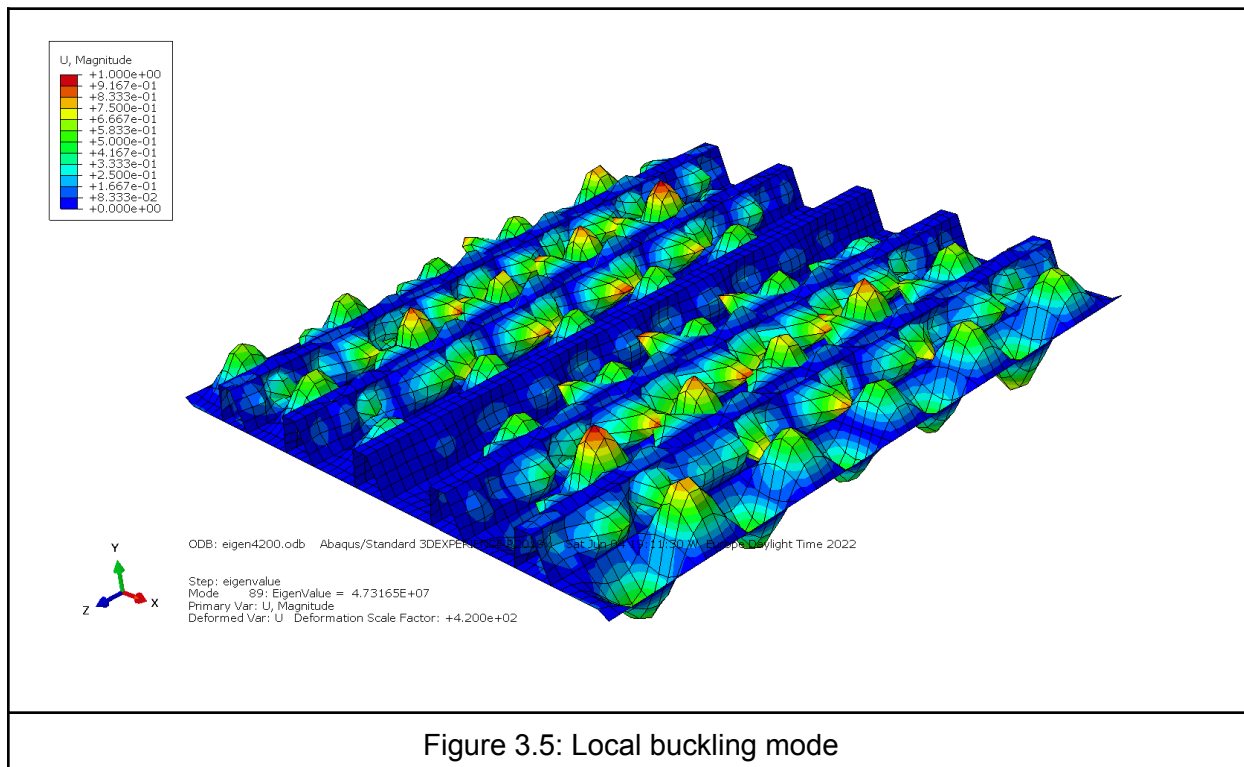
Figure 3.5: Local buckling mode

With this particular geometry, we were unable to determine a global buckling mode in the first 100 modes. This means that the plate is much more vulnerable to local buckling than it is to global buckling, because of a combination of large stiffeners and small thickness values.

The Eurocode accounts for local buckling by calculating an effective area, where the section is expected to fail as the whole effective area reaches the yield stress. This effective axial capacity is then used to calculate slenderness, or susceptibility to global buckling (more on this in chapters 4 and 5). As we were not able to determine a global buckling mode with FEM (to request more eigenvalues is computationally expensive and irrelevant in practice) we are not able to compare the FEM elastic global buckling force to the value from the Eurocode.

For loading in the transverse direction, the plate did buckle globally, which initially confused us. We assumed that we were performing the buckling analysis incorrectly when loading in the longitudinal direction. In fact, the large stiffener size provided enough resistance to global buckling so as to ensure local buckling be critical.

4. Calculations According to Eurocode

4.1 Buckling Analysis of Longitudinal Load

The process of buckling analysis according to the Eurocode (1, 2) is identifying a critical buckling stress for plate-like buckling behavior, as well as a critical buckling stress for column-like behavior. The calculations were performed on these three geometries:

- "Small" geometry, short stiffeners, see figure 3.6.
- "Slender" geometry, high stiffeners, see figure 3.6. The exact same geometry as the example from commentary (11)
- "Stiff" geometry, the same geometry as the "slender" except that the thickness of the plate and the stiffeners are doubled, see figure 3.6

Figure 3.6: From left to right, "small", "slender" and "stiff"
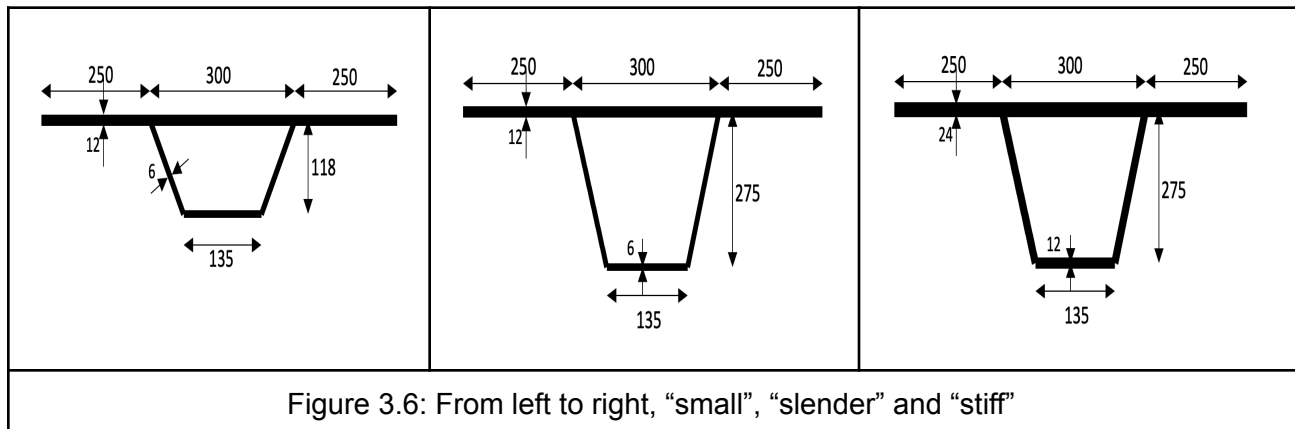
4.1.1 Plate-like Behavior

Unstiffened plates buckle in two directions (provided the boundary conditions prevent out-of-plane displacement), the longitudinal and the transverse. In a situation where the plate is loaded uniaxially, the center of the plate will have a significantly larger out-of-plane displacement than a point closer to the longitudinal edge, see figures 4.1 and 4.2. This is because the resistance provided by the boundary conditions on the long edges is reduced the closer the point is to the plate's center.

A plate without boundary conditions that prevent out-of-plane displacement along the longitudinal edge will not have this variation. One can also assume that the largest displacement will be as large or larger than an analogous plate with these boundary conditions.

Plate-like buckling behavior involves therefore a more or less quadratic or consistently "rounded" deformed shape in both the transverse and longitudinal directions
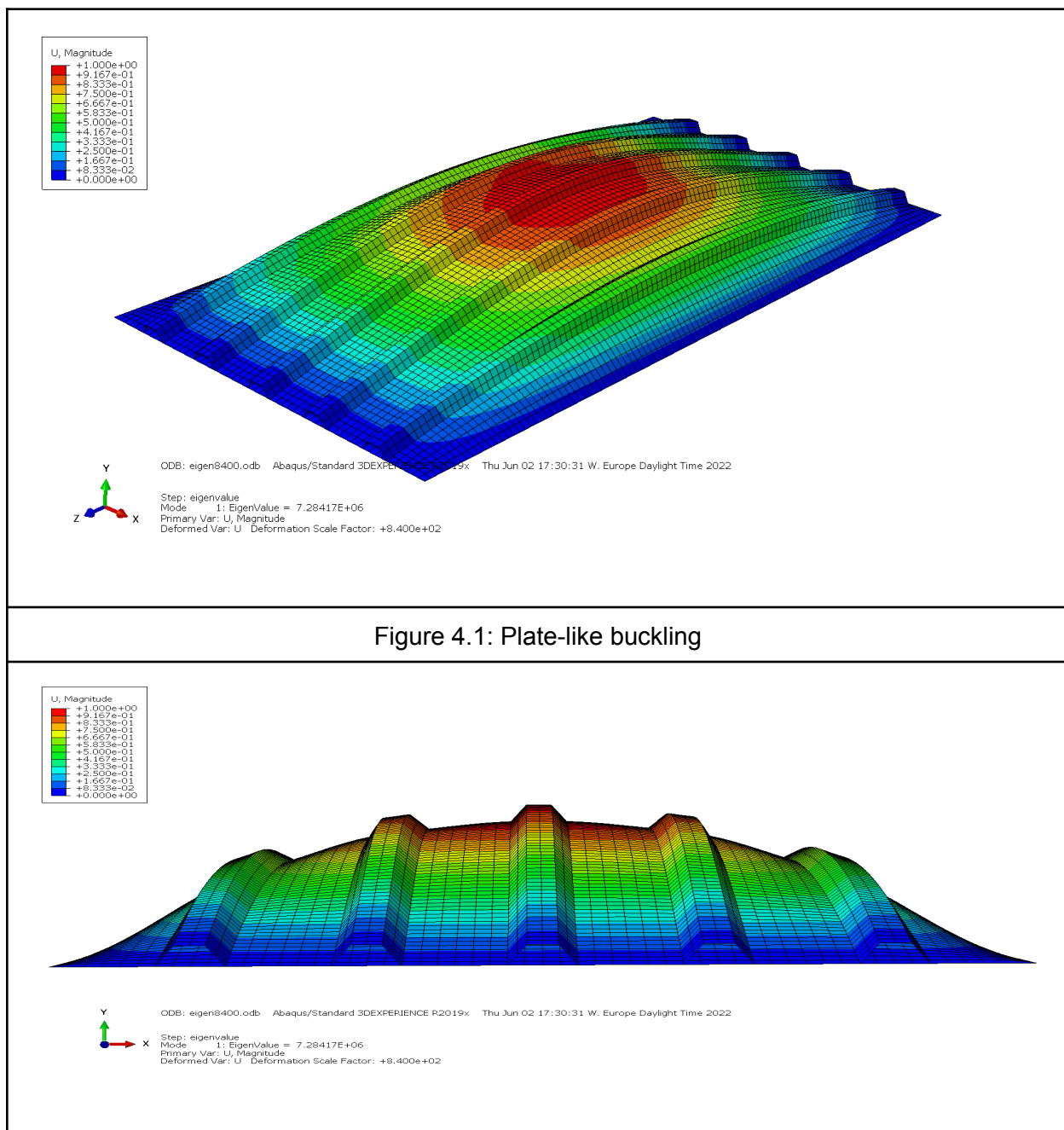
Figure 4.1: Plate-like buckling

Figure 4.2: Plate-like buckling

4.1.1 Column-like Behavior

Longitudinal stiffeners increase the second moment of area about the transverse axis for the section of the plate they cover, increasing the total buckling resistance and reducing out-of-plane displacement. In this way it can also be useful to model the buckling of a stiffened plate as a row of columns that buckle as a group (1).

At the same time, the boundary conditions provide an extra resistance to out of plane displacement, so a longitudinally loaded, longitudinally stiffened plate will always have a higher resistance to buckling than a true row of columns. This is why the Eurocode requires calculations of critical buckling stresses for **both** column-like and plate-like behavior.

A plate with relatively soft stiffeners will have a displacement field that more closely resembles a plate-like buckling shape, see figure 4.4 (that is, a large portion of the total resistance will come from the boundary conditions and membrane forces) while a plate with very large or stiff stiffeners will have a displacement field that more closely resembles the buckling shape of a row of columns, see figure 4.3.

In calculation of total axial capacity, the non-reduced axial capacity is multiplied with a reduction factor (see below) in order to account for buckling, and this reduction factor is an interpolation between the reduction factors for plate-like and column-like buckling, respectively. This equation is provided and explained below.

ODB: eigen2100.odb   Abaqus/Standard 3DEXPERIENCE R2019x   Thu Jun 02 17:29:39 W. Europe Daylight Time 2022

Step: eigenvalue
Mode   1: EigenValue = 3.73652E+07
Primary Var: U, Magnitude
Deformed Var: U   Deformation Scale Factor: +4.200e+02
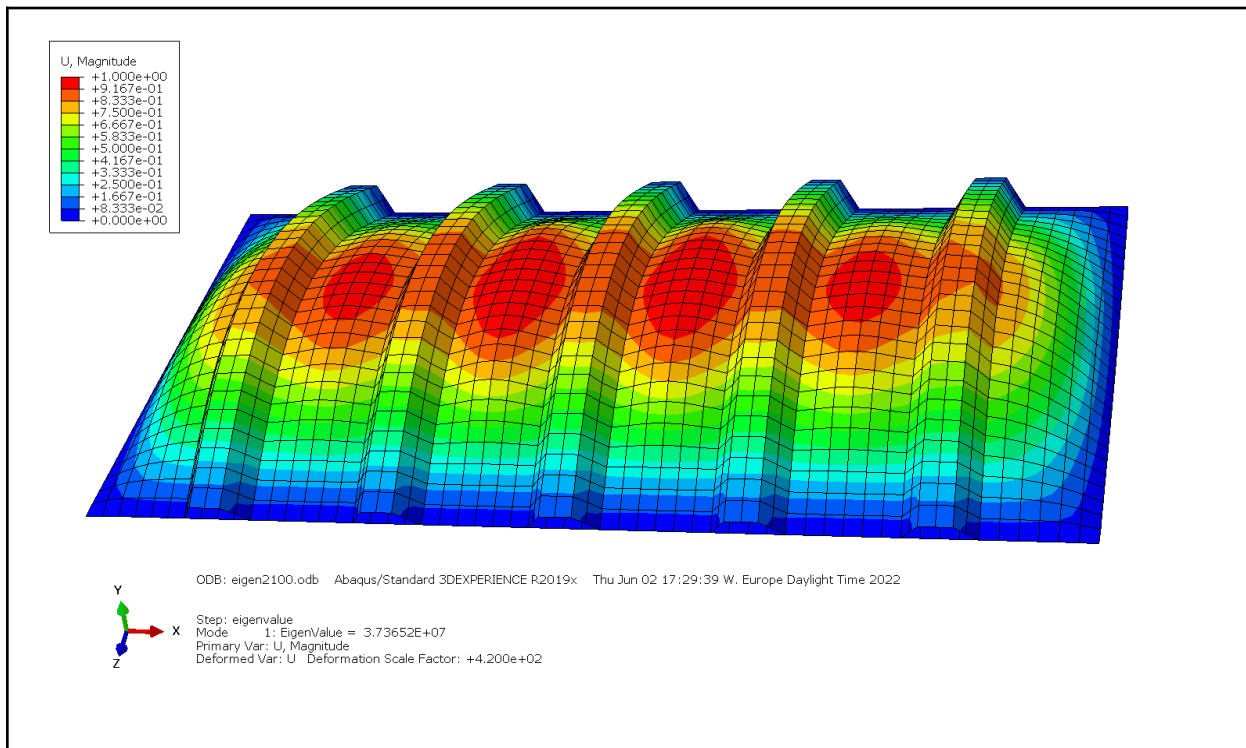
Figure 4.3: Column-like buckling

ODB: eigen2100.odb   Abaqus/Standard 3DEXPERIENCE R2019x   Thu Jun 02 17:29:39 W. Europe Daylight Time 2022

Step: eigenvalue
Mode   1: EigenValue = 3.73652E+07
Primary Var: U, Magnitude
Deformed Var: U   Deformation Scale Factor: +4.200e+02
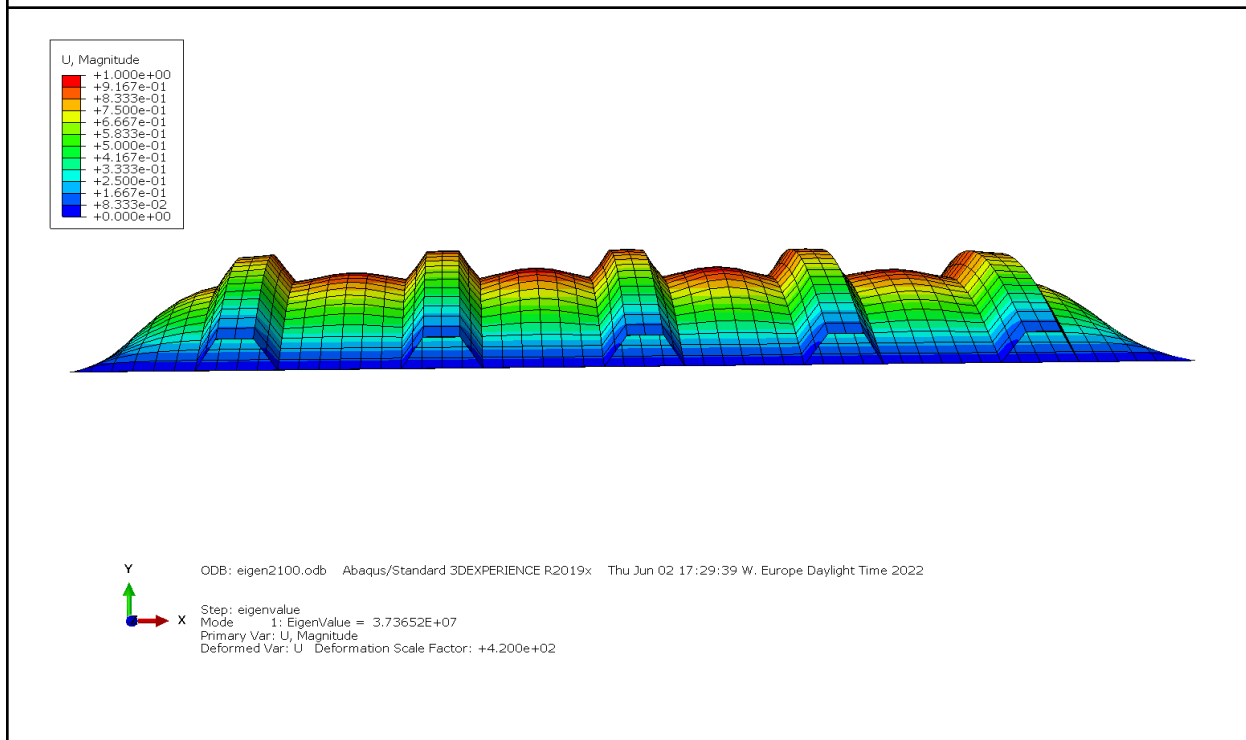
Figure 4.4: Column-like buckling

4.1.2 Capacity Analysis Following EC 3

Capacity analysis of the stiffened plate under axial load is described in chapters 4 and 5 of EC 1993-1-5, with capacity:

$$N_{c.Rd} := A_{c.eff} \cdot f_y$$

(4.1)

$A_{c,eff}$ is the effective compressive area, and differs from the gross area by taking into account reduction for local and global buckling. For the purposes of comparison between EC results and FEM analysis results, material factors are not included.

$$A_{c.eff} := \rho_c \cdot A_{c.eff.loc} + A_{eff.I}$$

(4.2)

- ρ_c is the reduction factor, derived from the interpolation function that takes into account both column and plate-like behavior

- $A_{c,eff,loc}$ is the net area that takes local buckling into account

- $A_{eff,I}$ is the area of the plate connected to other parts of the cross section

- If neither local nor global buckling are critical, $A_{c,eff}$ is equal to the gross area, and the capacity of the plate cross section is equal to unreduced axial capacity

Reduction factors for global buckling

The global reduction factor is an interpolation between the reduction factors for column and plate-like buckling behavior, respectively.

- Column-like behavior

$$\chi_c := \frac{1}{\phi + \sqrt{\phi^2 - \lambda_c^2}} \tag{4.3}$$

$$\phi := 0.5 \left(1.0 + \alpha_c \cdot (\lambda_c - 0.2) + \lambda_c^2\right) \tag{4.4}$$

$$\lambda_c := \sqrt{\frac{(\beta_{A.c} \cdot f_y)}{\sigma_{cr.sl}}} \tag{4.5}$$

– χ is the reduction factor

– α_c is the adjusted imperfection factor

– λ_c is the sections slenderness

– $\beta_{A,c}$ is the proportion between the effective and gross areas of the stiffener cross-section

– $\sigma_{cr,sl}$ is the critical buckling stress for the column (in uniform compression, this value is equal to the critical buckling stress $\sigma_{cr,c}$

●   Plate-like behavior

$$\rho := 1 \qquad\qquad \lambda_p \le 0.5 + \sqrt{0.085 - 0.055 \cdot \psi} \tag{4.6}$$

$$\rho := \frac{(\lambda_p - 0.055\,(3 + \psi))}{\lambda_p^2} \qquad\qquad \textbf{Otherwise} \tag{4.7}$$

where slenderness λ_p is the square root of the ratio of the nonreduced axial capacity $N_{a,Rd}$ to the critical plate-buckling load $N_{cr,p}$, identical as for columns.

$$N_{cr.p} := \sigma_{cr.p} \cdot A \qquad \text{(4.8)}$$

$$N_{cr.c} := \sigma_{cr.sl} \cdot A \qquad \text{(4.9)}$$

Nonreduced axial capacity (taking into account local buckling):

$$N_{a.Rd} := \left(A_{c.eff.loc} + A_{eff.I}\right) \cdot f_y \qquad \text{(4.10)}$$

Interpolation of reduction factor:

$$\rho_c := \left(\rho - \chi_c\right) \cdot \xi \cdot \left(2 - \xi\right) + \chi_c \qquad \text{(4.11)}$$

where

$$\xi := \frac{\sigma_{cr.p}}{\sigma_{cr.sl}} - 1 \qquad 0 \leq \xi \leq 1 \qquad \text{(4.12)}$$

The interpolation is an increase on the reduction factor for column-like behavior. Since membrane forces and boundary conditions increase resistance and decrease displacement, the resistance to buckling will always be slightly larger than the value calculated for an analogous row of columns.

A low value for variable ξ indicates that the stiffeners provide a high level of resistance on their own, and the membrane forces and boundary conditions provide a relatively small addition, while a high value of ξ indicates a larger role in membrane forces and boundary conditions in the total resistance.

It is important to note that the value of ξ is primarily dependent on the buckling resistance of the stiffeners. The calculated value of critical buckling stress for plate-like behavior can be calculated as lower than the corresponding value for column-like behavior. In practice, a stiffened plate will always have more resistance than the corresponding row of columns. It is therefore reasonable to conclude that the Eurocode will produce conservative capacities for plates with very large/stiff stiffeners, even before safety and material factors are included. Short plates with large stiffeners are particularly likely to encounter this problem.

The current Eurocode method also ignores torsional resistance of the stiffeners. Torsional stiffness is of limited significance for open stiffener sections, but in closed trapezoids it makes a larger difference. This is especially true for large stiffeners.

Length (mm)	$N_{cr.p}$ (MN)	$N_{cr.c}$ (MN)	λ_p	λ_c	ρ	χ_c	ρ_c	$N_{c.Rd}$ (MN)
600	470.231	505.334	0.213	0.205	1	0.997	0.997	21.172
1050	153.654	165.007	0.373	0.36	1	0.919	0.919	19.637
1500	75.378	80.853	0.532	0.514	1	0.835	0.835	18.015
2100	38.549	41.252	0.744	0.719	0.947	0.713	0.713	15.626
3000	18.999	20.213	1.06	1.027	0.748	0.524	0.524	11.948
4200	9.828	10.313	1.473	1.438	0.577	0.335	0.335	8.264
6300	4.596	4.584	2.154	2.157	0.417	0.172	0.173	5.103
7000	3.827	3.713	2.361	2.397	0.384	0.143	0.157	4.792
7700	3.273	3.068	2.553	2.637	0.358	0.12	0.151	4.667
8400	2.867	2.578	2.728	2.876	0.337	0.103	0.152	4.692

Table 4.1: Values for "small" geometry

Length (mm)	$N_{cr.p}$ (MN)	$N_{cr.c}$ (MN)	λ_p	λ_c	ρ	χ_c	ρ_c	$N_{c.Rd}$ (MN)
600	3297	3486	0.083	0.081	1	1	1	22.814
1050	1077	1138	0.146	0.142	1	1	1	22.814
1500	527.733	557.719	0.208	0.202	1	0.999	0.999	22.792
2100	269.342	284.551	0.291	0.283	1	0.961	0.961	21.988
3000	132.088	139.43	0.416	0.404	1	0.902	0.902	20.749
4200	67.526	71.138	0.581	0.566	1	0.817	0.817	18.946
6300	30.239	31.617	0.869	0.849	0.86	0.645	0.645	15.331
7000	24.598	25.61	0.963	0.944	0.801	0.587	0.587	14.094
7700	20.439	21.165	1.056	1.038	0.749	0.53	0.53	12.909
8400	17.291	17.784	1.149	1.133	0.704	0.478	0.478	11.807

Table 4.2: Values for "slender" geometry

Length (mm)	$N_{cr.p}$ (MN)	$N_{cr.c}$ (MN)	λ_p	λ_c	ρ	χ_c	ρ_c	$N_{c.Rd}$ (MN)
600	6617	6992	0.088	0.085	1	1	1	50.928
1050	2162	2283	0.153	0.149	1	1	1	50.928
1500	1060	1119	0.219	0.213	1	0.994	0.994	50.632
2100	541.478	570.785	0.307	0.299	1	0.953	0.953	48.737
3000	266.204	279.685	0.437	0.427	1	0.891	0.891	45.791
4200	136.892	142.696	0.61	0.597	1	0.799	0.799	41.463
6300	62.663	63.421	0.902	0.896	0.839	0.616	0.616	32.846
7000	51.591	51.371	0.994	0.996	0.784	0.555	0.557	30.077
7700	43.52	42.455	1.082	1.095	0.736	0.498	0.51	27.856
8400	37.503	35.674	1.165	1.195	0.696	0.446	0.471	26.028

Table 4.3: Values for "stiff" geometry

Figure 4.5: Reduction factors for buckling
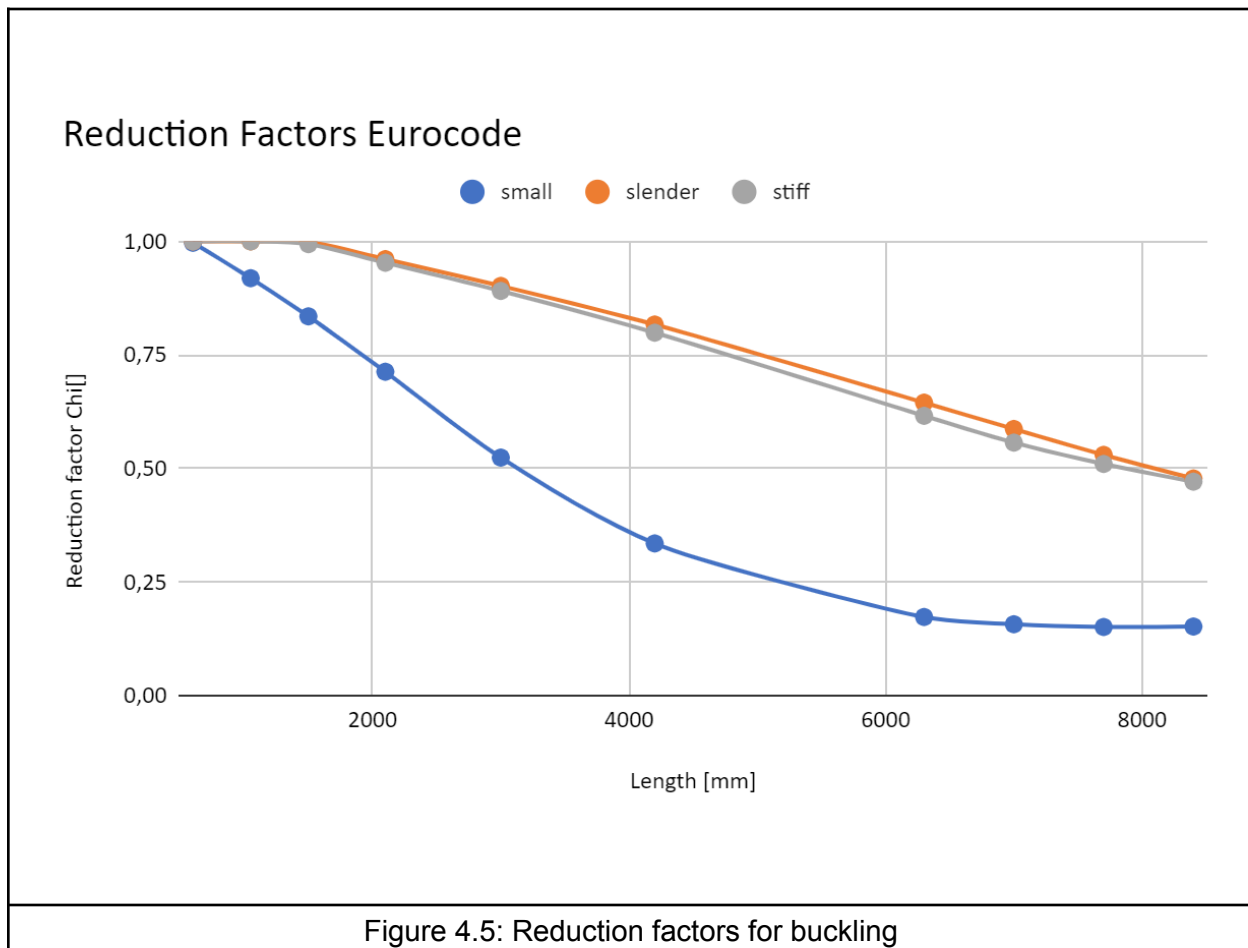
All three geometries are dominated by column buckling for plates with an aspect ratio less than or equal to one (read: length = 4200), while the slender and stiff geometries largely remain so for all lengths. This is why the curve for "small" geometry begins to flatten out as plate-like buckling takes on a larger role, while the other two continue in a fairly linear fashion. Meanwhile, "slender" and "stiff" geometries have curves that are very close, due to having large stiffeners with the same cross section, albeit of different thicknesses.

.

4.2 Compensation for Neglect of Torsional Stiffness

To compensate for the Eurocode's neglect of torsional stiffness of longitudinal stiffeners, we have included an alternate method of capacity calculation for comparison purposes.

4.2.1 Hybrid Method

In the Eurocode, critical buckling stress (and therefore critical buckling load) is determined by performing calculations on geometrical sizes, and then this critical buckling stress is used to determine slenderness and reduction factors for both plate-like and column-like behavior.
If, however, we instead retrieve critical buckling load from LBA performed in Abaqus, we can substitute this value for the ones calculated from the Eurocode to determine slenderness and a reduction factor.

Advantages

An advantage of this approach is simplicity. By retrieving the critical buckling load from Abaqus, we circumvent the need to calculate the critical buckling stresses and to evaluate values for both column-like and plate-like behavior. Since the "column" and "plate" critical buckling stresses are the same, ξ receives a value of zero and only the column-like reduction factor is relevant. This dovetails well with our specific chosen geometries, as column-like buckling dominates for the majority of them anyway.

Another advantage is that the resulting buckling curve can be compared to the Abaqus buckling curve for all lengths, and not only the ones where global buckling is critical.

Disadvantages

A possible disadvantage of this approach is that the Eurocode estimation of capacity is specifically tailored to the theoretical elastic buckling loads calculated from it. In this way, the neglect of torsional stiffness may be compensated for to some degree in a way of which we are unaware.

Pourostad's proposal hints to this being the case, as his interpolation formula is more conservative in order to allow for the inclusion of torsional stiffness. The results we received from this method, however, were conservative enough, as discussed later.

Results.

Included are our results. An example calculation sheet is included in the appendices.

Length (mm)	N_{cr} (MN)	λ_c	χ_c	$N_{c.Rd}$ (MN)	Length (mm)	N_{cr} (MN)	λ_c	χ_c	$N_{c.Rd}$ (MN)
600	45.9	0.68	0.751	15.932	600	47.8	0.691	0.744	16.974
1050	44.1	0.694	0.742	15.755	1050	42.3	0.734	0.717	16.366
1500	43.4	0.699	0.739	15.684	1500	42.0	0.737	0.716	16.329
2100	37.4	0.753	0.706	14.978	2100	41.6	0.741	0.714	16.279
3000	20.5	1.018	0.543	11.516	3000	41.1	0.745	0.711	16.216
4200	12.4	1.308	0.394	8.362	4200	40.7	0.749	0.709	16.164
6300	8.31	1.598	0.29	6.162	6300	36.8	0.787	0.684	15.614
7000	7.81	1.649	0.276	5.86	7000	31.9	0.846	0.648	14.778
7700	7.50	1.682	0.267	5.669	7700	28.4	0.896	0.616	14.056
8400	7.29	1.706	0.261	5.538	8400	26.0	0.937	0.591	13.485

Table 4.4: Hybrid "small" Table 4.5: Hybrid "slender"

Length	N_{cr}	λ_c	χ_c	$N_{c.Rd}$
(mm)	(MN)			(MN)
600	372	0.37	0.919	46.813
1050	330	0.393	0.908	46.241
1500	327	0.395	0.907	46.195
2100	324	0.396	0.906	46.149
3000	267	0.437	0.886	45.119
4200	156	0.571	0.814	41.452
6300	92.5	0.742	0.713	36.295
7000	83.5	0.781	0.688	35.059
7700	77.1	0.813	0.668	34.044
8400	72.4	0.839	0.652	33.213

Table 4.6: Hybrid "stiff"

4.2.2 Pourostad's Interpolation Formula

Another approach that takes torsional stiffness into account is Pourostad's suggestion for an alternate interpolation formula that adjusts it when the method includes torsional stiffness (10). This method, however, is more conservative than the current approach taken by the Eurocode. As such, it is not of much use for our particular geometries, where the Eurocode is already excessively conservative (see chapter 5). This section was included to clarify why the method is not included in the comparison graphs.

4.3 Transverse Load

Load perpendicular to the stiffener direction

Relevant load cases can often occur in the bottom plate of a hollow bridge cross section as a result of traffic load or the self weight of the construction during the launching phase. The shearing force is carried by the diagonal webs and transferred to the bottom plate partially as compressive axial force. During the bridge's use, the self-weight and traffic load provide a tensile stress on the bottom plate due to rotational moment. As such, the case of biaxial compression occurs in the launching phase.

A common way to install a bridge is through "launching" over the bridge's intended span. This setup poses a unique challenge to the design process, as the self-weight load of the bridge causes a "hogging moment" where compressive stresses occur in the bottom plate. Stated another way: during the launching phase the bridge behaves as a cantilever until it reaches the supports.

We have here analyzed a plate of aspect ratio 1 (4200x4200 mm). We have also chosen to apply the transverse load on all three sections that are also mentioned in the longitudinal load part. These sections are called "small", "slender" and "stiff".

4.3.1 Numerical Analysis

When calculating the capacity for transverse compressive axial load, hand calculations must be performed by adapting the Eurocode method (either effective width or reduced stress method) for plate buckling for unstiffened plates. This is because there is no current recommended method for dimensioning a stiffened plate when the plate's stiffener direction is perpendicular to the compressive load, see chapter 6.

Meanwhile, numerical analysis can be utilized via FEM software like ABAQUS, which we have also used to determine capacity in the longitudinal direction.

In order to model the transverse behavior, we adjusted boundary conditions slightly because of the change in the load direction. These changes can be seen on the figures below. Otherwise, we first performed a linear buckling analysis to determine the critical buckling load and shape,

and then included the critical mode as an imperfection when running the capacity analysis, with maximum deflection 1 mm. We also performed a capacity analysis on the perfect geometry first, in order to ensure that our choice of boundary conditions was appropriate.

Figure 4.6: Load perpendicular to the stiffener direction

Figure 4.7: Section A-A from the figure 4.6
  Section B-B
Figure 4.8: Section B-B from the figure 4.6
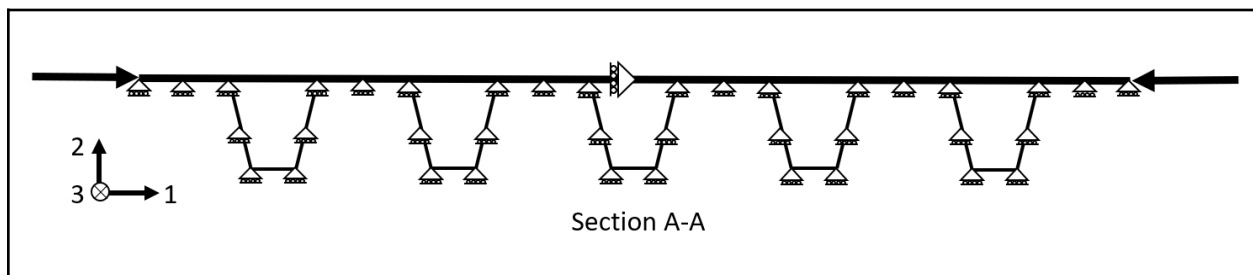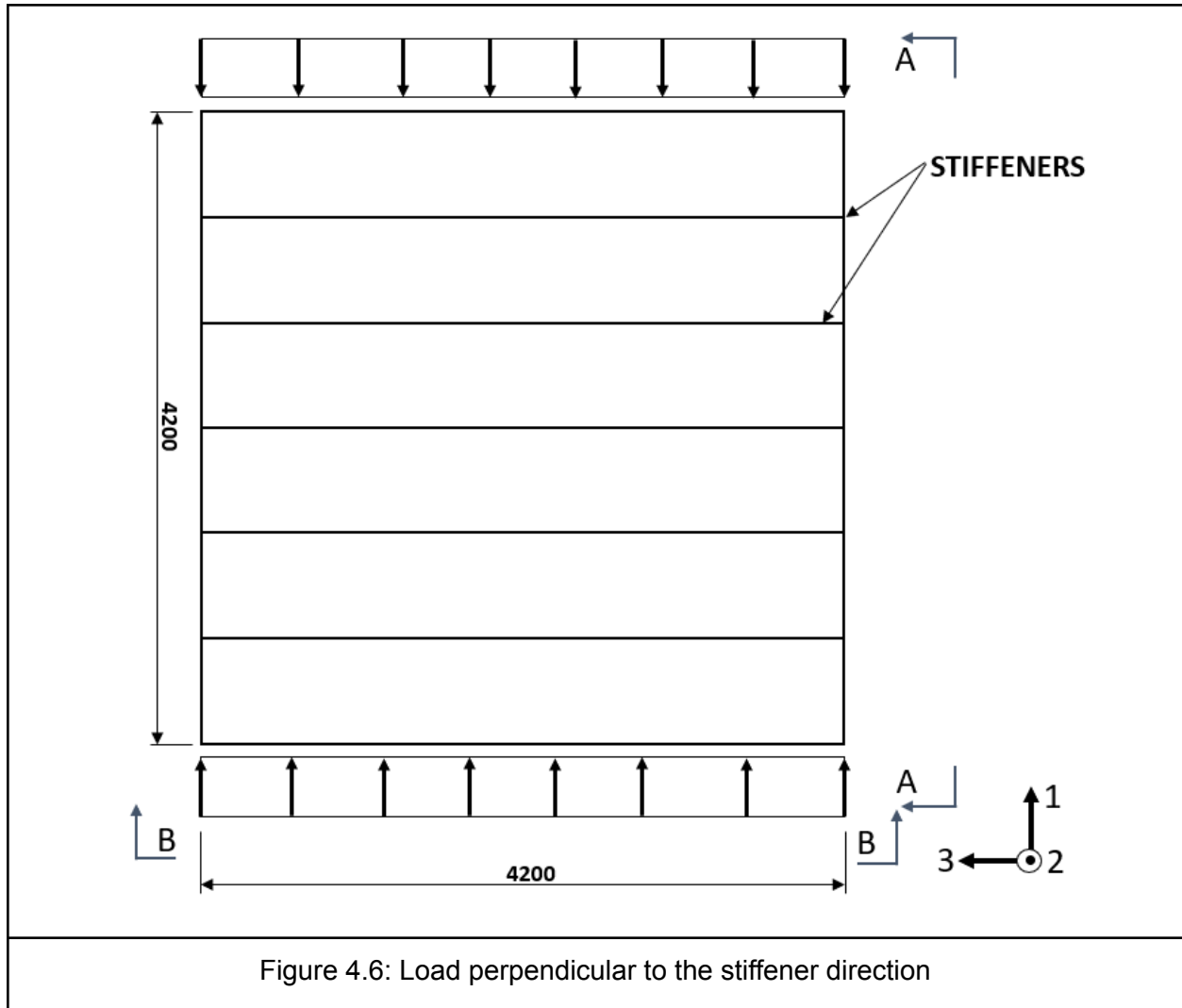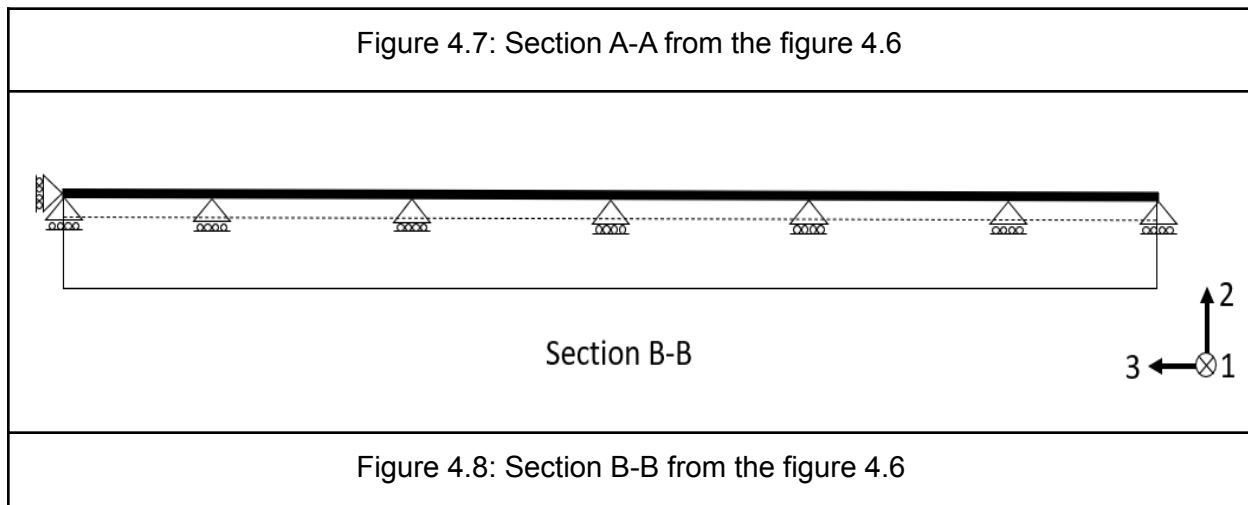
Figure 4.6 shows how the transverse load was applied to the plate. The load was as shown in the figure, applied as a distributed load along the edge on both sides of the plate. The 1-, 2- and 3-direction on the figures reflect the x-,y- and z-direction, respectively. The directions are the same as the ones used in ABAQUS. 1-direction is along the width of the plate, 2-direction along the length of the plate and 3-direction along the height of the plate.

Figures 4.7 and 4.8 show two different sections from the plate which are closely examined with respect to the boundary conditions of the plate. Section A-A shows that displacement is prevented in the 1-direction (x-direction) by restraining the node in the center of the plate's edge. The plate and the stiffeners are also restrained along the edge against displacement in the 2 direction (y direction).

Section B-B which is shown in the figure 4.8 above shows the loaded edge and its boundary conditions. It is worth mentioning that the boundary conditions of the opposite edge of the plate are the exact same as the one shown in the figure. On this edge the plate is restrained along the edge against displacement in the 2-direction. There is also one node in the corner of the plate which can be seen on the left side of the figure 4.8, that is restraining the plate against displacement in the 3-direction (z-direction).

4.3.2 Capacity

When running the capacity analysis with perfect geometry, we noticed that there was a slight downward deflection of the plate members between the edge and first stiffener on both sides.

The buckling shape from the LBA, however, showed an upward deflection of these same sections. For this reason we included an imperfection with scale factor -1 in addition to 1, in order to find the lowest strength, presumed to be the design strength.
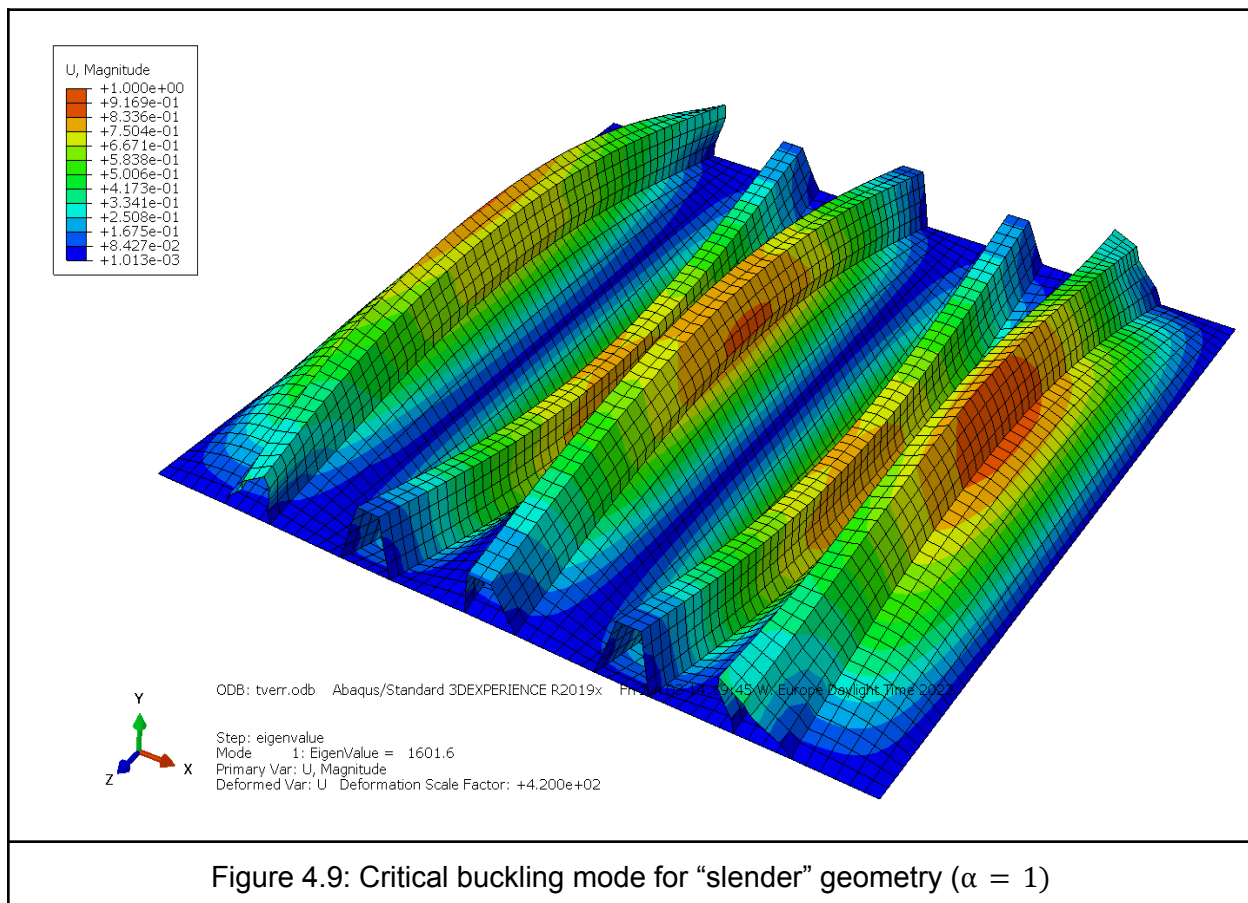
Figure 4.9: Critical buckling mode for "slender" geometry ($\alpha = 1$)

Figure 4.10: Critical buckling mode for "slender" geometry ($\alpha = 1$)
Side view
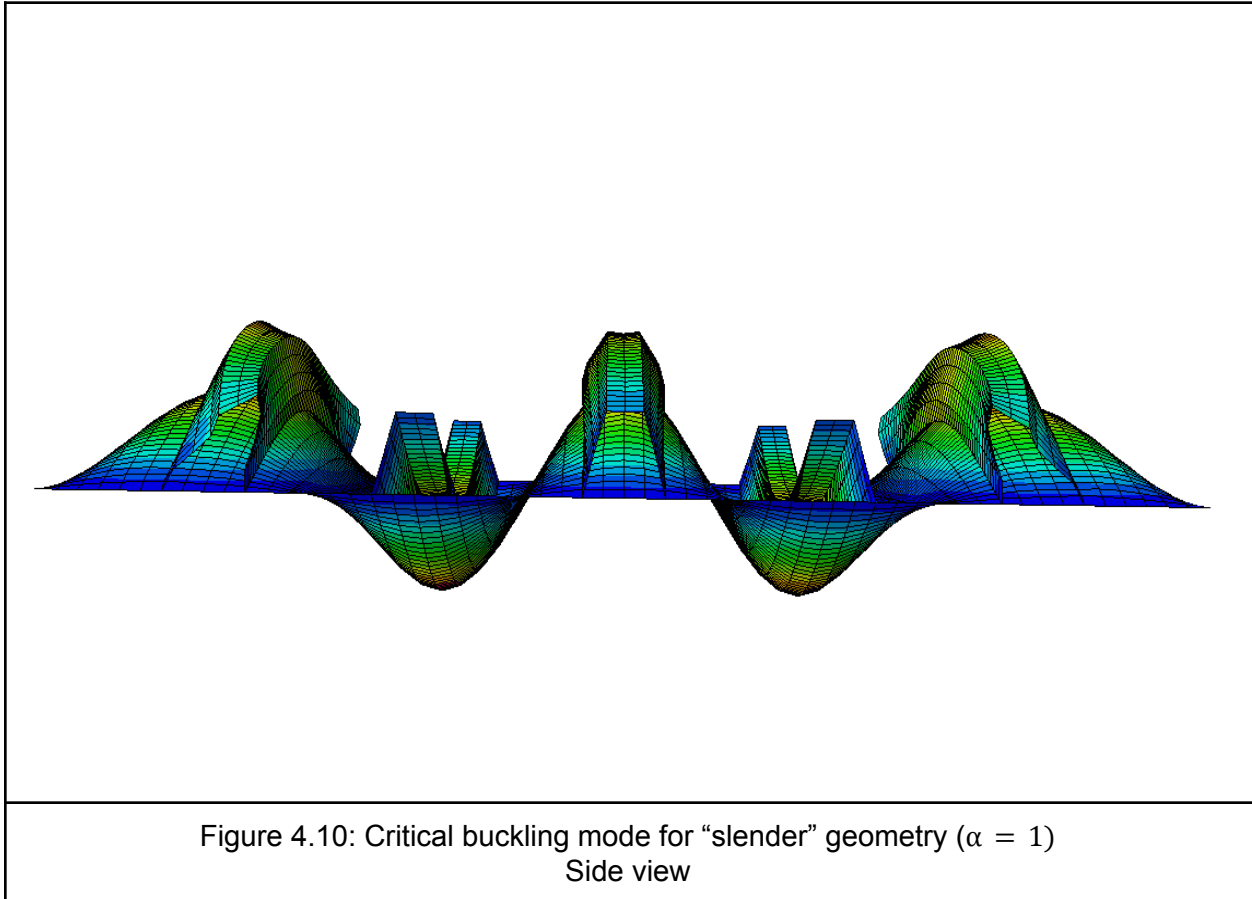
Below is the shape of the perfect geometry in deformed condition at section yield (note that the deformations are scaled larger for visibility purposes.)
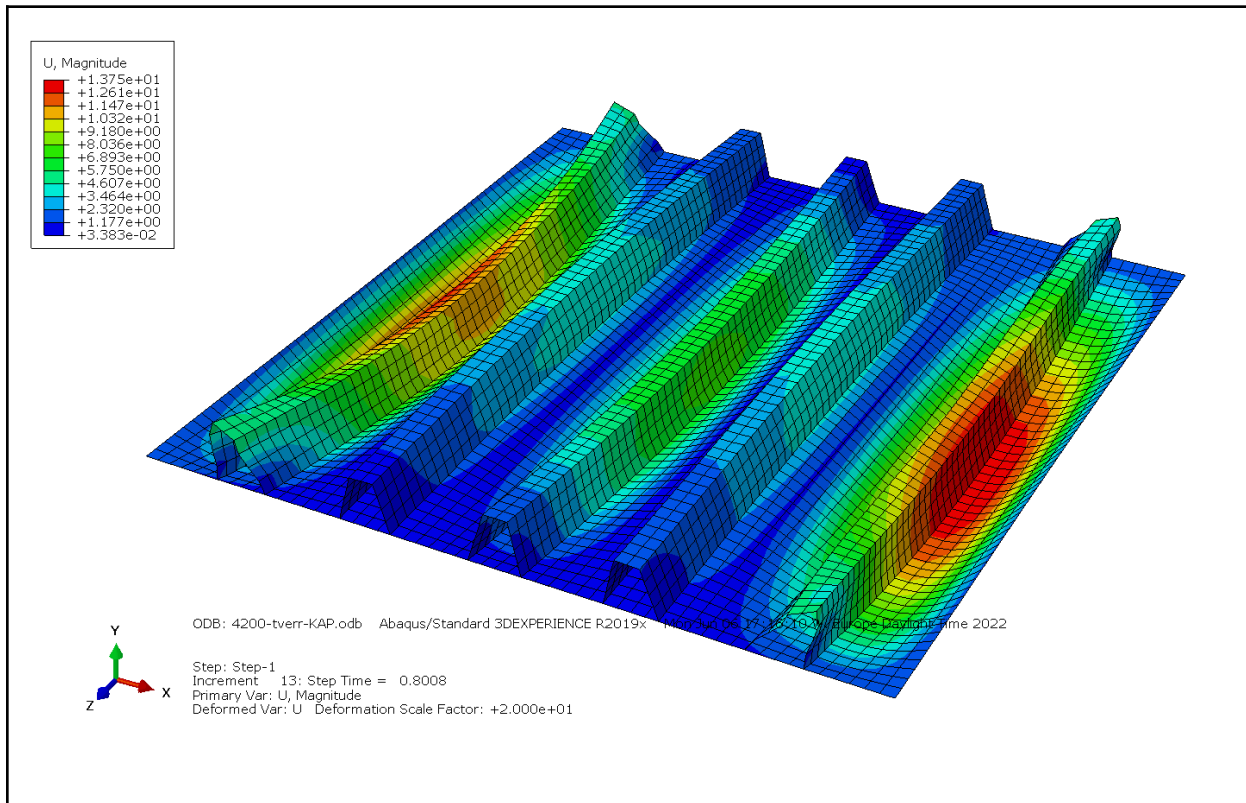
Figure 4.11: Failure mode for "slender" geometry ($\alpha = 1$). Imperfection factor 0
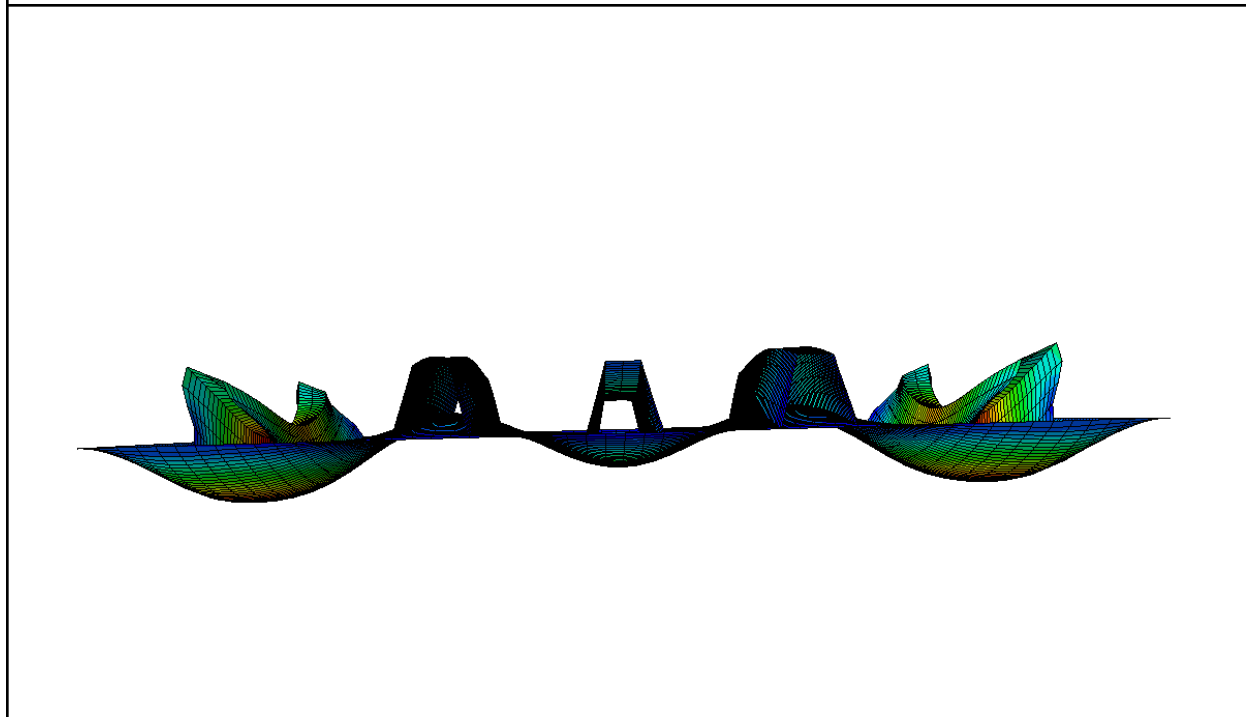
Figure 4.12: Failure mode for "slender" geometry ($\alpha = 1$). Imperfection factor 0. Side view

It is clear that the deformation of the perfect geometry is analogous to the eigenvalue shape (note also that Abaqus's linear analysis stopped at the same load as the critical buckling load. The buckling load gives a stiffness matrix with determinant zero and therefore will not provide a convergent result.) As a result of this, it is logical to include an imperfection that is a negatively scaled form of the buckling mode. We therefore include two capacities in our results.

Imperfection scale factor	Capacity[MN]
1	6.68
-1	6.325
Table 4.7: Capacities including imperfections	

The capacity with the negatively scaled buckling mode is slightly smaller, with a difference of about 5.6%. The most unfavorable imperfection shape is generally preferable, since the shape of any real imperfections are unpredictable, so it is better to take the conservative estimate despite the LBA suggesting an upward deflection of the side panels during buckling.

5. Abaqus analysis

5.1 Model Description

5.1.1 Imperfections

When performing a static linear-geometry capacity analysis, Abaqus operates with the assumption of perfect geometry. In practice, this is never the case. Material safety factors are intended to compensate for non-uniformities in the building material (in this case steel) but do not address the issue of buckling. For this reason we have included an imperfection in the model geometry by first running a buckling analysis and including the lowest mode as a scaled imperfection in the geometry when running a static capacity analysis. The lowest mode would give an imperfection that is presumably the weakest possible construction of the plate with regards to buckling, and therefore should give reasonable results in the capacity analysis.

EC 1993-1-5 states that a plate can be considered planar so long as the curvature radius satisfies the following condition (2).

$$r \geq \frac{a^2}{t} \qquad (5.1)$$

where *r* is the radius of curvature, *a* is the width of the plate (here interpreted as longest in-plane dimension), and *t* is the plate's thickness.

If we assume the largest displacement occurs in the middle of the plate, we can use the pythagorean theorem and algebra to determine a maximum central displacement for a plate to still be considered planar.

$$\delta := r - \sqrt{r^2 - \left(\frac{a}{2}\right)^2} \qquad (5.2)$$

For all the chosen plate lengths, this equation produced a displacement of just over 3 mm (for t=24) or 1.5 (for t=12). As a result, for all geometries where the critical buckling mode was global, we used an imperfection factor of 3 and 1.5 respectively for a maximum central out-of-plane displacement of 3 mm or 1.5 mm. For geometries where the critical buckling mode was a local buckling mode, we used a scale factor of 0.5. For transverse applied load, failure with perfect geometry produced a displacement field resembling the first buckling mode, but in the opposite direction. We have therefore applied a scale factor of both 1 and -1 to identify the weakest imperfect geometry.

In 1993-1-1, chapter 5.1 discusses imperfections. For columns an imperfection eccentricity is placed at the vertical center of the column, and can range from 1/150 times the length to 1/350 times the length, depending on the buckling curve.Our shape factor was 0.452, which is closest to buckling curve c, with a shape factor of 0.49. This means that if we included the imperfection suggested for columns, the imperfection should be 1/200th of the length, or 42mm for the longest length. This is 14 times larger than the imperfection we have chosen. If the manufacturer of a plated structure is following the Eurocode, this is far too large an imperfection to be allowed in the context of plated structures, and we have therefore chosen to use imperfection size 3 mm.

For a few of the geometries (3 out of 30), introduction of imperfection in this manner provided a capacity higher than that of the perfect geometry. Since this only occurred in very short plates with local buckling modes where the reduced and nonreduced axial capacities were very close, we deemed the capacity of the perfect geometry adequate. This will be further discussed later in the chapter.

5.1.2 Geometries

Our chosen geometries consist of combinations of ten plate lengths and three cross sections.

"Slender" cross section

The "Slender" cross-section comes from the example retrieved from the commentary and included in chapter 3, see figure 3.6. As a compressive class 4 cross section with very slender stiffeners, six of our ten chosen lengths resulted in local buckling being critical. This made us

curious about the behavior of similar cross sections that were less slender, leading to our two other cross-section choices.

"Stiff" cross section

The "Stiff" cross section has the same dimensions as the "Slender" section apart from plate and stiffener thicknesses, which were both doubled to 24 and 12 mm, respectively. The cross-sectional area is twice that of the "Slender" section, see figure 3.6. The "Stiff" section is of compressive class 1.

"Small" cross section

As shown in figure 3.6, the "Small" cross section is a modification of the "Slender" cross section in which the stiffener's angular height was halved in order to reduce the second moment of area about the transverse axis. The cross-sectional area is about 14,8 percent lower than that of the "Slender" section. The "Small" section is of compressive class 4.

We chose 10 lengths ranging from 600 mm to 8400mm (aspect ratio range of 0.143 to 2) in order to get an idea of how axial capacity changes along with aspect ratio.

5.2.2 Boundary Conditions

The Abaqus axes corresponded to the plate axes thus:

●   The X axis was the transverse axis

●   The Y axis was the orthogonal or out-of-plane axis

●   The Z axis was the longitudinal axis.

The following figures demonstrate the boundary conditions.
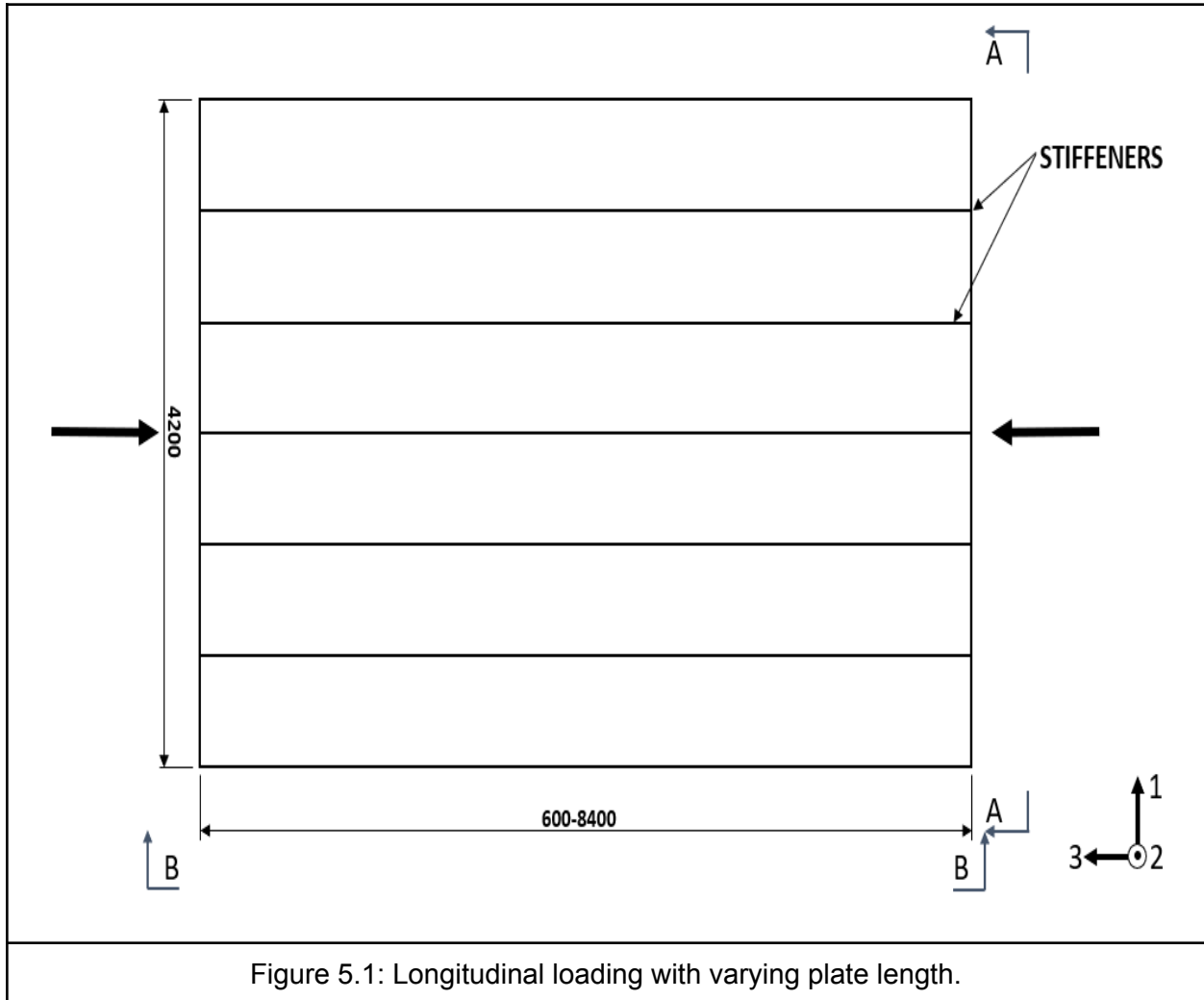
Figure 5.1: Longitudinal loading with varying plate length.
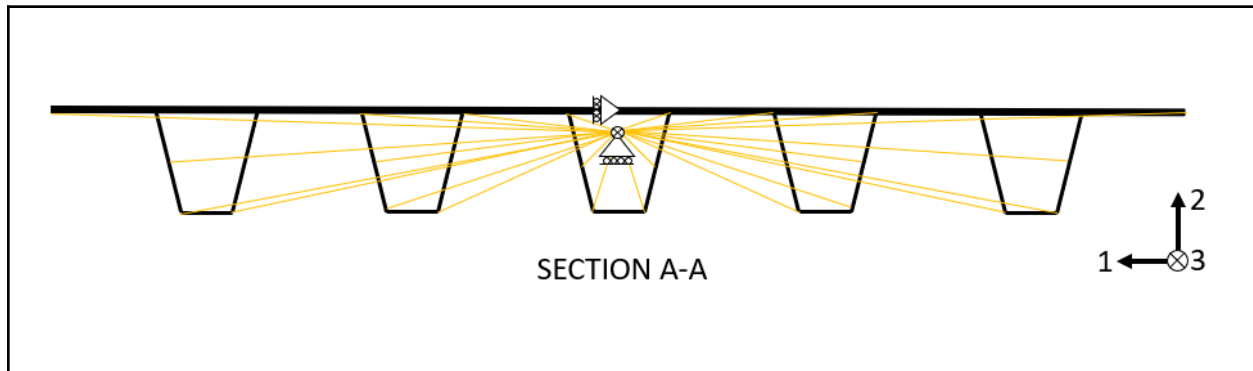
Figure 5.2: Section A-A, boundary conditions and constraints
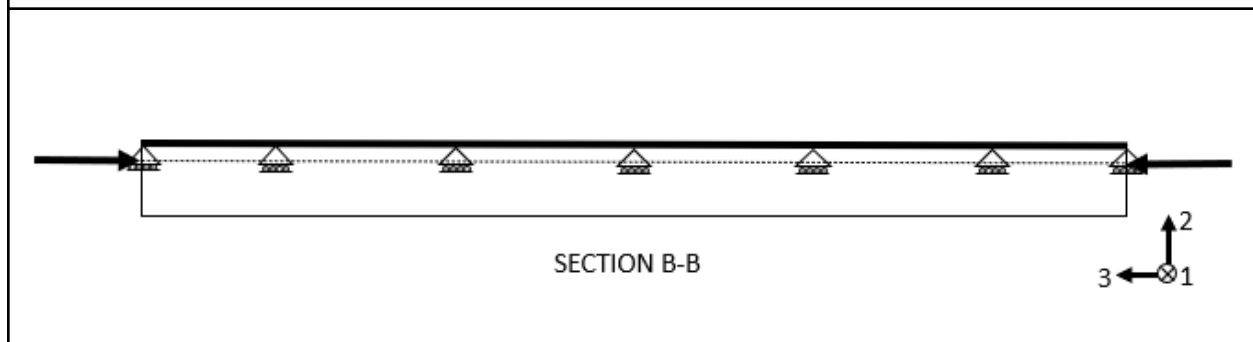
Figure 5.3: Section B-B, boundary conditions and constraints

In order to distribute longitudinal load throughout the section without including an unintentional rotational moment about the transverse axis, we placed a reference point in the center of area, see figure 5.2, and then constrained the section edge to the reference point using kinematic coupling (see section 5.2.3). Note that the center of area is the center of area for the entirety of the plate section. In reality, the three central stiffeners could be loaded about their own center of area (including the corresponding plate sections) which is slightly higher, while the two edge stiffeners have a center of area slightly lower than our reference point.

Our options were to choose the column center of area, the edge column center of area, or the global center of area. Though the global center of area introduces slight inaccuracies to both central and edge columns, we deemed it the best of the three options, and the differences are small enough to not interfere with our results to a significant extent.

5.2.3 Kinematic Coupling Constraints

Applying load is more complicated in sections with longitudinal stiffeners, as the load needs to be applied at the center of area so as to not cause an unintentional rotational moment. This was achieved by adding a reference point in the Assembly module, placing it in the center of area for the section, and using kinematic coupling constraints to control the displacement behavior of the section.

The constraints did not include the corner nodes of the plate. When performing a triaxially loaded capacity analysis, including the corners causes distortion in the displacement field, and we chose to use the same constraints for consistency's sake.

Boundary conditions were applied to the reference point, creating a pinned reference point at one end of the plate and a sliding reference point at the other. The constraints allow for the section to rotate about the transverse axis.

5.3 Analysis

5.3.1 Longitudinal and Transverse Elastic Buckling

As previously mentioned, we performed a linear buckling analysis by including a linear perturbation step of type buckling.

Before running the analysis, we added a reference load of 1 Newton to the sliding reference point. Our results provided a set of eigenvalues for 3 buckling modes, the eigenvalue being a multiplier to the reference load. This means that an eigenvalue result of 8E7 indicates an elastic buckling load of 80 MN.

The first eigenvalue produced by Abaqus for each geometry is the lowest mode, and is therefore the critical elastic buckling load. This can be either a global or a local buckling mode, whereas the Eurocode determines the elastic buckling load specifically for global buckling (see buckling curves in figures 5.4-5.6). One consequence of this is that it is meaningless to compare critical buckling loads retrieved from Abaqus to critical buckling loads calculated using the Eurocode specifically in cases where local buckling modes are critical.

For the "small" section, this was the three lengths with an aspect ratio less than 0.5. Meanwhile, the "stiff" section had global buckling modes for all plates of 3000 mm (aspect ratio 0.714) and up. The "slender" sections buckled locally up to and including the plate of length 4200 mm (aspect ratio 1). This is likely because of a combination of large stiffeners and slender plate members; the large stiffeners provide high resistance to global buckling while the thin plates make the section more susceptible to local buckling. Both of these characteristics contributed to higher likelihood of local buckling.

Low aspect ratios, in particular, tend to be susceptible to local buckling because of the low level of column slenderness. This effect begins to wane around aspect ratios of 1.

Length (mm)	N_{cr} (MN)	Length (mm)	N_{cr} (MN)	Length (mm)	N_{cr} (MN)
600	45.9	600	47.8	600	372
1050	44.1	1050	42.3	1050	330
1500	43.4	1500	42.0	1500	327
2100	37.4	2100	41.6	2100	324
3000	20.5	3000	41.1	3000	267
4200	12.4	4200	40.7	4200	156
6300	8.31	6300	36.8	6300	92.5
7000	7.81	7000	31.9	7000	83.5
7700	7.50	7700	28.4	7700	77.1
8400	7.29	8400	26.0	8400	72.4

Table 5.1: left to right small, slender, stiff. Critical buckling load per Abaqus

Figure 5.4: Buckling curve for "small" geometry

Figure 5.5: Buckling curve for "slender" geometry
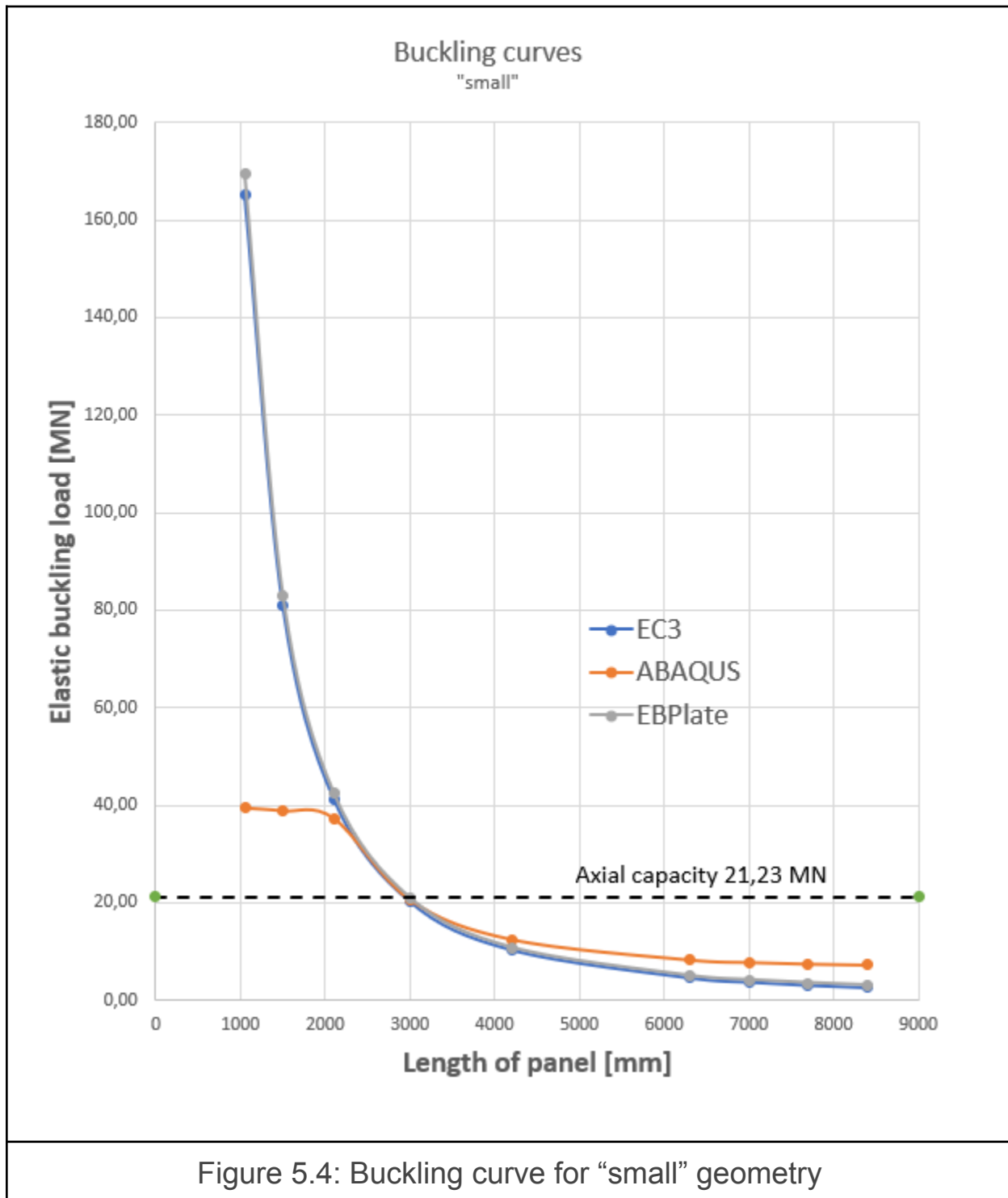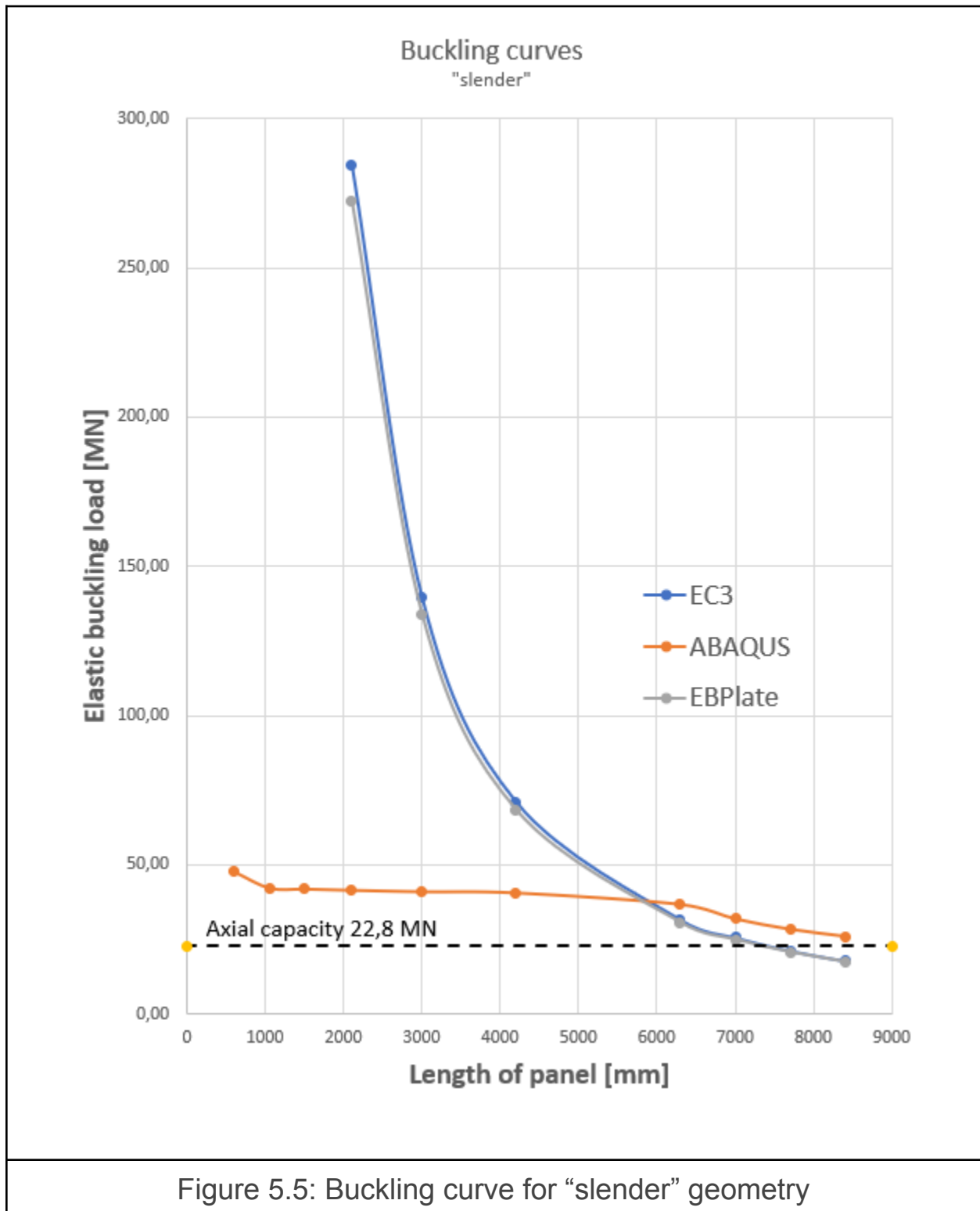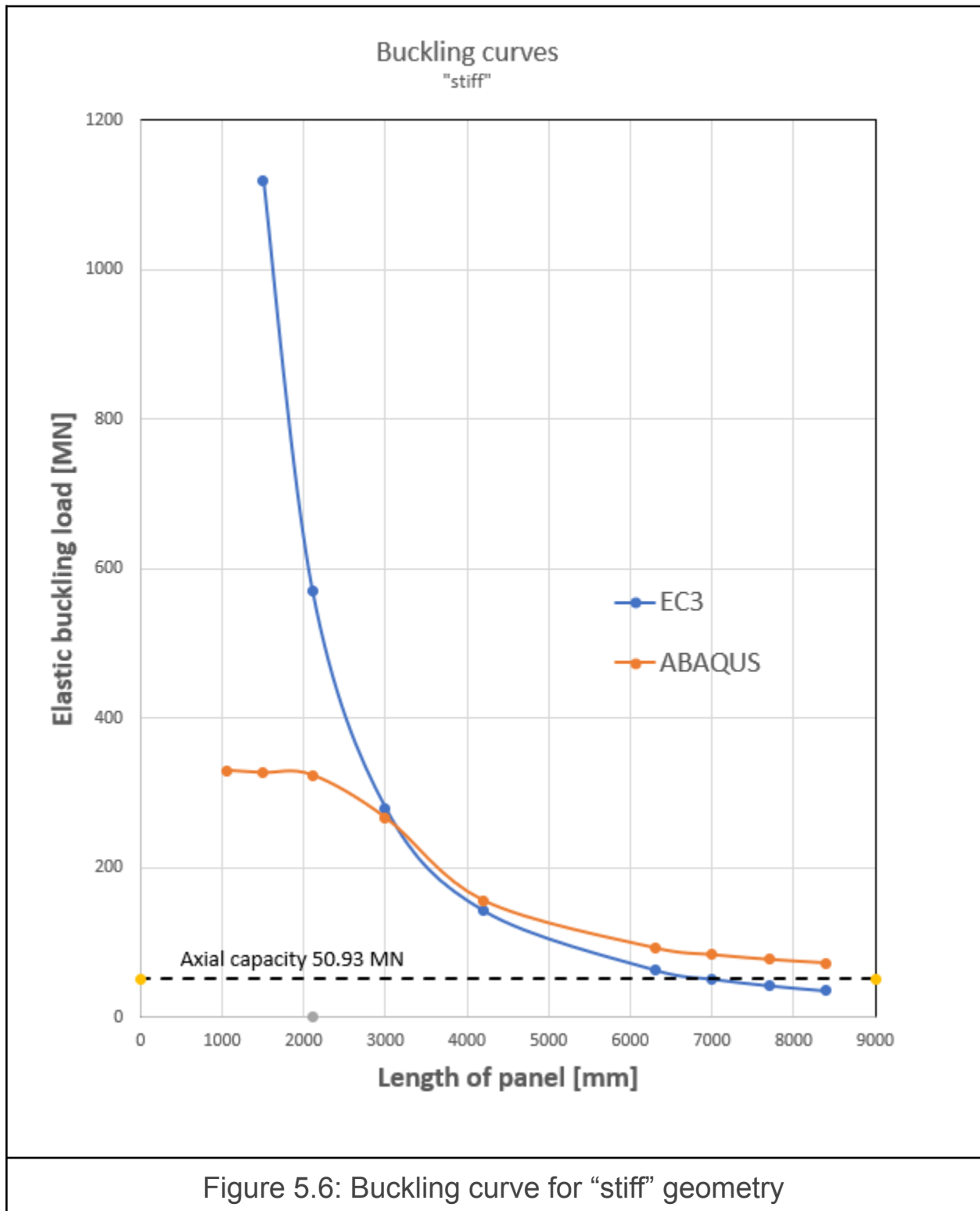
Figure 5.6: Buckling curve for "stiff" geometry

We can clearly see the region on the left where Abaqus begins to identify local buckling modes as critical while the Eurocode and values retrieved from EB plate diverge.

The point where the EC3 curve crosses the curve is the point at which torsional resistance begins to play a larger role. It makes sense that this occurs for long plates since it is here the column buckling resistance begins to significantly decline.

For stiff geometry, the EB plate curve is not included because it provided values that were so large as to be irrelevant. The cause of this presumably has something to do with the cross-sectional class and stiffener size, as the EB plate curves and the Eurocode curves are very close for the other two sections, which are both of class 4.

5.3.4 Capacity Analyses

The capacities of the various geometries are included here:

Length [mm]	Small [MN]	Slender [MN]	Stiff [MN]
600	22.212	25.4925	51.1555
1050	21.99	25.4815	50.996
1500	21.978	25.432	50.9575
2100	20.823	24.992	50.6935
3000	17.922	24.6125	49.115
4200	12.546	24.662	49.049
6300	9.387	23.925	49.06
7000	9.126	23.694	49.093
7700	9.012	23.3475	49.137
8400	8.982	22.8635	49.1975
Table 5.2: Axial longitudinal resistance capacities			

Note that for "Stiff," the capacities for the two shortest plates are higher than the total theoretical capacity for the section (50.928 MN). This section is class 1 and therefore includes no reduction to account for local buckling of members and must be the maximum capacity. The error is likely caused by the exclusion of the corner nodes by the kinematic coupling constraints used to apply axial load.

This error need not compromise the results, however, because it is very small (0.4%) even for maximum error.

Note that for all lengths of the "slender" section, capacity is higher than the axial capacity (disregarding buckling) determined by the Eurocode. This is interesting, as the areal reduction is

supposed to protect against the risk of local buckling, and in our case has produced conservative results. This is similarly true for the "small" plates with lengths of 1500 or shorter.

5.5 Comparison to Eurocode and Discussion

With regard to critical elastic buckling load it is, as previously mentioned, meaningless to compare Abaqus values to those of the Eurocode for geometries for which the critical buckling mode is a local one. This tends to occur in situations where the plate is particularly short or particularly vulnerable to local buckling because of slender geometry (class 4 sections).

Another large difference is, as noted by Pourostad (10), the Eurocode does not take torsional stiffness of stiffeners into account when calculating the critical elastic buckling load. For this reason, for long plates, Abaqus produces a critical elastic buckling load that is significantly higher than the value suggested by the Eurocode.

It should be noted that for the geometries we have chosen all have buckling curves that are partially (for "Small" geometries shorter than 4200 mm) or entirely ("Slender" and "Stiff") above the nonreduced axial capacity according to Abaqus. Additionally, even while neglecting torsional stiffness, the Eurocode produced buckling curves for the "slender" and "stiff" geometries that were largely above the non-reduced axial capacity. This doesn't mean that the sections are immune to buckling, but rather that they are not particularly vulnerable. Combined with the Eurocode's neglect of torsional stiffness and the size of the error in capacities, this suggests that the Eurocode produces overly conservative results when slenderness values are low and the section has closed stiffeners. This is interesting to note, especially in the case of "slender" geometry, a class 4 section with stiffeners that are prone to local buckling.

Additionally, in the case of column-buckling, the Eurocode suggests including a much larger imperfection than what we have used in order to calculate the resistance to buckling. This implies that with such small scale factors for the imperfections, it may be useful to test them in the opposite direction as well to confirm that it is indeed buckling and not failure due to other imperfections that are decisive.
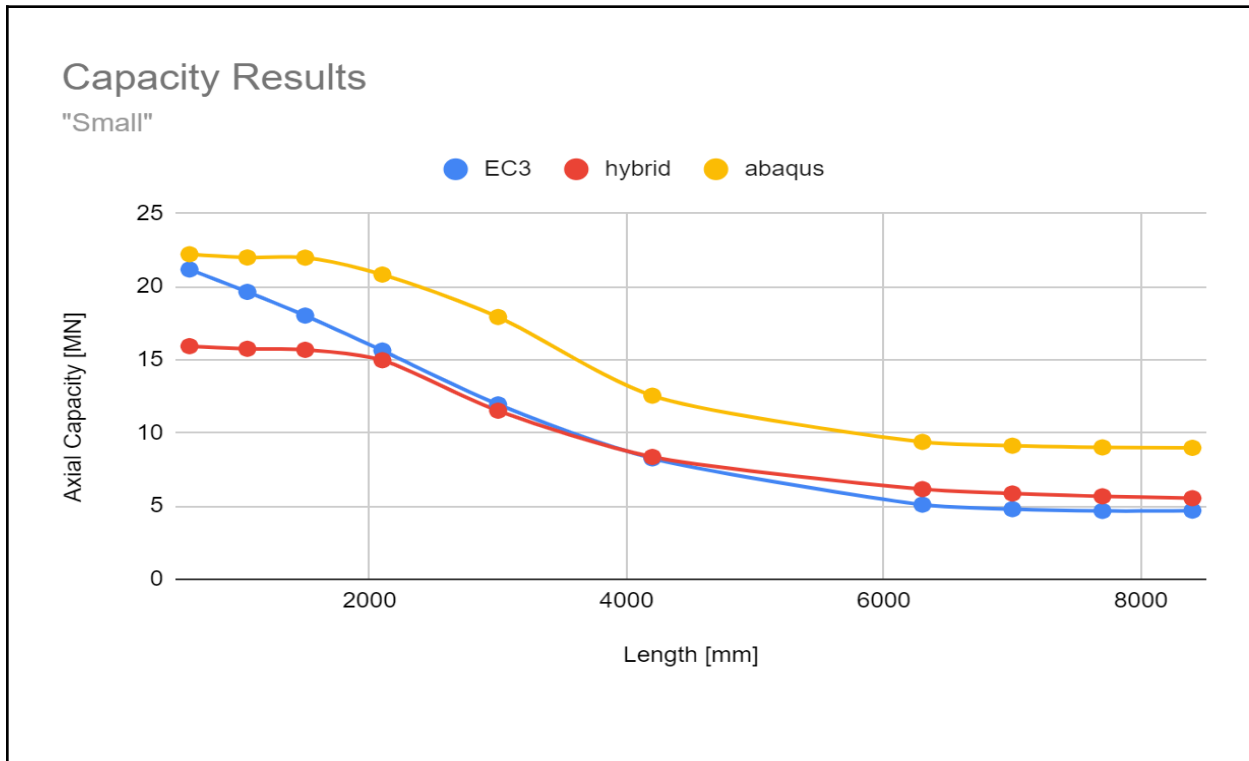
Figure 5.7: Axial capacity for "small" geometry, buckling included
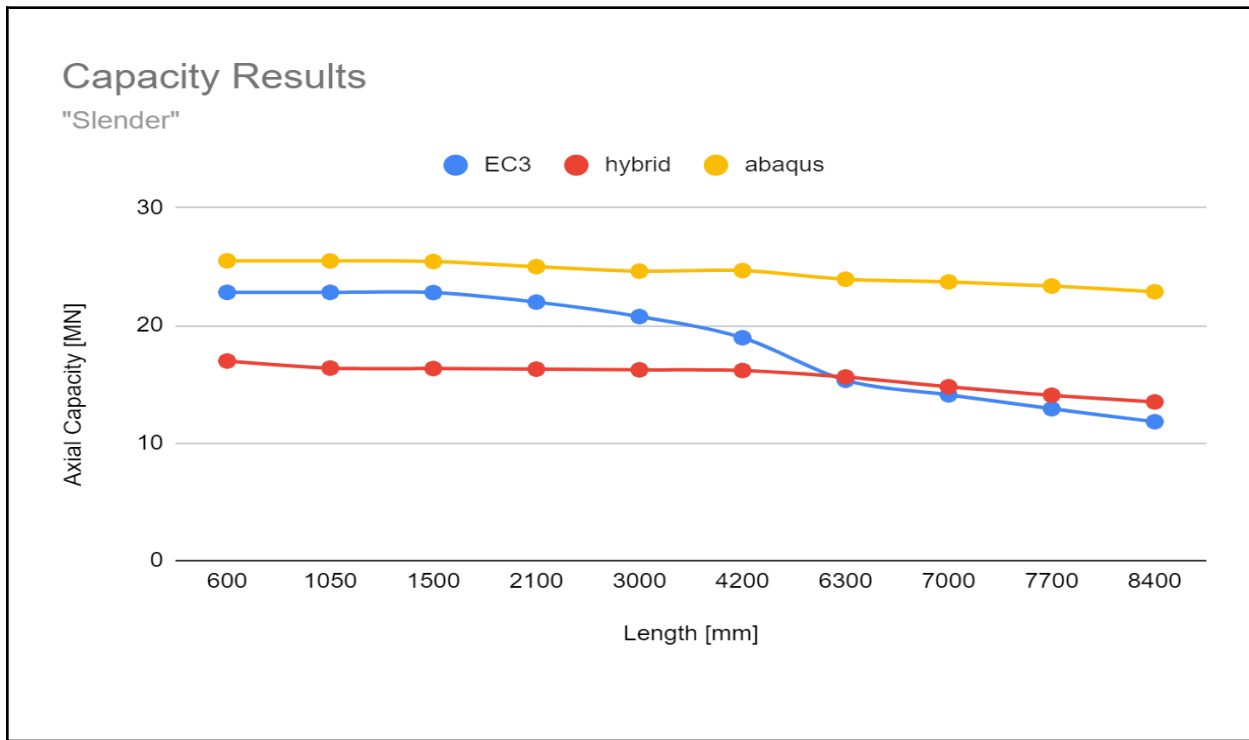
Figure 5.8: Axial capacity for "slender" geometry, buckling included

Figure 5.9: Axial capacity for "stiff" geometry, buckling included
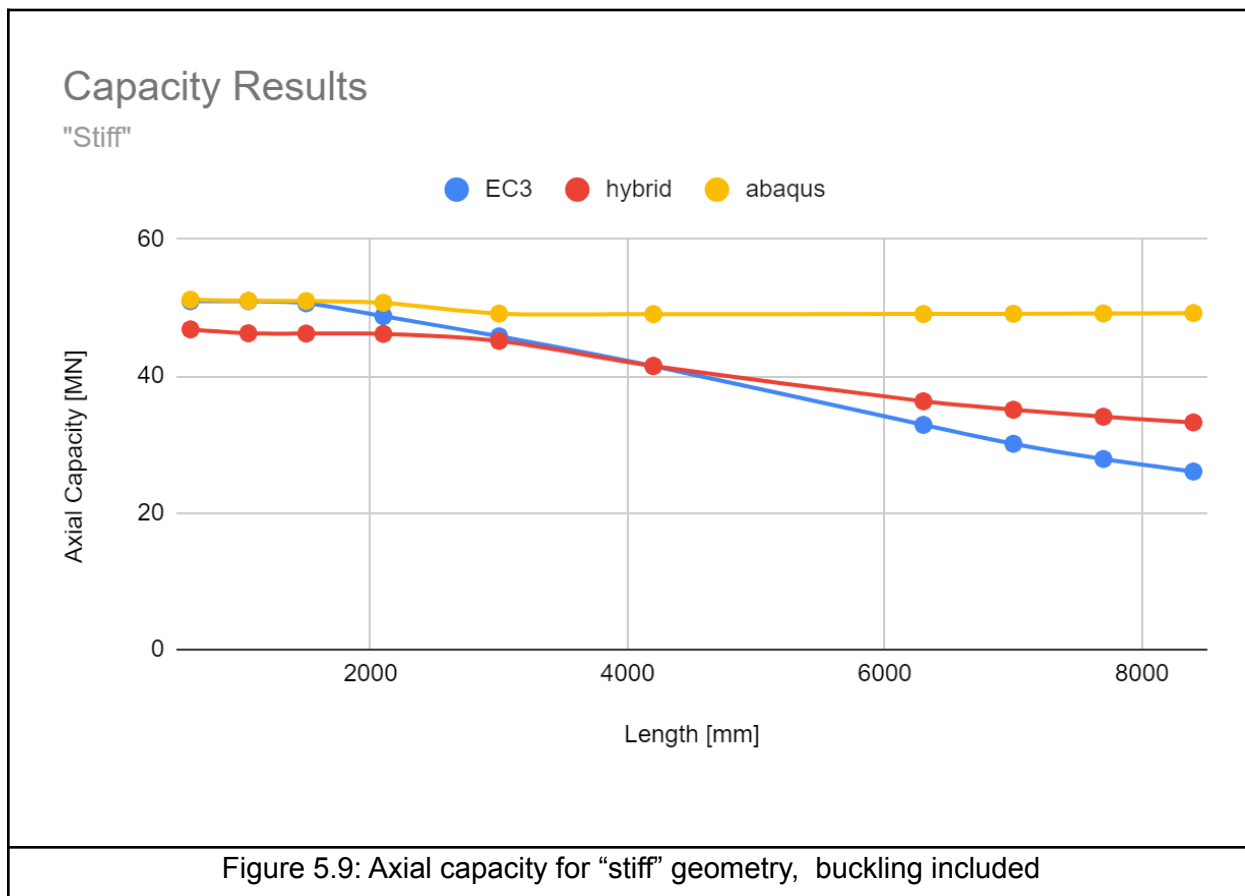
Both EC3 and hybrid methods are conservative, but for long plates the Eurocode deviates further from the capacity determined in FEM analysis than the hybrid method. For both "small" and "stiff" geometries, the hybrid method and EC3 curves cross around aspect ratio 1, or length 4200. This is not the case for "slender" geometry, but the relevant "slender" plate is vulnerable to local rather than global buckling, and this has the function of reducing the capacity in the hybrid method to a value lower than that of the Eurocode. The next plate length (aspect ratio 1.5) does see this cross.

This suggests that the hybrid method is preferable to the Eurocode for plates with aspect ratios above 1, provided they have low slenderness for global buckling; however, the hybrid method is still conservative, and underestimates capacity by around 30%, suggesting that it is inadequate. It is also worse than the Eurocode in situations where local buckling is critical, rather than global buckling.

6. Hand Calculations of Transverse Capacity

Capacity for axial loads in the transverse direction was determined by the effective width method according to EC3. Here there is only plate-like behavior, as there are no longitudinal stiffeners to add to the capacity.

Because of the five stiffeners, and the LBA results, it is reasonable to conclude that the lowest relevant buckling mode will have 5 half-sine waves perpendicular to the stiffener direction, see figure 6.1. This is a necessary adaptation to the Eurocode method, as it is unreasonable to assume it would behave exactly as an unstiffened plate would.

Figure 6.1: Critical buckling mode for "slender" geometry
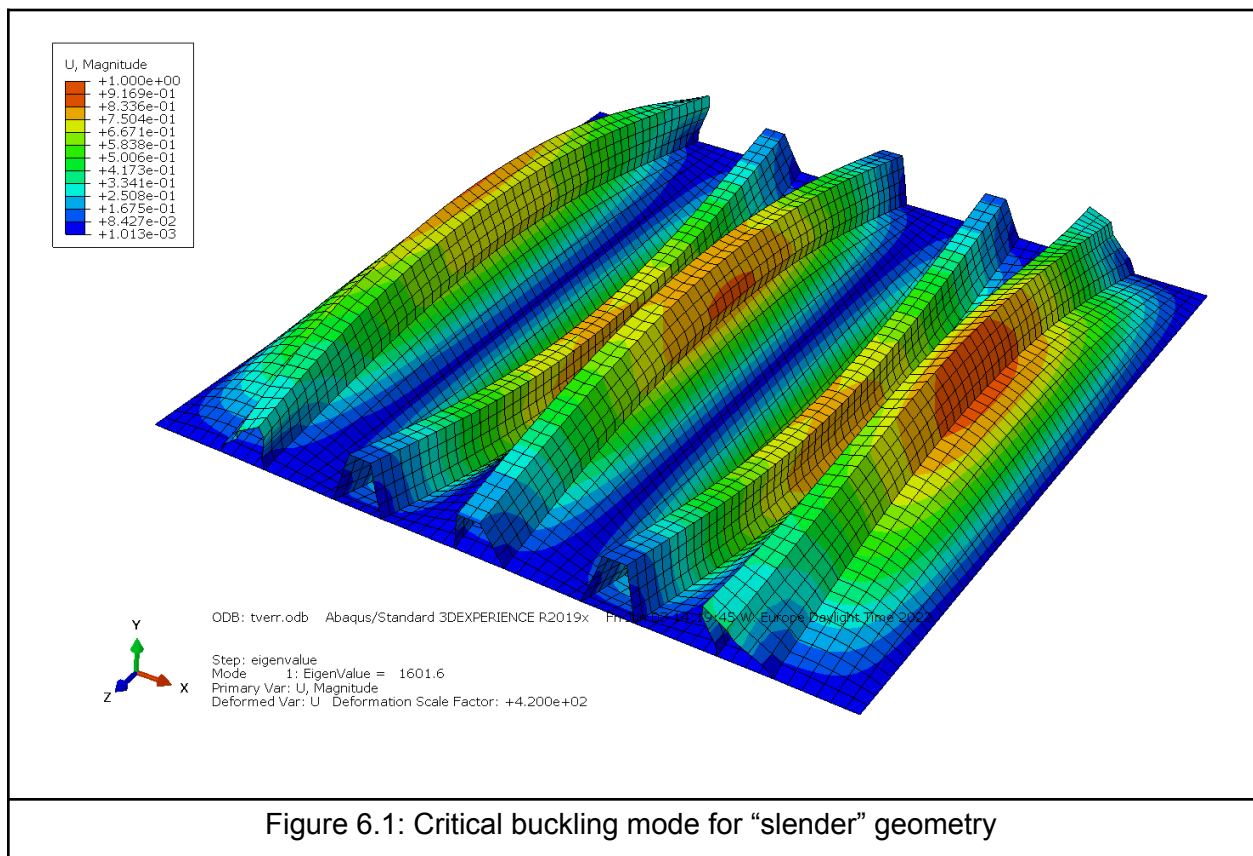
 Otherwise, we treated the plate as unstiffened. In reality, the longitudinal stiffeners aid in providing some stiffness, but the Eurocode says nothing about the buckling behavior of a plate when uniaxially loaded perpendicular to the stiffener direction.

This example is for the "Slender" section with an aspect ratio of 1. This method is retrieved from source (4)

We begin by calculating the buckling factor k_σ

$$k_\sigma := \left(m \cdot \frac{b}{a} + \frac{n^2}{m} \cdot \frac{a}{b} \right)^2 \tag{6.1}$$

Here a is the length of the plate, b is the width, m is the number of half-sine waves in the relevant buckling shape in the longitudinal direction, and n is the number of half-sine waves in the transverse direction. Notice that since the plate is being loaded perpendicular to the stiffeners, what we have earlier referred to as the longitudinal and transverse axes have now switched places.

$$k_\sigma := \left(m \cdot \frac{b}{a} + \frac{n^2}{m} \cdot \frac{a}{b} \right)^2 = 27.04 \tag{6.2}$$

$$\lambda_{p.tr} := \frac{\dfrac{b}{t}}{28.4 \cdot 0.814 \cdot \sqrt{k_\sigma}} = 2.912 \tag{6.3}$$

$$\rho := \frac{\lambda_{p.tr} - 0.22}{\lambda_{p.tr}^2} = 0.318 \tag{6.4}$$

$$N_{a.Rd.tr} := b \cdot t \cdot f_y \cdot \rho = 5.681 \ \mathit{MN} \tag{6.5}$$

The FEM analysis determined the value to be 6.325 MN, meaning the Eurocode has about 10% error. This is interesting considering that the error was much larger for axial load in the longitudinal direction (parallel to stiffeners).

The lowest buckling mode for "stiff" geometry had an asymmetrical form, with 4 half-sine waves.

Figure 6.2: Critical buckling mode for "stiff" geometry

Figure 6.3: Critical buckling mode for "stiff" geometry, side view

Though the half-sine waves are not of uniform size, we performed calculations with an m-value of 4 in addition to the m-value of 5, in order to compare.
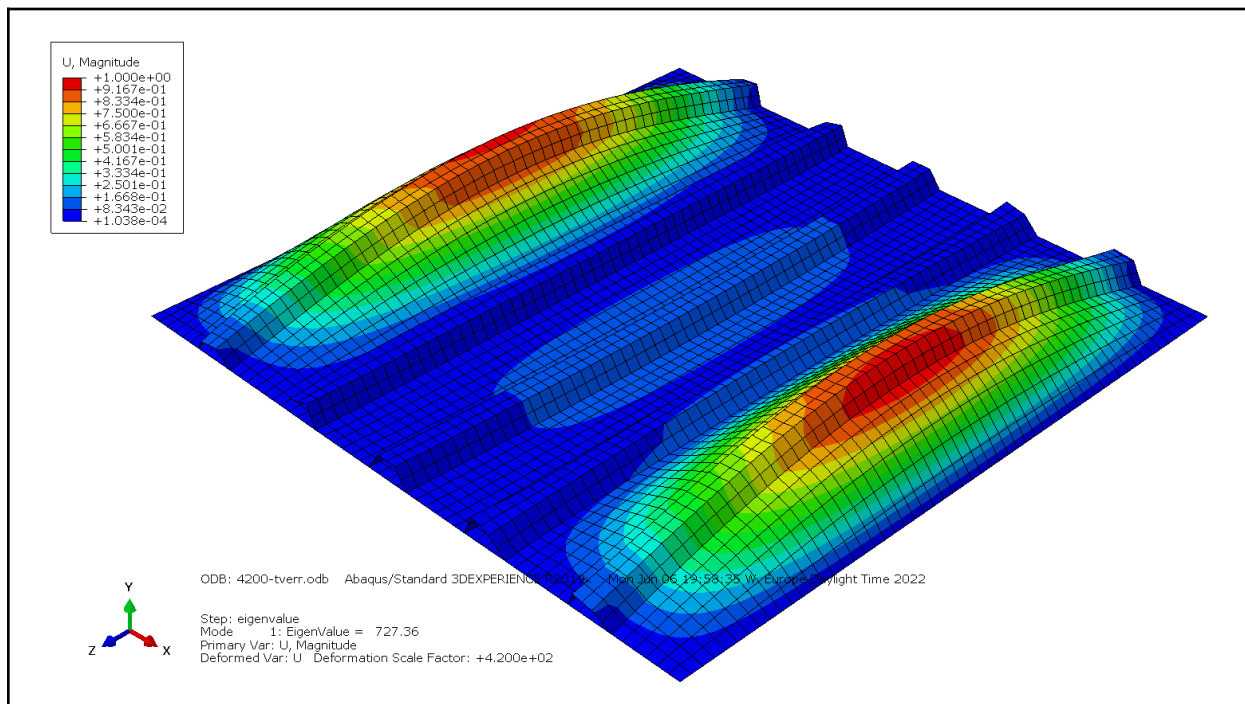
Figure 6.4: Critical buckling mode for "small" geometry
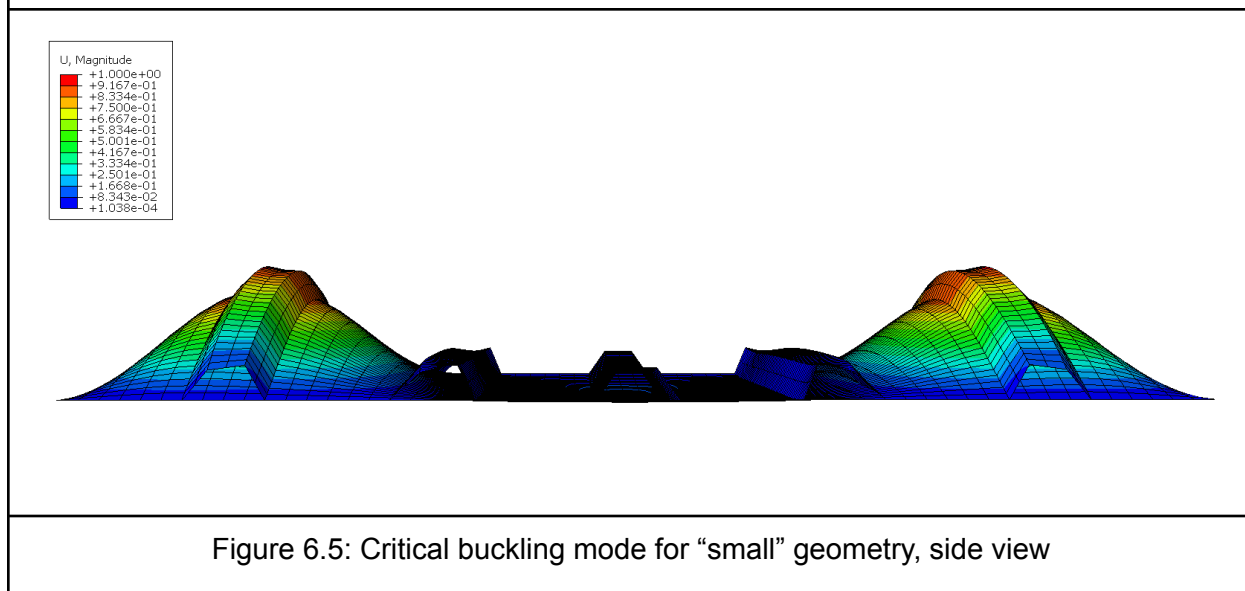
Figure 6.5: Critical buckling mode for "small" geometry, side view

For small geometry, we chose an m-value of 3.This seemed most appropriate as the middle three stiffeners did not appear to aid much against buckling.

Geometry	Capacity according to hand calculations [MN]	Capacity according to FEM analysis [MN]	Deviation [% of FEM capacity]
Stiff (m=4)	17.61	22.62	22.1% (safe)
Stiff (m=5)	20.86	22.62	7.8% (safe)
Small (m=3)	3.75	2.992	25.3% (unsafe)
Table 6.1: Capacity comparison of Eurocode and Abaqus			

It is interesting to note that for "stiff" geometry, the m-value of 4 gave a conservative value for the capacity. Even with an m-value of 5, the capacity is still on the safe side. Keep in mind that the imperfection that gave the lowest capacity was a scaled mode 1, which is closer to the shape of plate buckling with m-value 4.

For small geometry however, this method was unsafe, producing a value 25% larger than the true capacity. It is clear, then, that the current methods for plate buckling should not be applied to stiffened plates in this way, and an alternative should be developed.

The method does work for sections with large stiffeners due to higher bending resistance, but if the point is to be able to use this method without first confirming or checking against more exact methods of design, this adapted method is still insufficient.

7. Out-of-plane Loads

Figure 7.1: Loading model for out-of-plate loading
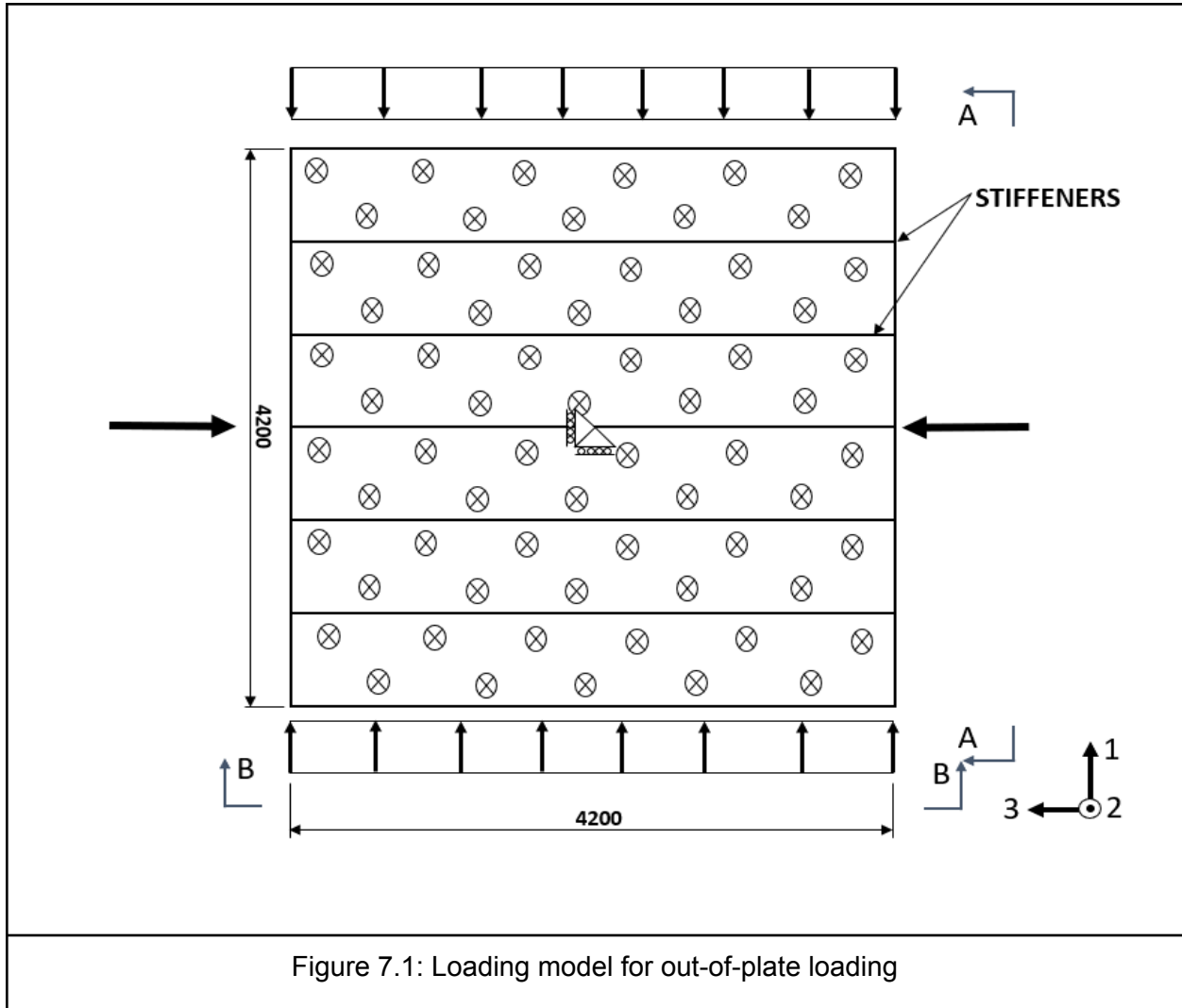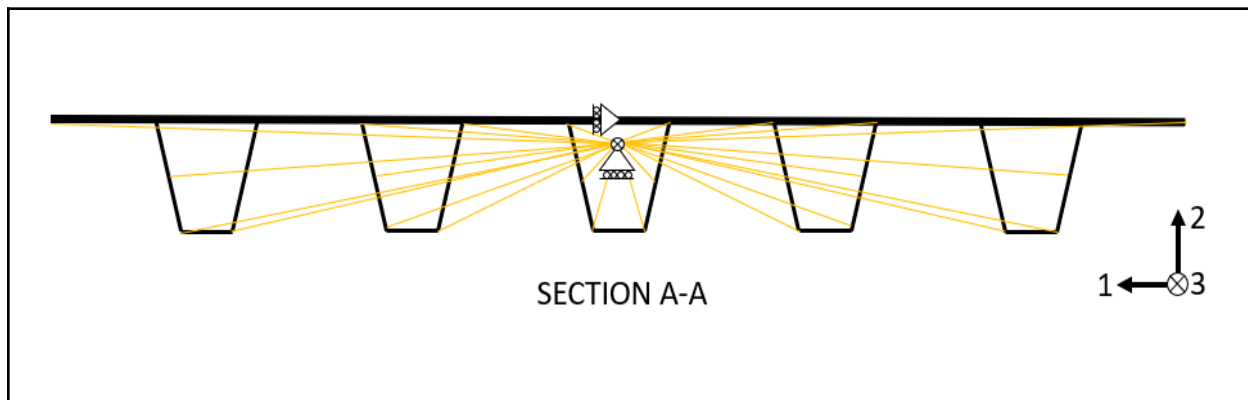
Figure 7.2: Cross section A-A with constraints and boundary conditions
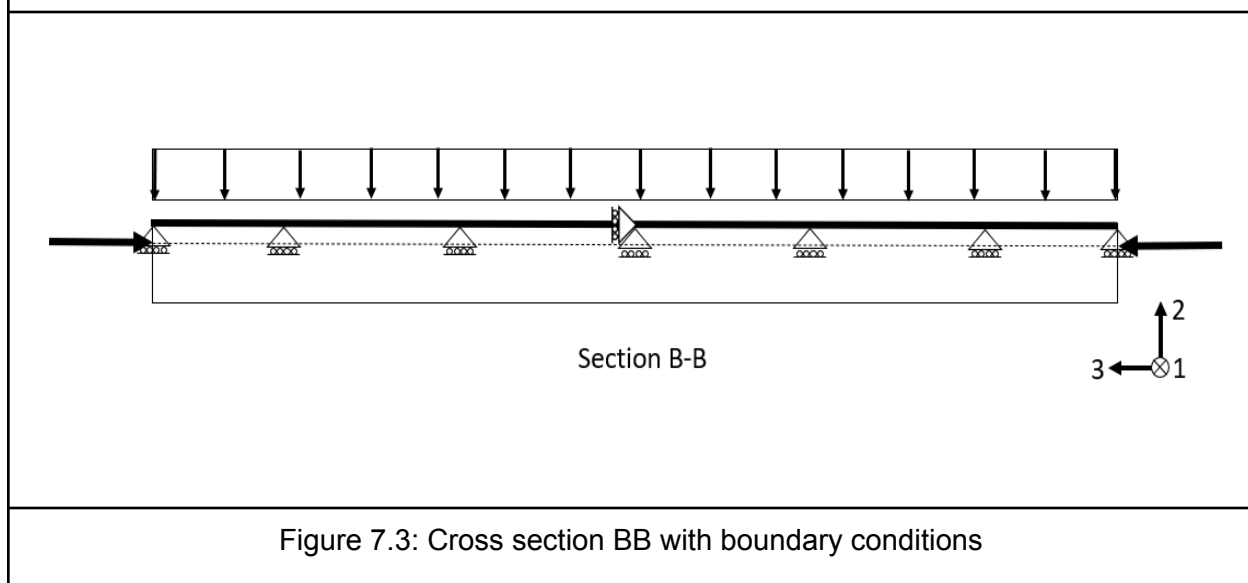
Figure 7.3: Cross section BB with boundary conditions

In modeling the plate behavior under out of plane loads, we used the FEM software ABAQUS. Unlike in our axial analyses, the behavior of the plate is not as simple as a capacity that, when reached, necessarily results in the plate buckling/failing.

In a plate that is only loaded out of plane, without axial loads in the longitudinal and transverse directions, the resistance of the plate is determined by first bending behavior and then membrane behavior in tension (see section 7.3). If the plate is biaxially loaded in addition to its out-of-plane load, the deflection of the midpoint will cause the plate to begin taking on a shape resembling a global buckling mode. This deflection is therefore comparable to an imperfection in global buckling analysis, and reduces the axial resistance of the plate.

As such, when the deflection of the midpoint becomes too large, the plate will buckle, similarly to the plates in earlier chapters.

7.1 Description of Load Combinations

To investigate this loading situation, we modeled a plate of aspect ratio 1 (4200x4200 mm), for each section ("Small," "Slender" and "Stiff") and included three load combinations for each geometry.

- Control: The control situation had no axial loads, and a gradually increasing out-of-plane load (pressure or suction)
- 10% group: The 10% load combination included axial loads that were 10% of the capacities for axial load in the longitudinal and transverse directions, respectively. These load capacities are taken from our Abaqus results in chapter 5.
- 30% group: Similar to 10% group, but with 30% of the axial capacities applied in each direction.

For both the 10% and 30% groups, we added a step in Abaqus to ensure that they were held constant during the progressive loading of the pressure/suction load

7.2 Interpretation of Results

Initially, we had difficulty understanding the results we produced. When performing static analyses (provided that nonlinear geometry is enabled), Abaqus exits with an error once it is unable to produce a convergent result within the increment bounds set by the user. Provided the minimum time increment is sufficiently small (default is 1E-5) this means that the equilibrium curve has reached a nonlinearity. For the purposes of axial capacity analysis, this is adequate, as the relevant nonlinearity is buckling or section failure. In the case of plates with zero axial load, the analysis continues past any semblance of what one could reasonably call its resistance capacity.

This is due to the pressure forces causing such large deformation that additional load is taken by deformed sections of the plate as tension loads.

Figure 7.4: Ultimate deformation of slender plate when analysis continues until non-convergence
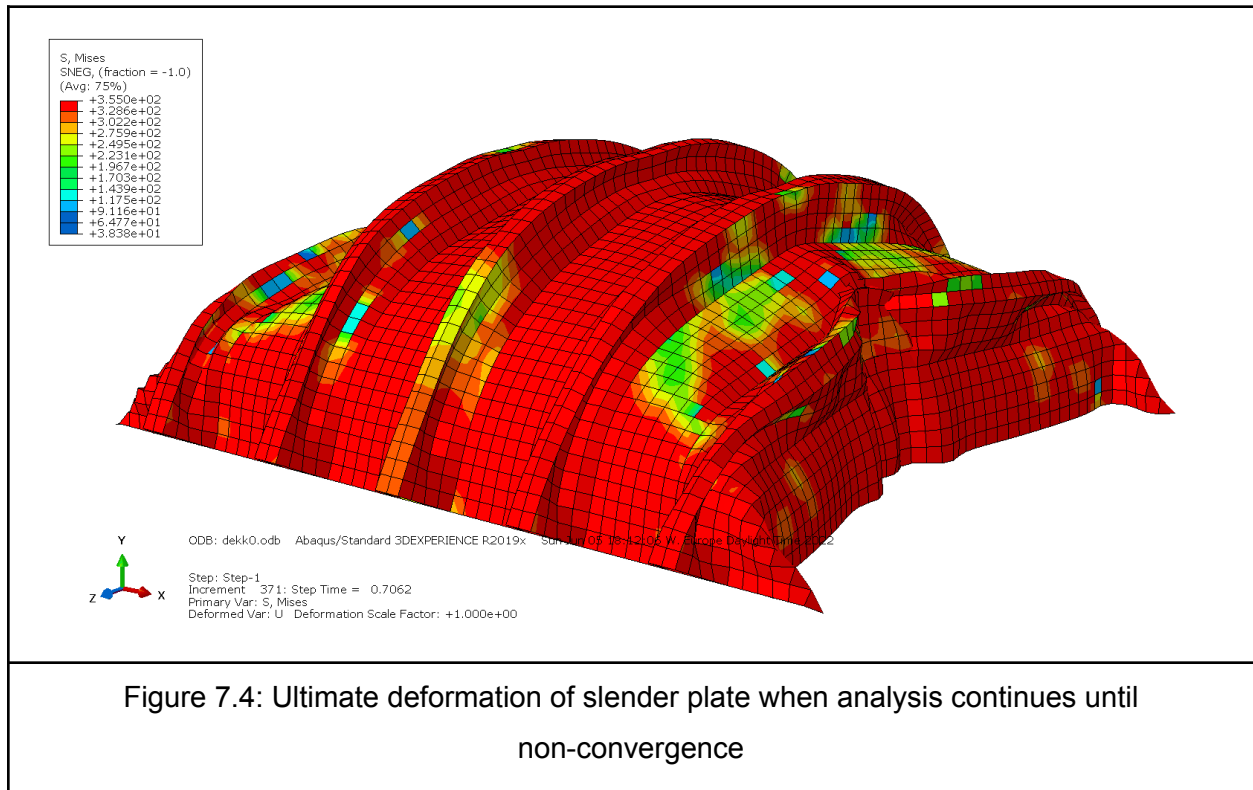
It is more relevant to constructions to evaluate the capacity in terms of bending resistance of the stiffeners. There is no current method for this in the EC3, but the EC9, which gives guidelines for dimensioning aluminum members, includes a method that we have used for comparison purposes (see chapter 8).

Meanwhile, we have taken an observational approach to capacity determination based on our results.

7.2 Results

We requested a History Output for the out-of-plane deflection of the center point of the plate, and plotted its displacement against the total force acting upon the plate out of plane.

7.2.1 Pressure

The Force-Displacement graphs for each geometry follow. The curves for the control, 10% and 30% groups are presented on the same graphs for clarity and comparison's sake.
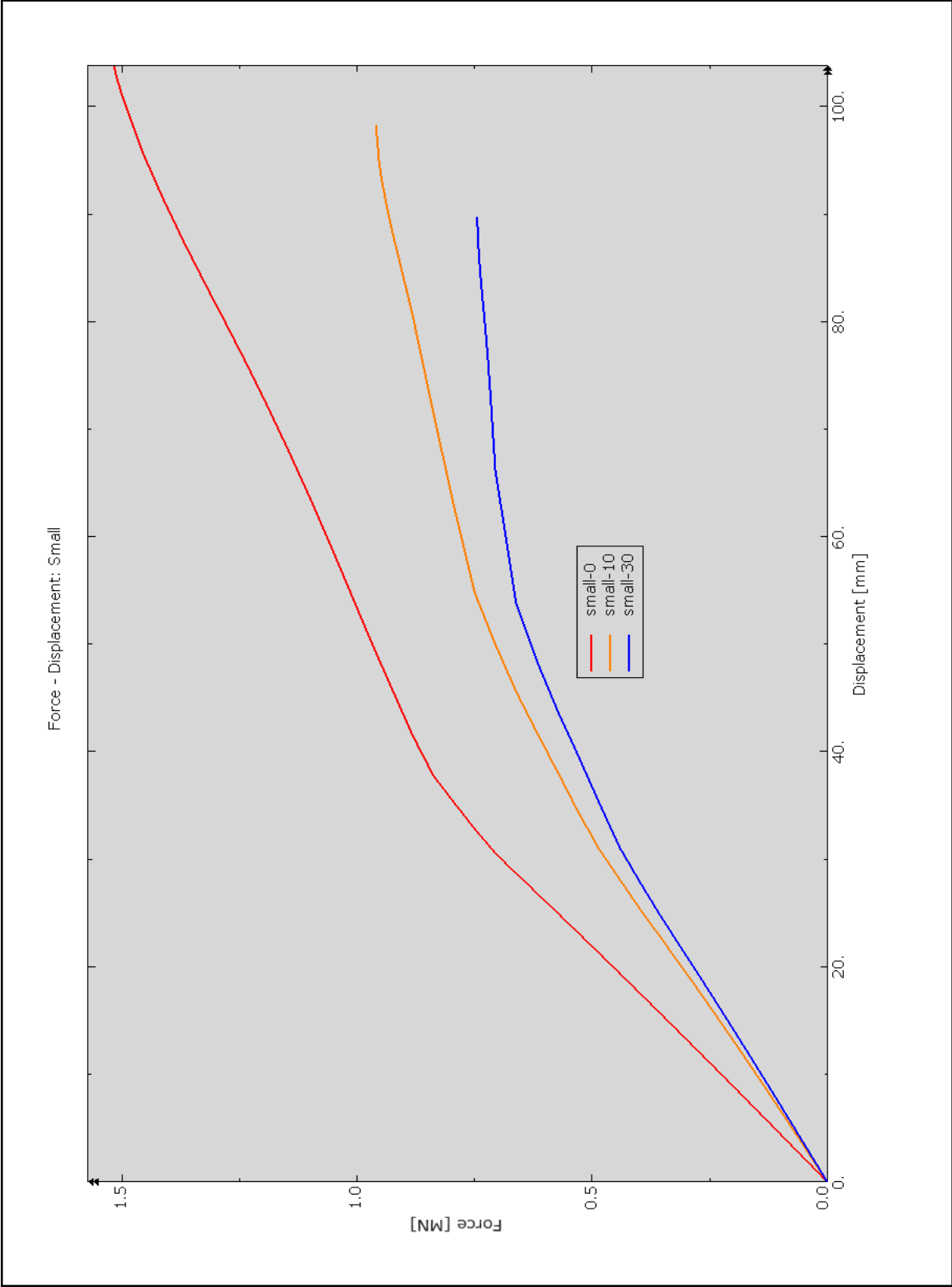
Figure 7.5: F-D curve: small
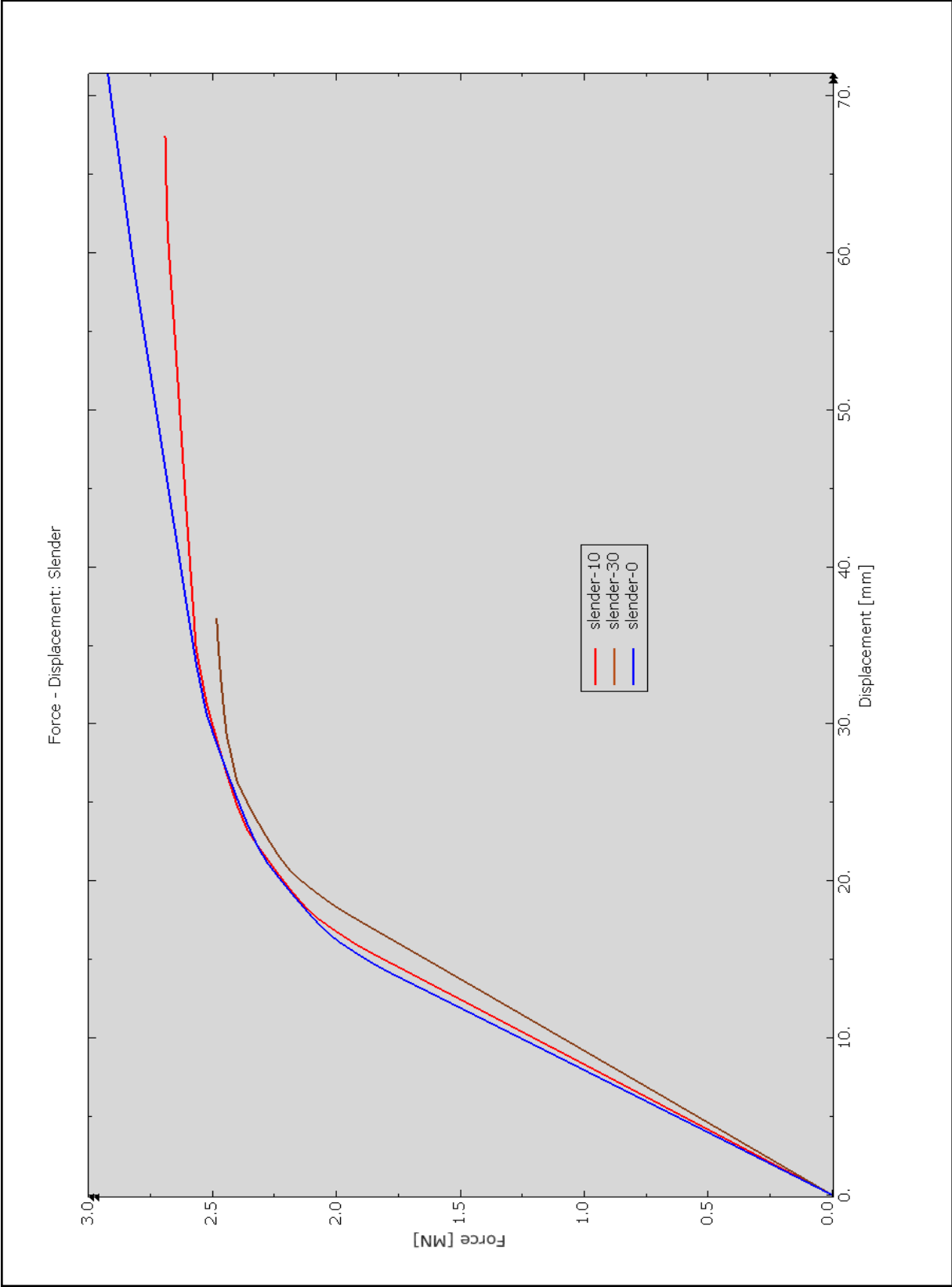
Figure 7.6: F-D curve: slender
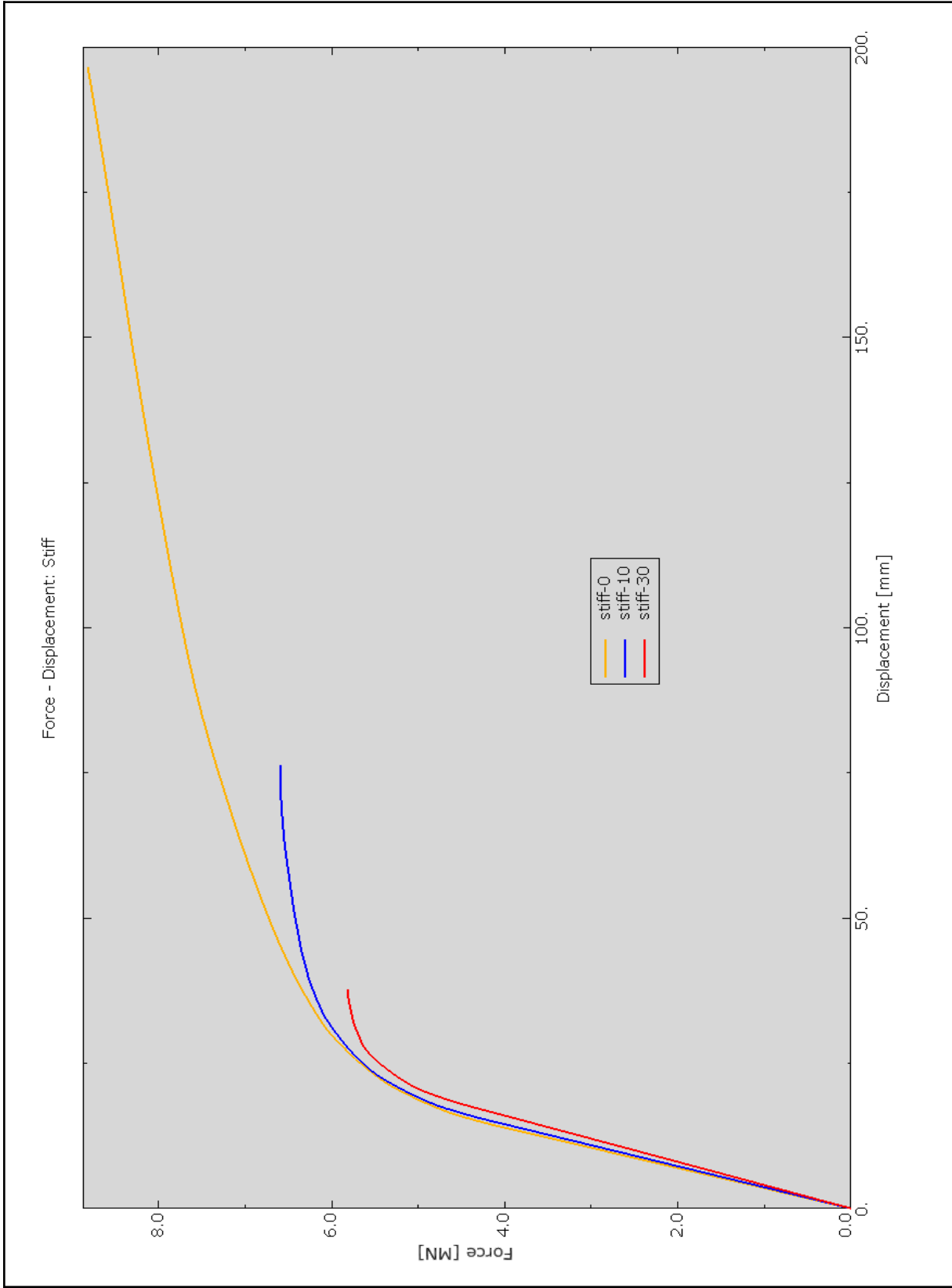
Figure 7.7: F-D curve: stiff

The pressure graph for "stiff" geometry is the easiest to interpret. The curves resemble a stress-strain curve for a tensile material test, in that there is a fairly linear section initially, followed by a region of softening, where the rate of displacement relative to force increases. This effect is more obvious for the axially loaded groups than for the control group, where the curve does not flatten as much. Still, there is a clear linear region presumably dominated by bending, followed by a softer region where the stiffeners provide less resistance as they deform.

For the "Slender" geometry, the curves for the control and 10% groups actually overlap briefly, though this could be due to imprecisions in the calculations. The general behavior is the same, with a clear linear region followed by a region of softening. Though the 10% and control group curves are very close even during a large portion of this softening region, the 10% curve flattens more, due to axial loads accelerating the deflection of the plate center.

The "Small" plate has an equilibrium curve that is less clear. It too has a softening region, but this is more difficult to identify. The initial linear area has a shallow slope to begin with, and does not flatten as much in relative terms. This is visible despite scale differences because of the failure points on the 10% and 30% curves.

Note the points at which the 10% and 30% groups stop. These are the aforementioned points at which Abaqus is no longer able to find a convergent value. This is because the displacement is increasing so quickly (while the equilibrium load is either decreasing or behaving with a nonlinearity) that Abaqus can no longer determine a solution using the Newton Raphson method, where buckling of the plate occurs. Still, we suggest that a better value for the plate's resistance capacity can be determined from the region of the curve at which the slope begins to decline.

7.2.2 Suction

The Force-Displacement curves for suction follow on the next three pages.
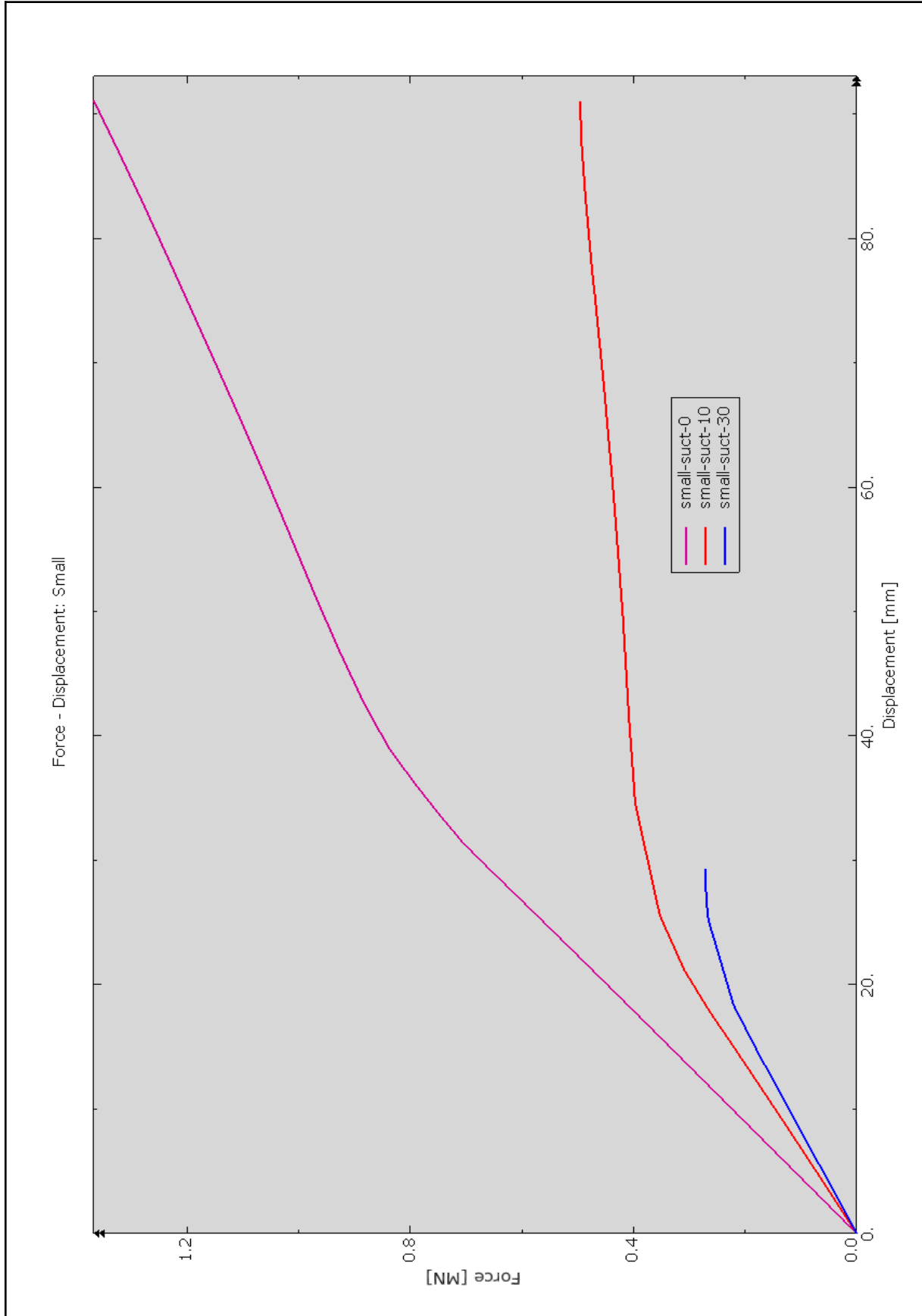
Figure 7.8: F-D curve: small, suction
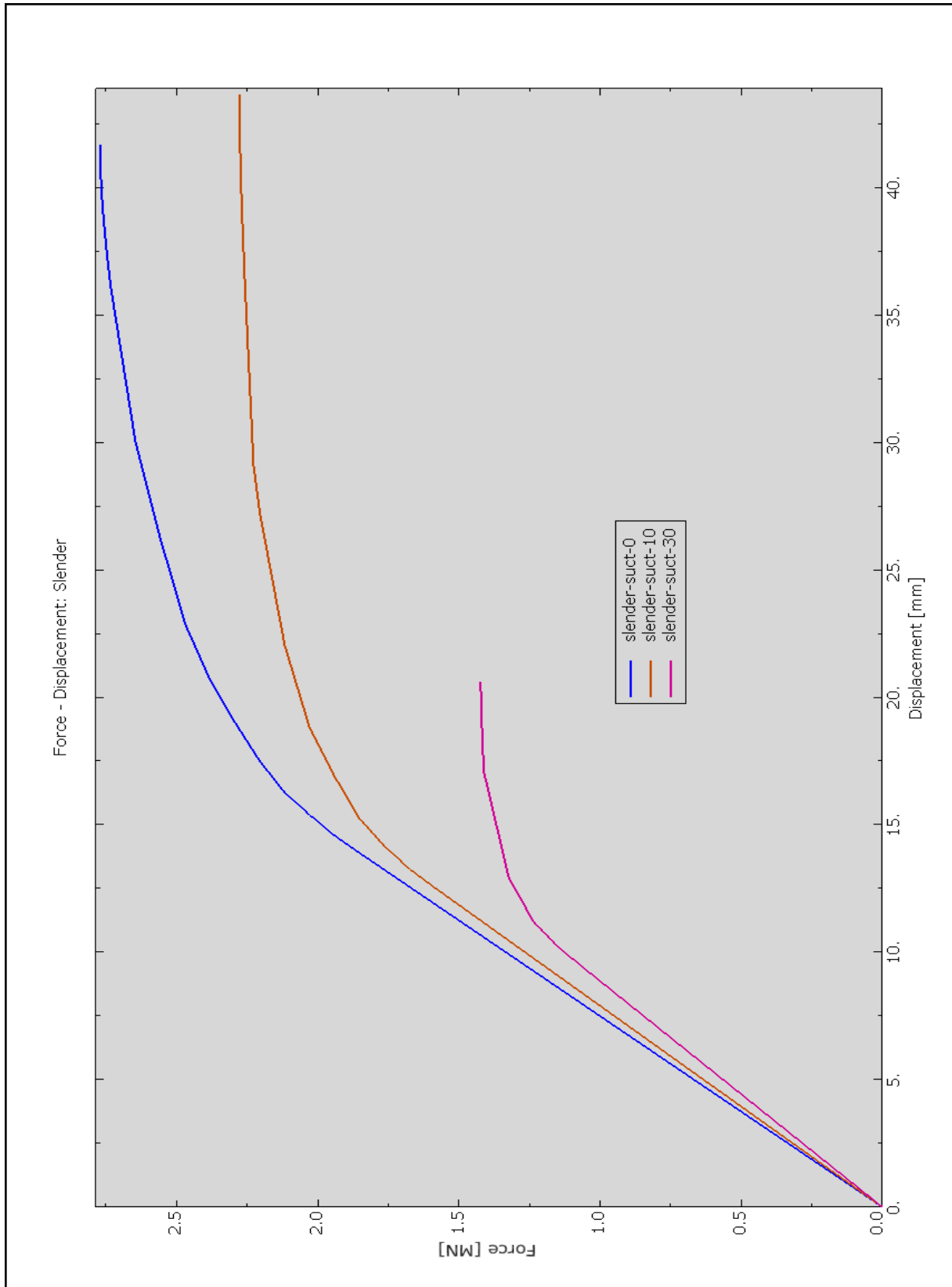
Figure 7.9: F-D curve: slender, suciton
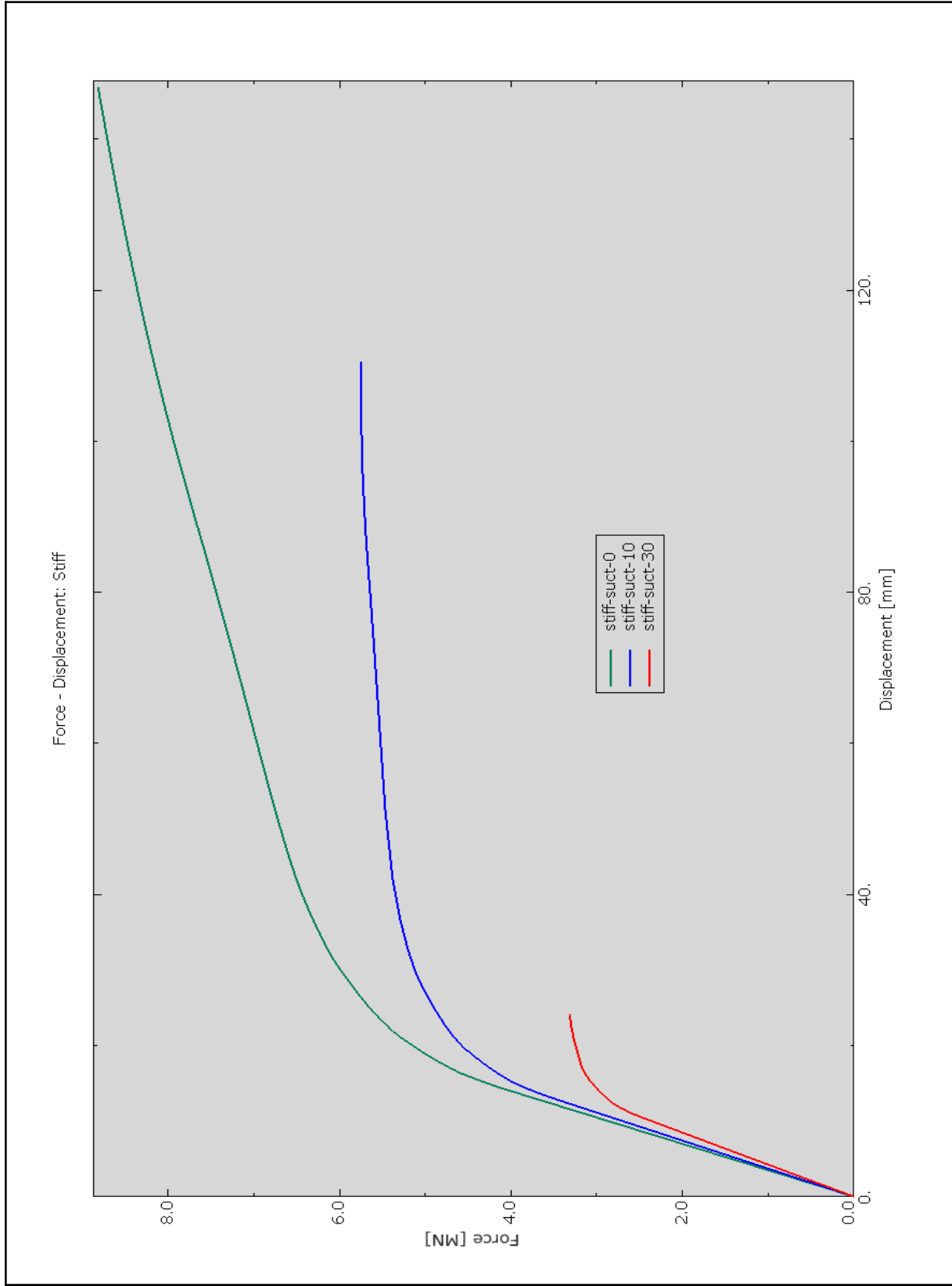
Figure 7.10: F-D curve: stiff, suction

The shape of the curves in suction is analogous to the shape for pressure load, but there are larger capacity differences between the curves for different groups of the same geometry.

A part of this effect comes from the reversal of the bending moment about the transverse axis. When the plate is under a pressure load, most of the stiffener is in tension, and the plate is in compression. Because the center of area is very close to the plate, the magnitude of the stresses due to bending are significantly larger at the top of the stiffener than at the bottom of the plate. This large tension stress is offset somewhat by the compressive stress from the axial loads. Though this does increase the stress in the plate, the total stress distribution is more favorable.

In suction, however, the top flange of the stiffener has a compressive stress due to bending moment and compressive stress from the axial loads. Though this reduces the overall stress in the plate, it increases the compressive stress in the flange and is altogether a more vulnerable loading situation. In the slender geometry, this is further compounded by the stiffener web's vulnerability to local buckling. This is perhaps an explanation for why the slender curve for suction without axial loads flattens and fails, while the other two continue in a shallower pattern.

Figure 7.11: Stress distribution throughout section, suction

Figure 7.12: Stress distribution throughout section, pressure
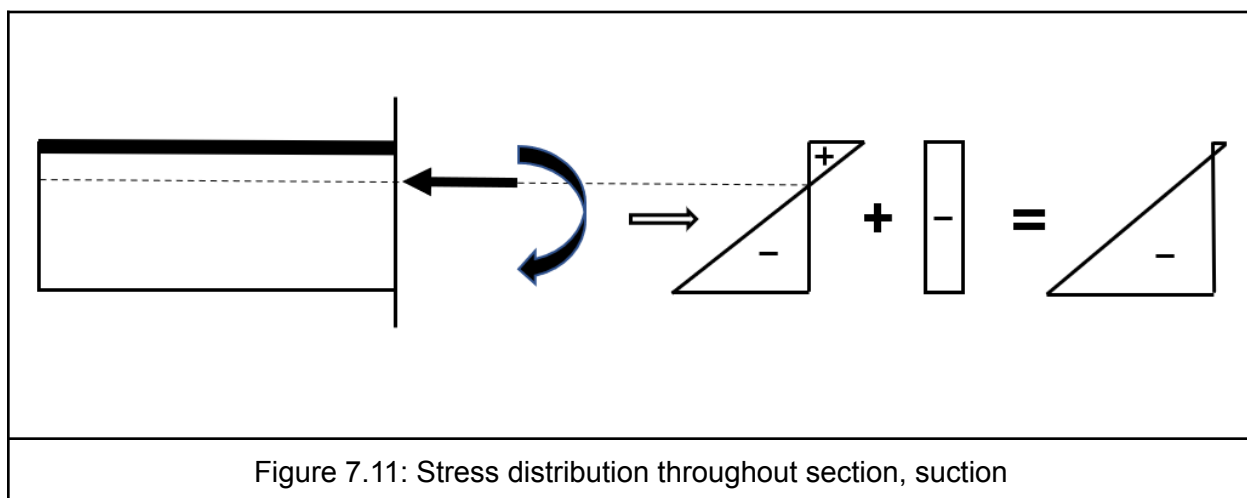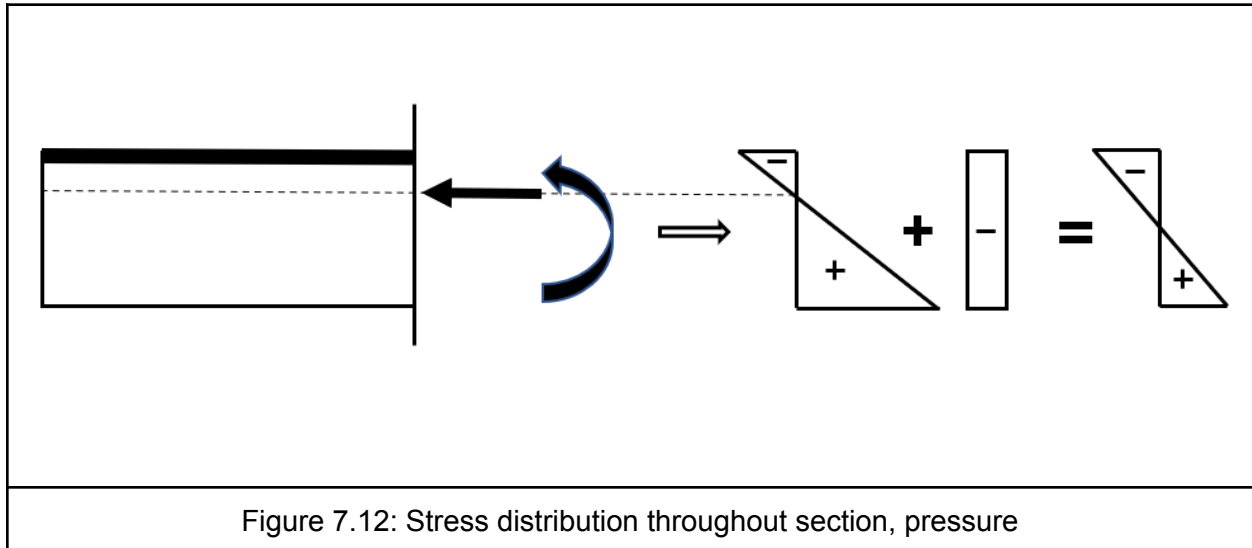
In bending about the longitudinal axis, the plate has a much lower resistance, due to the slenderness of the plate. We therefore consider bending about the transverse axis to be more relevant for determination of resistance.

7.2.3 Stress Distribution Throughout the Plate

Figure 7.13: Stress distribution throughout plate, pressure

Figure 7.14: Stress distribution throughout plate, suction
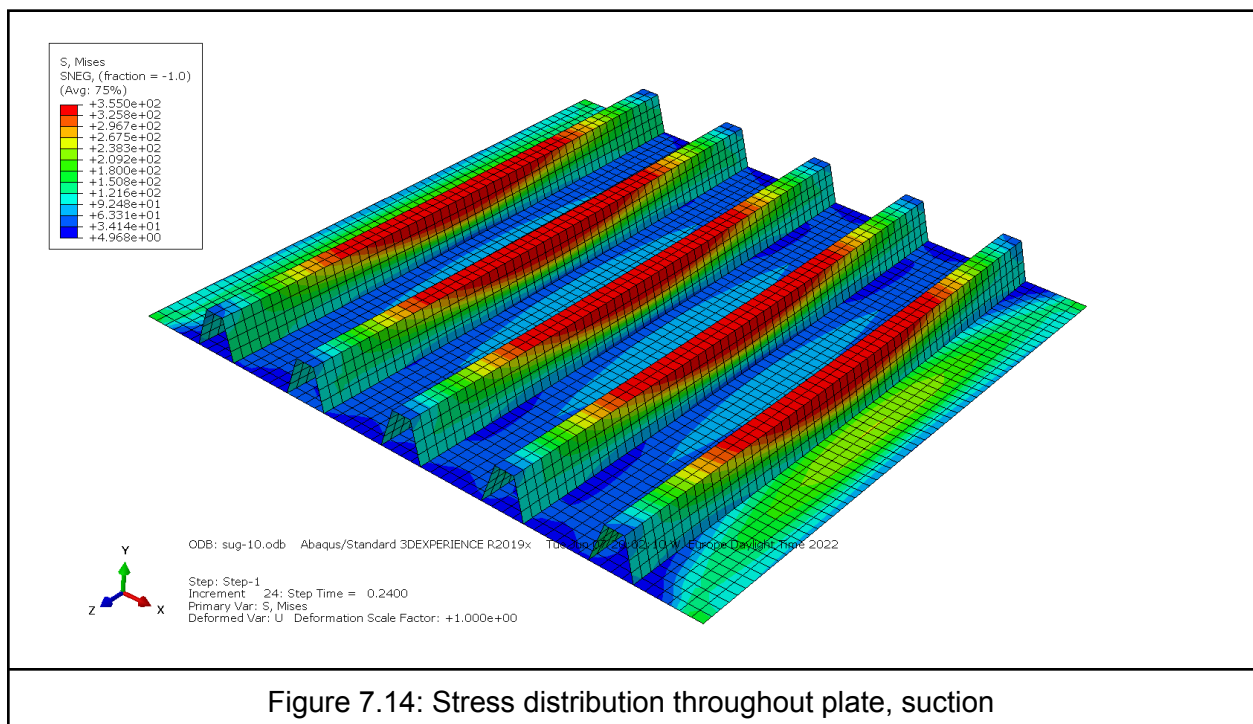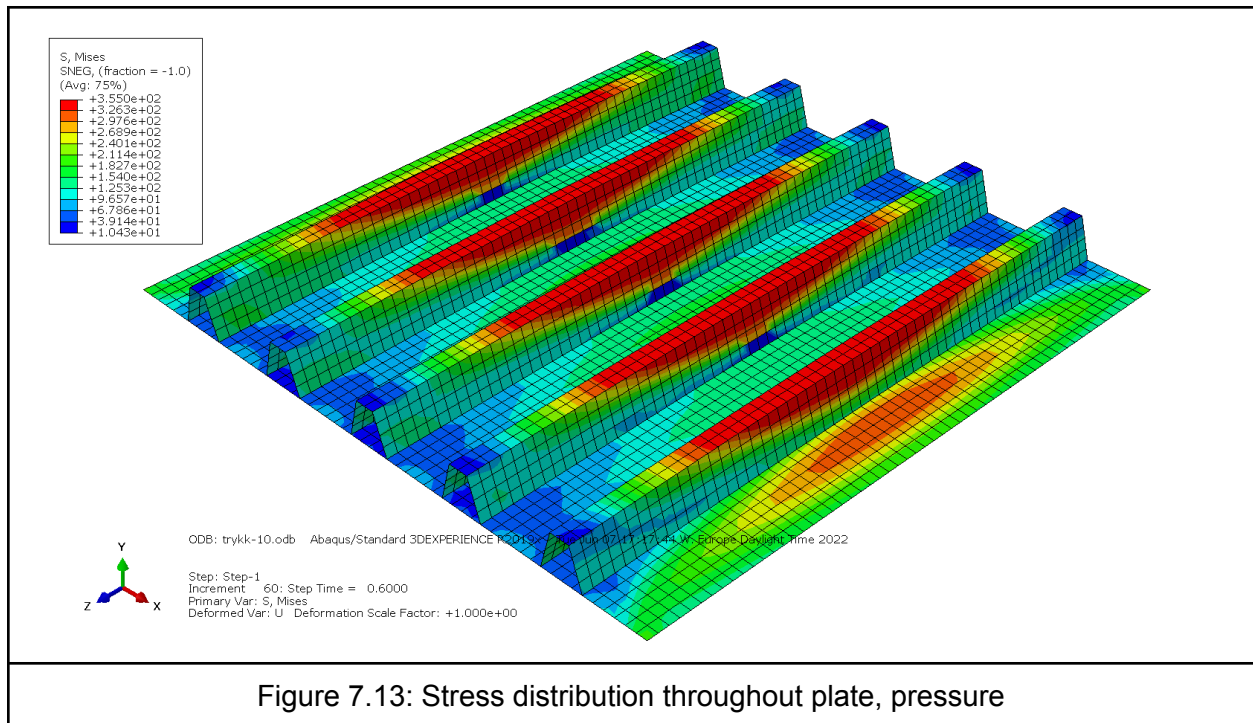
These figures are retrieved from the Abaqus output database around the time the flattening of the curves begins. In both the pressure and suction scenarios, it is the stiffeners that begin to yield first. This is what causes the flattening of the curves, as the red sections on the figures are unable to provide the resistance they did before.

Note the lower levels of stress in the plate in the suction scenario. This is a result of the dynamic discussed above; the offset of the stresses in the plates by the axial loads exacerbates the stress scenario in the stiffeners and reduces the tension stress in the plate, causing a scenario where the stiffeners are at a much higher stress level than the plate in relative terms.

7.3 Discussion of Procedure

As mentioned above, when determining the capacity of a plate loaded in this way, there is no current Eurocode guideline to assess how the resistance strength changes with different axial load combinations. Therefore, when running the analysis in Abaqus, the user has to use his or her best judgment in deciding what the true resistance capacity of the plate is. Ideally, this would also be standardized, so that different geometries and load situations could be easily compared.

By standardized, we mean that capacity should be determined as the load that causes a certain displacement, in terms of, for example, the height of the total cross section. Another suggestion would be when the slope of the Force-Displacement curve is reduced to a predetermined proportion of the slope in the linear region. An advantage of this suggestion is that a small deviation in the load size from the design load would not necessarily produce a much larger displacement, since the slope of the curve has not yet reached the shallow region.

More research is needed, and analyses performed on different geometries in order to determine a reasonable window for either of these suggestions. The variation is large (see curves for "small" vs "stiff" geometry) and three geometries is not adequate for making this determination. Additionally, we have assumed an aspect ratio of 1, and the plate may behave differently under different aspect ratios.

A Note on Membrane Forces:

When designings constructions, deflections and deformations are critical to understanding the behavior of both the component and the entire constructions. In the case of a plate loaded out of plane, it is the deformation that accounts for much of the strength after a certain point.

The plate in figure 7.4 in its deformed state is clearly too deformed to be of any use, despite its retention of some resistance strength. This resistance strength comes from the membrane forces in the plate. Along the plate's edges, the plate has deformed so much as to be practically perpendicular to its original orientation, causing the pressure load to be carried by tension in the plate.

8. Comparison to The Aluminum Standard

To calculate the theoretical capacity against pressure and suction, we used the interaction method, (eq 2.10) from the aluminum standard, EN 1999-1-1 (3). We calculated as mentioned in the previous chapter the out-of-plane load capacities in combination with axial loads for these three cases, 0%, 10% and 30% of the total axial capacity from both longitudinal and transverse direction.

8.1 Suction

In our case, the studied layer was the plate and this was under tension when we applied suction to the stiffened plate. The results of this analysis is shown in figure 8.4. The figure shows the results for all three geometries that were analyzed. As we can see the capacity against suction decreases with the size of the geometry and the increasing percentage of total axial load. The mentioned tendencies follow the observations made in chapter 7. However, when we compare the final results from EC9 against ABAQUS, it is obvious that the results from EC9 are unsafe, see figures below.

The results from EC9 are added on the Abaqus graphs, in order to be able to compare the curves. EC9 results are shown by horizontal lines with the same color as the corresponding ABAQUS result.The difference between the two methods is clearer as the axial load grows.
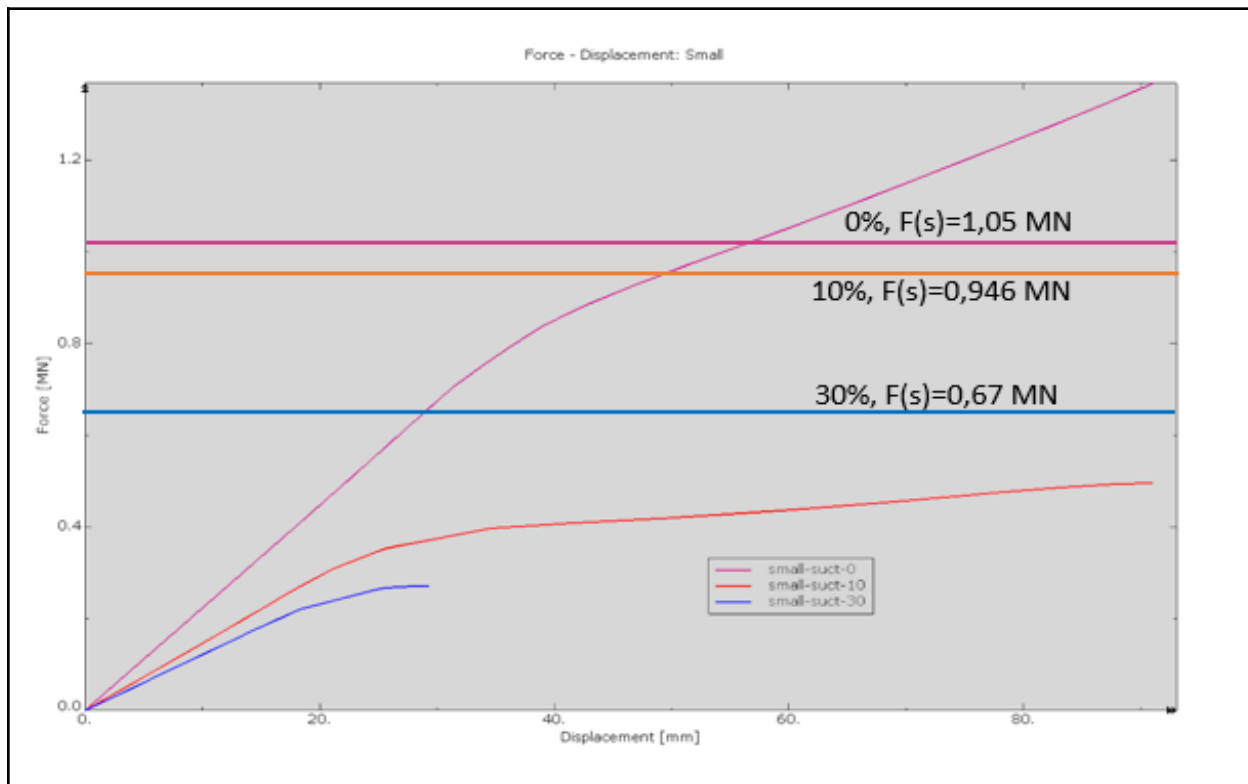
Figure 8.1: "Small" geometry plotted as horizontal lines (EC9)
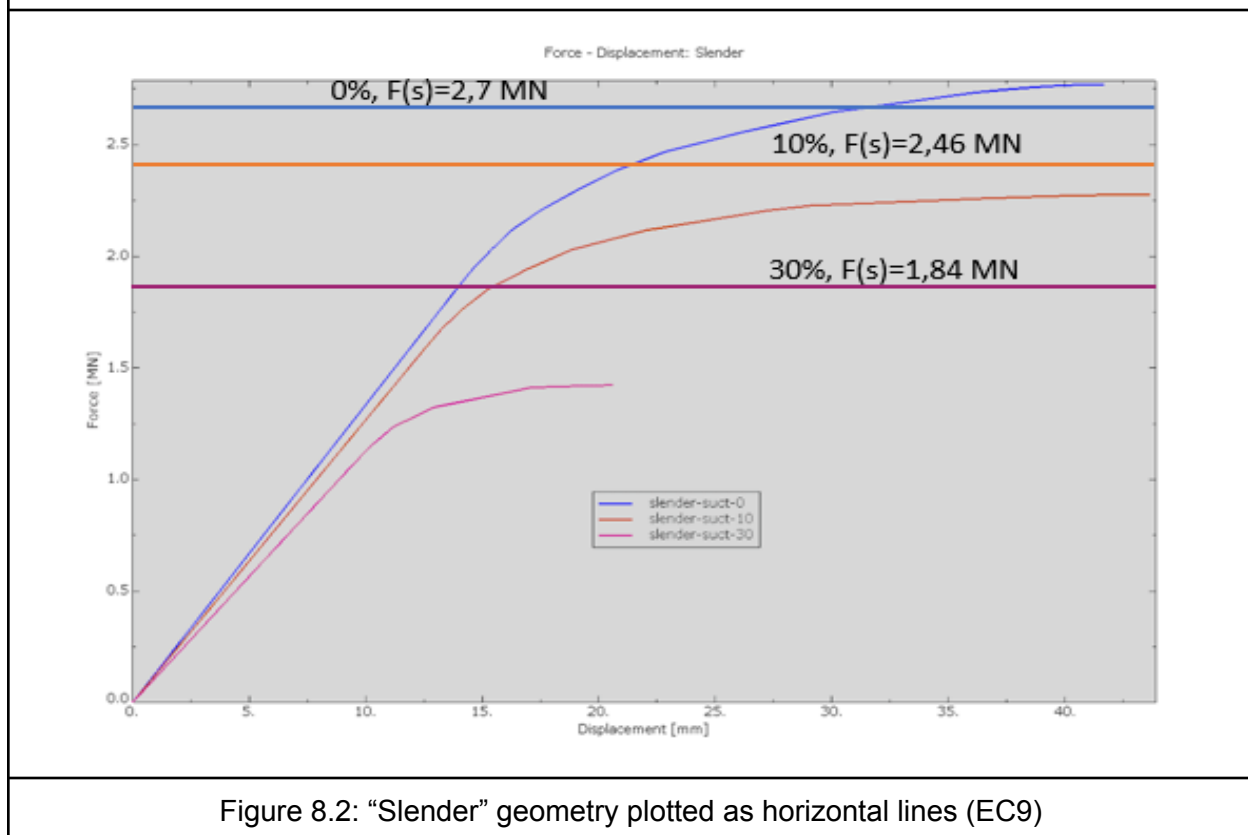
Figure 8.2: "Slender" geometry plotted as horizontal lines (EC9)

Figure 8.3: "Stiff" geometry plotted as horizontal lines (EC9)
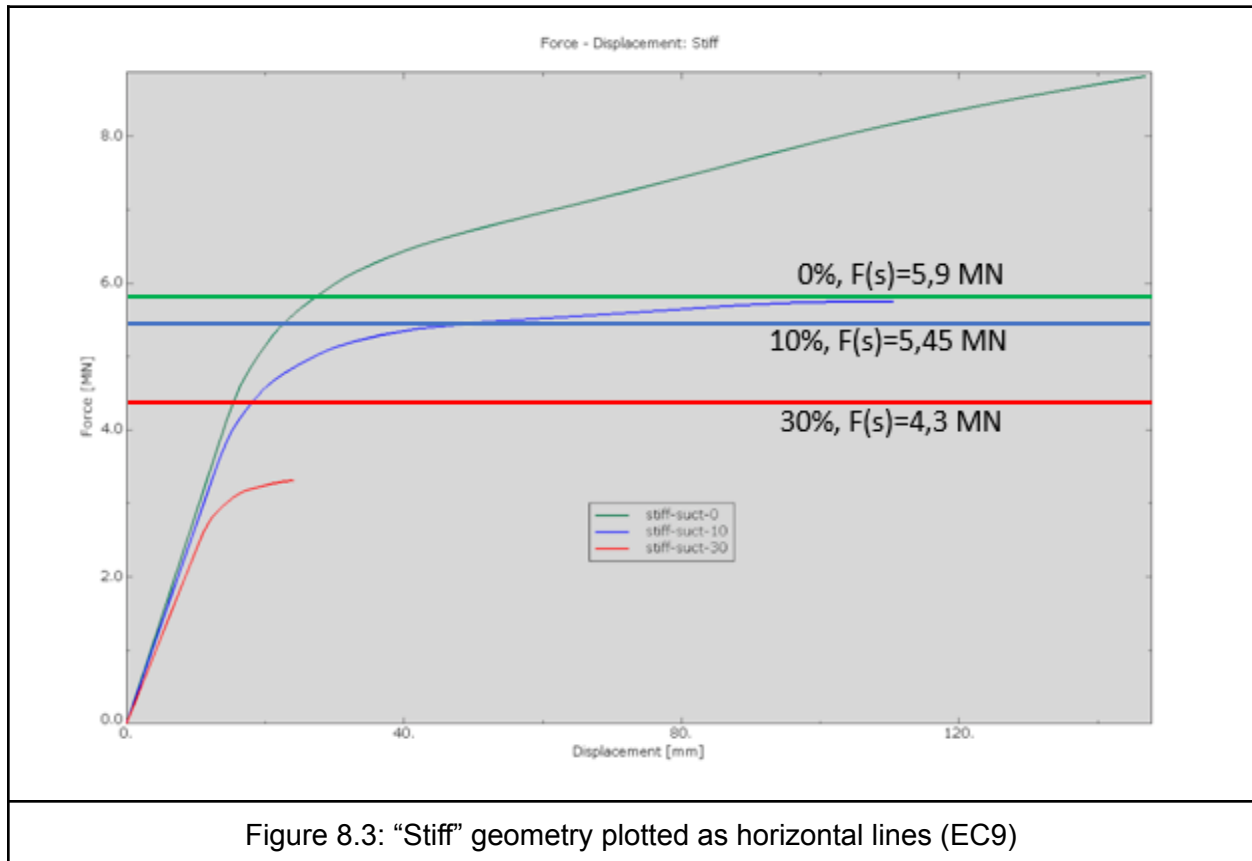
8.2 Pressure

The EC9 results from the pressure loading are inconsistent with findings from chapter 7 because of the increase of the out-of-plane pressure capacity with the bigger axial loads, as shown in figure 8.5. The only difference we made here compared to the suction, was that we changed the k_{Nm} value from 1 to -1. This change caused the capacity to trend in the opposite direction of the results from ABAQUS, where it is obvious that the pressure capacity decreases when the axial load increases. As such, plotting these results is meaningless, and has been omitted.

Our results show that the interaction method from EC9 is not fully suitable nor trustworthy. The reason behind this is that the interaction method requires adjustment. Another possible reason is that the differences between steel and aluminum are critical here, since this interaction method is derived from the aluminum standard.
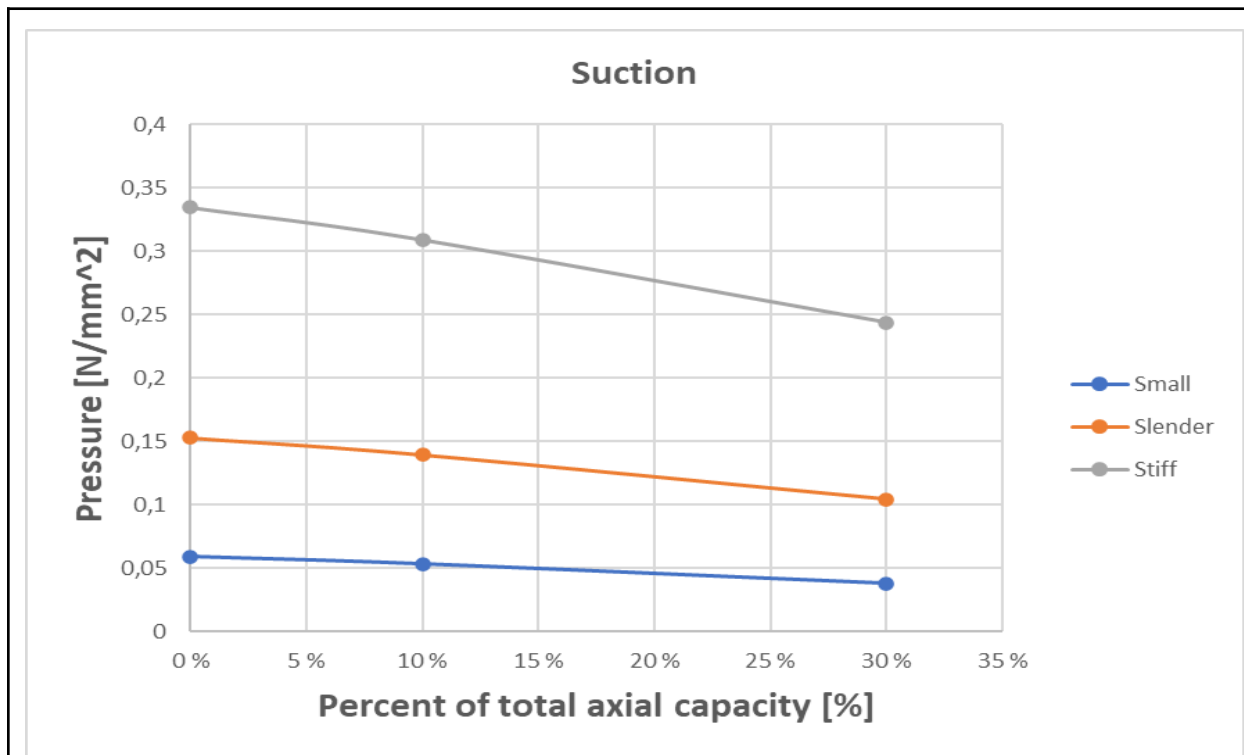
Figure 8.4: Plate loaded by suction, $k_{Nm} = -1$
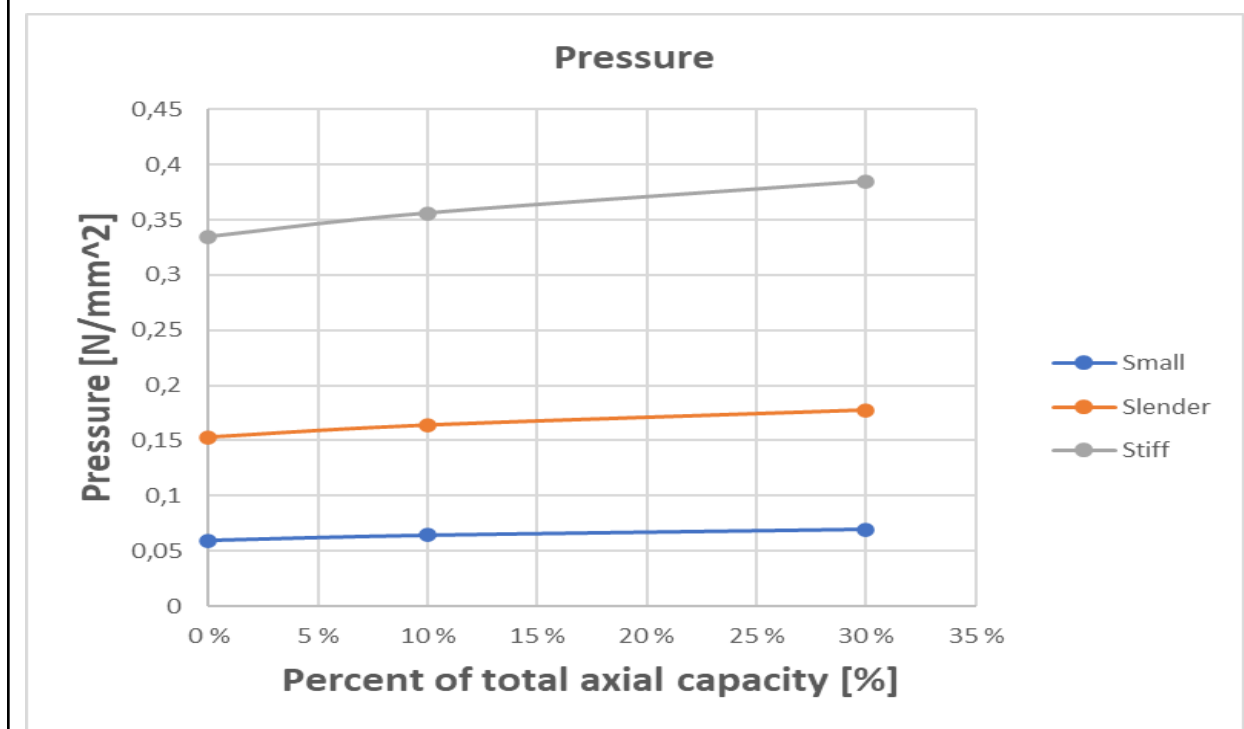
Figure 8.5: Plate loaded by pressure, $k_{Nm} = 1$

9. Conclusion

Longitudinally stiffened steel plates currently have an incomplete procedure for design according to the Eurocode. In determination of axial capacity, our results show that, in the longitudinal direction, it tends to be conservative, at least for our choices of geometry. Earlier studies have shown that the method is not sufficiently conservative, while our study has produced opposite results. This implies that the Eurocode does not account for different geometries in consistent ways, since it does not provide consistently conservative or consistently unsafe results. To adjust or adapt the current method, therefore, more complicated measures should be implemented. For axial capacity, at least, the current method can be safely used for geometries similar to ours, as it is conservative.

Note that our geometries have relatively large, closed section stiffeners and are not particularly susceptible to global buckling. The risk of local buckling for two of our three geometries reduced the slenderness with regard to global buckling, and the size of the stiffeners in the third geometry also reduced slenderness via its large stiffeners and significant torsional strength.

For transverse uniaxial loading of stiffened plates, the adapted methods for determination of resistance capacities worked to a reasonable extent for the geometries with large stiffeners with a high degree of bending resistance, but produced unsafe results for the "small" geometry, even when the difference in bending stiffness is partially accounted for via analysis of the lower buckling modes (showing fewer half-sine waves and therefore lower resistance than intuition implies). This suggests that, similarly to axial capacity, whether the method is easily adapted in this way is more dependent on the specific geometry as opposed to the method itself. The torsional stiffness is likely of value here.

When it comes to out-of-plane loading of the stiffened plate, it is clear that increased compressive axial load reduces the plate's resistance capacity. Especially for plates whose stiffeners have a high level of bending resistance, one method for determining capacity could be found by analyzing the displacement of the center of the plate. Due to membrane forces, the plate has some post-buckling resistance strength as well, but the global deformation at this point is likely to be undesirable. While there is no current method for steel plates, the 2021 version of the EC9, or aluminum standard, includes a method for determining capacity via utilization grade, but this appears as well to be unsafe and inadequate in its current form.

10. Bibliography

[1] NS-EN 1993-1-1:2005+A1:2014+NA:2015 Prosjektering av stålkonstruksjoner. Del 1-1 Allmenne regler og regler for bygninger

[2] NS-EN 1993-1-1:2005+A1:2014+NA:2015 Prosjektering av stålkonstruksjoner. Del 1-5 Plater påkjent i plateplanet

[3] prEN 1999-1-1:2022 Design of aluminium structures - Part 1-1: General structural rules

[4] Larsen, P.K. (2010) *Dimensjonering av stålkonstruksjoner*. Tapir Akademisk Forlag, second edition

[5] Zahlquist, R.(2013) Knekklast for platefelt med aksiallast. Master's thesis, NTNU

[6] Valen, W. (1998) Platefelt i aluminium med stivere av lukket profil. Master's thesis, NTNU

[7] Rønning, Y. (2006) Kapasitet av avstivede platefelt. Project thesis, NTNU

[8] Derik, A.M. (2013) Stiffened plates - Reduced Stress Method. Master's thesis, NTNU

[9] Beg, D.; Kuhlmann, U.; Davaine, L.; & Braun, B. (2010). *Design of Plated Structures*: *Eurocode 3: Design of Steel Structures, Part 1-5: Design of Plated Structures*. ECCS

[10] Pourostad, V; Kuhlmann, U. (2021) Interpolation of plate- and column-like behavior under multiaxial loading. ECCS

[11] Johansson, B.; Maquoi, R.; Sedlacek, G. ;Müller, C.;Beg, D. (2007). Commentary and worked examples to en 1993-1-5 "Plated structural elements."

[12] Couto, C; Real, P.V.; Lopes, N.; Zhao, B. Effective Width Method [Internet]. Trondheim (NO): Science Direct NTNU; 2014 [updated 2014; cited 2022]. Available from: https://reader.elsevier.com/reader/sd/pii/S0263823114001761?token=190053F2D4A44008C2D DC7F5289D69DC6128166604BFAD08A79ABB86D43C8DF10B8683FD4B06DFB50D7DC1757 E1EA40A&originRegion=eu-west-1&originCreation=20220525154439

Appendix A

Longitudinal buckling load for slender geometry:

- Orthotropic plate with trapezoid stiffeners

Dimensions:

$$a := \begin{bmatrix} 600 \\ 1050 \\ 1500 \\ 2100 \\ 3000 \\ 4200 \\ 6300 \\ 7000 \\ 7700 \\ 8400 \end{bmatrix} mm$$
Plate lengths

$b := 4200 \ mm$	Plate width
$b_I := 450 \ mm$	Plate width between stiffeners
$b_{II} := 300 \ mm$	Plate width between one stiffener
$b_{III} := 288 \ mm$	Angled height of stiffener
$b_{IV} := 135 \ mm$	Width of stiffener parallell to plate
$h := 275 \ mm$	Vertical height of stiffener
$t := 12 \ mm$	Plate thickness
$t_{sl} := 6 \ mm$	Stiffener thickness

Material Data:

$f_y := 355 \ MPa$
$E := 210000 \ MPa$
$\nu := 0.3$

$$\varepsilon := \sqrt[2]{\frac{235 \ MPa}{f_y}} = 0.814$$

$\gamma_{M0} := 1.00$
$\gamma_{M1} := 1.05$
$\psi := 1$
$k_\sigma := 4$

Note that for comparison purposed we will neglect material factors

Calculation of effective areas of subpanels:

$$reduction(var) := \begin{Vmatrix} \text{if } var < 0.673 \\ \quad \begin{Vmatrix} 1 \end{Vmatrix} \\ \text{else} \\ \quad \begin{Vmatrix} \dfrac{(var - 0.055 \ (3+\psi))}{var^2} \end{Vmatrix} \end{Vmatrix}$$

$$vecred(var) := \begin{Vmatrix} \text{for } i \in 0..9 \\ \quad \begin{Vmatrix} \text{if } var_i < 0.673 \\ \quad \begin{Vmatrix} vec_i \leftarrow 1 \end{Vmatrix} \\ \text{else} \\ \quad \begin{Vmatrix} vec_i \leftarrow \dfrac{\left(var_i - 0.055 \ (3+\psi)\right)}{var_i^2} \end{Vmatrix} \end{Vmatrix} \\ vec \end{Vmatrix}$$

Plate between two longitudianl stiffeners:

$$\lambda_{p.I} := \frac{\left(\dfrac{b_I}{t}\right)}{28.4 \ \varepsilon \ \sqrt{k_\sigma}} = 0.811$$

$$\rho_I := reduction\left(\lambda_{p.I}\right) = 0.898$$

$$b_{eff.I} := \rho_I \cdot b_I = 404.209 \ \textit{mm}$$

$$A_{eff.I} := \rho_I \cdot b_I \cdot t = \left(4.851 \cdot 10^3\right) \ \textit{mm}^2$$

Plate between one longitudinal stiffener:

$$\lambda_{p.II} := \frac{\left(\dfrac{b_{II}}{t}\right)}{28.4 \ \varepsilon \ \sqrt{k_\sigma}} = 0.541$$

$$\rho_{II} := reduction\left(\lambda_{p.II}\right) = 1$$

$$A_{eff.II} := b_{II} \cdot t = \left(3.6 \cdot 10^3\right) \ mm^2 \qquad \text{No reduction for local buckling}$$

$$b_{eff.II} := b_{II} = 300 \ mm$$

Inclined part of the stiffener:

$$\lambda_{p.III} := \frac{\left(\dfrac{b_{III}}{t_{sl}}\right)}{28.4 \ \varepsilon \ \sqrt{k_\sigma}} = 1.039$$

$$\rho_{III} := reduction\left(\lambda_{p.III}\right) = 0.759$$

$$b_{eff.III} := \rho_{III} \cdot b_{III} = 218.549 \ mm$$

$$A_{eff.III} := \rho_{III} \cdot b_{III} \cdot t_{sl} = \left(1.311 \cdot 10^3\right) \ mm^2$$

Stiffener, part parallell to the plate:

$$\lambda_{p.IV} := \frac{\left(\dfrac{b_{IV}}{t_{sl}}\right)}{28.4 \ \varepsilon \ \sqrt{k_\sigma}} = 0.487$$

$$\rho_{IV} := reduction\left(\lambda_{p.IV}\right) = 1$$

$$b_{eff.IV} := \rho_{IV} \cdot b_{IV} = 135 \ mm \qquad \text{No reduction for local buckling}$$

$$A_{eff.IV} := \rho_{IV} \cdot b_{IV} \cdot t_{sl} = 810 \ mm^2$$

Relevant cross sections:

$$A := b_I \cdot t \cdot 6 + b_{II} \cdot t \cdot 5 + b_{III} \cdot t_{sl} \cdot 10 + b_{IV} \cdot t_{sl} \cdot 5 = \left(7.173 \cdot 10^4\right) \ mm^2$$

$$A_{sl} := 5 \cdot \left(2 \cdot b_{III} \cdot t_{sl} + b_{IV} \cdot t_{sl}\right) = \left(2.133 \cdot 10^4\right) \ mm^2$$

$$A_{sl.1.eff} := A_{eff.I} + A_{eff.II} + 2 \cdot A_{eff.III} + A_{eff.IV} = \left(1.188 \cdot 10^4\right) \ mm^2$$

$$A_p := b \cdot t = \left(5.04 \cdot 10^4\right) \ mm^2$$

$$A_{adj.p} := b_I \cdot t = \left(5.4 \cdot 10^3\right) \ mm^2$$

$$A_c := A - A_{adj.p} = \left(6.633 \cdot 10^4\right) \ mm^2$$

$$A_{c.eff.loc} := \left(5 \cdot A_{eff.IV} + 10 \cdot A_{eff.III}\right) + 5 \ \left(A_{eff.I} + A_{eff.II}\right) = \left(5.942 \cdot 10^4\right) \ mm^2$$

Second moment of area of the whole stiffened plate:

$$\theta := \mathrm{acos}\left(\frac{h}{b_{III}}\right) = 17.281 \ \textbf{\textit{deg}}$$

$$z_{c.1} := \frac{\left(b_{IV} \cdot t_{sl} \cdot \left(h + \frac{t}{2}\right) + 2 \cdot b_{III} \cdot t_{sl} \cdot \left(\frac{h}{2} + \frac{t}{2}\right)\right) + \left(b_{II} + 2\,\frac{b_I}{2}\right) \cdot t \cdot \frac{t}{2} + \frac{b_I}{5} \cdot t \cdot \frac{t}{2}}{b_{IV} \cdot t_{sl} + 2 \cdot b_{III} \cdot t_{sl} + \left(b_{II} + 2 \cdot \frac{b_I}{2}\right) \cdot t + \frac{b_I}{5} \cdot t} = 54.651 \ \textbf{\textit{mm}}$$

$$I_{adj.p} := \frac{\left(\left(b_{II} + 2 \cdot \frac{b_I}{2}\right) \cdot t^3\right)}{12} + \left(b_{II} + 2 \cdot \frac{b_I}{2}\right) \cdot t \cdot \left(z_{c.1} - \frac{t}{2}\right)^2 = \left(2.141 \cdot 10^7\right) \ \textbf{\textit{mm}}^4$$

$$I_{adj.s.\|} := \frac{\left(b_{IV} \cdot t_{sl}^{\ 3}\right)}{12} + b_{IV} \cdot t_{sl} \cdot \left(h + \frac{t}{2} - z_{c.1}\right)^2 = \left(4.15 \cdot 10^7\right) \ \textbf{\textit{mm}}^4$$

$$I_{adj.s.ang} := \frac{\left(t_{sl} \cdot b_{III}^{\ 3}\right)}{12} \cdot \cos(\theta)^2 + b_{III} \cdot t_{sl} \cdot \left(\frac{h}{2} + \frac{t}{2} - z_{c.1}\right)^2 = \left(2.453 \cdot 10^7\right) \ \textbf{\textit{mm}}^4$$

$$I_{sidep} := \frac{\left(\left(\frac{b_I}{2}\right) \cdot t^3\right)}{12} + \frac{b_I}{2} \cdot t \cdot \left(z_{c.1} - \frac{t}{2}\right)^2 = \left(6.423 \cdot 10^6\right) \ \textbf{\textit{mm}}^4$$

$$I_{sl} := 5 \cdot \left(I_{adj.p} + I_{adj.s.\|} + 2 \cdot I_{adj.s.ang}\right) + 2 \cdot I_{sidep} = \left(5.727 \cdot 10^8\right) \ \textbf{\textit{mm}}^4$$

Plate type buckling behaviour:

$$I_p := \frac{\left(b \cdot t^3\right)}{12\,\left(1 - \nu^2\right)} = \left(6.646 \cdot 10^5\right) \ \textbf{\textit{mm}}^4$$

$$\gamma := \frac{I_{sl}}{I_p} = 861.728 \qquad\qquad \delta := \frac{A_{sl}}{A_p} = 0.423$$

$$\alpha := \frac{a}{b} = \begin{bmatrix} 0.143 \\ 0.25 \\ 0.357 \\ 0.5 \\ 0.714 \\ 1 \\ 1.5 \\ 1.667 \\ 1.833 \\ 2 \end{bmatrix}$$

$$k_{\sigma.p} := \begin{Vmatrix} \text{for } i \in 0..9 \\ \quad \begin{Vmatrix} \text{if } \alpha_i \leq \sqrt[4]{\gamma} \\ \quad \begin{Vmatrix} k_{\sigma.p_i} \leftarrow \left(2 \, \dfrac{\left(\left(1+\alpha_i^2\right)^2 + \gamma - 1 \right)}{\alpha_i^2 \, (\psi+1)(1+\delta)} \right) \end{Vmatrix} \\ \text{else} \\ \quad \begin{Vmatrix} k_{\sigma.p_i} \leftarrow \left(4 \, \dfrac{\left(1+\sqrt{\gamma}\right)}{(\psi+1)(1+\delta)} \right) \end{Vmatrix} \end{Vmatrix} \\ k_{\sigma.p} \end{Vmatrix} = \begin{bmatrix} 2.967 \cdot 10^4 \\ 9.689 \cdot 10^3 \\ 4.748 \cdot 10^3 \\ 2.424 \cdot 10^3 \\ 1.189 \cdot 10^3 \\ 607.588 \\ 272.088 \\ 221.33 \\ 183.91 \\ 155.586 \end{bmatrix}$$

Calculation of elastic critical plate buckling stress:

$$\sigma_E := \frac{\left(\pi^2 \, E \cdot t^2\right)}{12 \left(1 - \nu^2\right) b^2} = 1.549 \; \boldsymbol{MPa}$$

$$\sigma_{cr.p} := k_{\sigma.p} \cdot \sigma_E = \begin{bmatrix} 4.597 \cdot 10^4 \\ 1.501 \cdot 10^4 \\ 7.357 \cdot 10^3 \\ 3.755 \cdot 10^3 \\ 1.841 \cdot 10^3 \\ 941.39 \\ 421.571 \\ 342.926 \\ 284.948 \\ 241.063 \end{bmatrix} \; \boldsymbol{MPa}$$

Slenderness of stiffened plate:

$$\beta_{A.c} := \frac{A_{c.eff.loc}}{A_c} = 0.896$$

$$\lambda_p := \sqrt{\frac{\left(\beta_{A.c} \cdot f_y\right)}{\sigma_{cr.p}}} = \begin{bmatrix} 0.083 \\ 0.146 \\ 0.208 \\ 0.291 \\ 0.416 \\ 0.581 \\ 0.869 \\ 0.963 \\ 1.056 \\ 1.149 \end{bmatrix}$$

$$\rho := vecred\left(\lambda_p\right) = \begin{bmatrix} 1 \\ 1 \\ 1 \\ 1 \\ 1 \\ 1 \\ 0.86 \\ 0.801 \\ 0.749 \\ 0.704 \end{bmatrix}$$

Column type buckling behaviour:

$$I_{sl.1} := I_{adj.p} + I_{adj.s.\parallel} + 2 \cdot I_{adj.s.ang} = \left(1.12 \cdot 10^8\right) \; mm^4$$

$$A_{sl.1} := \left(2 \cdot b_{III} \cdot t_{sl} + b_{IV} \cdot t_{sl}\right) + t \cdot \left(2 \cdot \frac{b_I}{2} + b_{II}\right) = \left(1.327 \cdot 10^4\right) \; mm^2$$

$$\sigma_{cr.sl} := \frac{\left(\pi^2 \; E \cdot I_{sl.1}\right)}{A_{sl.1} \cdot a^2} = \begin{bmatrix} 4.86 \cdot 10^4 \\ 1.587 \cdot 10^4 \\ 7.775 \cdot 10^3 \\ 3.967 \cdot 10^3 \\ 1.944 \cdot 10^3 \\ 991.742 \\ 440.774 \\ 357.027 \\ 295.064 \\ 247.936 \end{bmatrix} \; MPa$$

Slenderness of a stiffener as a column:

$$\beta_{A.c} := \frac{A_{sl.1.eff}}{A_{sl.1}} = 0.896$$

$$\lambda_c := \sqrt{\frac{\left(\beta_{A.c} \cdot f_y\right)}{\sigma_{cr.sl}}} = \begin{bmatrix} 0.081 \\ 0.142 \\ 0.202 \\ 0.283 \\ 0.404 \\ 0.566 \\ 0.849 \\ 0.944 \\ 1.038 \\ 1.133 \end{bmatrix}$$

Reduction factor χ

$$i := \sqrt{\frac{I_{sl.1}}{A_{sl.1}}} = 91.873 \ mm$$

$\alpha := 0.34$ Curve b for closed section stiffeners

$$e := \frac{\left(b_{IV} \cdot t_{sl} \cdot \left(h + \frac{t}{2}\right) + 2 \cdot b_{III} \cdot t_{sl} \cdot \left(\frac{h}{2} + \frac{t}{2}\right)\right)}{b_{IV} \cdot t_{sl} + 2 \cdot b_{III} \cdot t_{sl}} - z_{c.1} = 114.956 \ mm$$

$$\alpha_c := \alpha + \frac{0.09}{\dfrac{i}{e}} = 0.453$$

$$\phi := 0.5 \ \left(1.0 + \alpha_c \cdot \left(\lambda_c - 0.2\right) + \lambda_c{}^2\right) = \begin{bmatrix} 0.476 \\ 0.497 \\ 0.521 \\ 0.559 \\ 0.628 \\ 0.743 \\ 1.008 \\ 1.114 \\ 1.229 \\ 1.352 \end{bmatrix}$$

$$\chi_c := \frac{1}{\phi + \sqrt{\phi^2 - \lambda_c{}^2}} = \begin{bmatrix} 1.057 \\ 1.028 \\ 0.999 \\ 0.961 \\ 0.902 \\ 0.817 \\ 0.645 \\ 0.587 \\ 0.53 \\ 0.478 \end{bmatrix}$$

$$\chi_c := \begin{array}{l} \text{for } i \in 0..9 \\ \quad \left\| \begin{array}{l} \text{if } \chi_{c_i} > 1 \\ \quad \left\| \chi_{c_i} \leftarrow 1 \right. \\ \chi_c \end{array} \right. \end{array} = \begin{bmatrix} 1 \\ 1 \\ 0.999 \\ 0.961 \\ 0.902 \\ 0.817 \\ 0.645 \\ 0.587 \\ 0.53 \\ 0.478 \end{bmatrix}$$

Interaction between plate and column buckling:

$$\xi := \frac{\sigma_{cr.p}}{\sigma_{cr.sl}} - 1 = \begin{bmatrix} -0.054 \\ -0.054 \\ -0.054 \\ -0.053 \\ -0.053 \\ -0.051 \\ -0.044 \\ -0.039 \\ -0.034 \\ -0.028 \end{bmatrix}$$

$$\xi := \begin{array}{l} \text{for } i \in 0..9 \\ \quad \left\| \begin{array}{l} \text{if } \xi_i < 0 \\ \quad \left\| \xi_i \leftarrow 0 \right. \\ \xi \end{array} \right. \end{array} = \begin{bmatrix} 0 \\ 0 \\ 0 \\ 0 \\ 0 \\ 0 \\ 0 \\ 0 \\ 0 \\ 0 \end{bmatrix}$$

$$\rho_c := \left\| \begin{array}{l} \text{for } i \in 0..9 \\ \quad \left\| \rho_{c_i} \leftarrow \left(\rho_i - \chi_{c_i} \right) \cdot \xi_i \cdot \left(2 - \xi_i \right) + \chi_{c_i} \right. \\ \rho_c \end{array} \right. = \begin{bmatrix} 1 \\ 1 \\ 0.999 \\ 0.961 \\ 0.902 \\ 0.817 \\ 0.645 \\ 0.587 \\ 0.53 \\ 0.478 \end{bmatrix}$$

Verification for uniform compression:

$$A_{c.eff} := \rho_c \cdot A_{c.eff.loc} + A_{eff.I}$$

$$A = \left(7.173 \cdot 10^4\right) \, mm^2$$

$$N_{cr.p} := \sigma_{cr.p} \cdot A = \begin{bmatrix} 3.297 \cdot 10^3 \\ 1.077 \cdot 10^3 \\ 527.733 \\ 269.342 \\ 132.088 \\ 67.526 \\ 30.239 \\ 24.598 \\ 20.439 \\ 17.291 \end{bmatrix} MN \quad N_{cr.c} := \sigma_{cr.sl} \cdot A = \begin{bmatrix} 3.486 \cdot 10^3 \\ 1.138 \cdot 10^3 \\ 557.719 \\ 284.551 \\ 139.43 \\ 71.138 \\ 31.617 \\ 25.61 \\ 21.165 \\ 17.784 \end{bmatrix} MN$$

Note that the Eurocode does not take torsional stiffness into account, and therefore can produce a resistance capacity above

$$N_{a.Rd} := \left(A_{c.eff.loc} + A_{eff.I}\right) \cdot f_y = 22.814 \, MN$$

$$N_{b.Rd} := A_{c.eff} \cdot f_y = \begin{bmatrix} 22.814 \\ 22.814 \\ 22.792 \\ 21.988 \\ 20.749 \\ 18.946 \\ 15.331 \\ 14.094 \\ 12.909 \\ 11.807 \end{bmatrix} MN$$

$$N_{c.Rd} := \begin{array}{l} \text{for } i \in 0..9 \\ \quad \left\| \begin{array}{l} \text{if } N_{b.Rd_i} \leq N_{a.Rd} \\ \quad \left\| N_{c.Rd_i} \leftarrow N_{b.Rd_i} \right. \\ \text{else} \\ \quad \left\| N_{c.Rd_i} \leftarrow N_{a.Rd} \right. \end{array} \right. \\ N_{c.Rd} \end{array} = \begin{bmatrix} 22.814 \\ 22.814 \\ 22.792 \\ 21.988 \\ 20.749 \\ 18.946 \\ 15.331 \\ 14.094 \\ 12.909 \\ 11.807 \end{bmatrix} MN$$

Length	$N_{cr.p}$	$N_{cr.c}$	λ_p	λ_c	ρ	χ_c	ρ_c	$N_{c.Rd}$
(mm)	(MN)	(MN)						(MN)
600	3297	3486	0.083	0.081	1	1	1	22.814
1050	1077	1138	0.146	0.142	1	1	1	22.814
1500	527.733	557.719	0.208	0.202	1	0.999	0.999	22.792
2100	269.342	284.551	0.291	0.283	1	0.961	0.961	21.988
3000	132.088	139.43	0.416	0.404	1	0.902	0.902	20.749
4200	67.526	71.138	0.581	0.566	1	0.817	0.817	18.946
6300	30.239	31.617	0.869	0.849	0.86	0.645	0.645	15.331
7000	24.598	25.61	0.963	0.944	0.801	0.587	0.587	14.094
7700	20.439	21.165	1.056	1.038	0.749	0.53	0.53	12.909
8400	17.291	17.784	1.149	1.133	0.704	0.478	0.478	11.807

Appendix B

Hybrid method for calculating buckling load:
- Slender geometry

$$N_{cr.ab} := \begin{bmatrix} 47.8 \\ 42.3 \\ 42.0 \\ 41.6 \\ 41.1 \\ 40.7 \\ 36.8 \\ 31.9 \\ 28.4 \\ 26.0 \end{bmatrix} \; MN$$

$$N_{a.Rd} = 22.814 \; MN$$

$$\lambda_c := \sqrt{\frac{N_{a.Rd}}{N_{cr.ab}}} = \begin{bmatrix} 0.691 \\ 0.734 \\ 0.737 \\ 0.741 \\ 0.745 \\ 0.749 \\ 0.787 \\ 0.846 \\ 0.896 \\ 0.937 \end{bmatrix}$$

$$\alpha_c := 0.452$$

$$\phi := 0.5 \; \left(1.0 + \alpha_c \cdot \left(\lambda_c - 0.2 \right) + \lambda_c^{\,2} \right) = \begin{bmatrix} 0.85 \\ 0.89 \\ 0.893 \\ 0.896 \\ 0.901 \\ 0.904 \\ 0.943 \\ 1.004 \\ 1.059 \\ 1.105 \end{bmatrix}$$

$$\chi_c := \dfrac{1}{\phi + \sqrt{\phi^2 - \lambda_c^2}} = \begin{bmatrix} 0.744 \\ 0.717 \\ 0.716 \\ 0.714 \\ 0.711 \\ 0.709 \\ 0.684 \\ 0.648 \\ 0.616 \\ 0.591 \end{bmatrix} \qquad N_{c.Rd} := \chi_c \cdot N_{a.Rd} = \begin{bmatrix} 16.974 \\ 16.366 \\ 16.329 \\ 16.279 \\ 16.216 \\ 16.164 \\ 15.614 \\ 14.778 \\ 14.056 \\ 13.485 \end{bmatrix} MN$$

Length	N_{cr}	λ_c	χ_c	$N_{c.Rd}$
(*mm*)	(*MN*)			(*MN*)
600	47.8	0.691	0.744	16.974
1050	42.3	0.734	0.717	16.366
1500	42.0	0.737	0.716	16.329
2100	41.6	0.741	0.714	16.279
3000	41.1	0.745	0.711	16.216
4200	40.7	0.749	0.709	16.164
6300	36.8	0.787	0.684	15.614
7000	31.9	0.846	0.648	14.778
7700	28.4	0.896	0.616	14.056
8400	26.0	0.937	0.591	13.485

Appendix C

Interaction Method by EN1999-1-1

- Slender geometry with 10% axial load

Dimensions:

$L := 4200 \ mm$	Plate length
$b := 4200 \ mm$	Plate width
$b_I := 450 \ mm$	Plate width between stiffeners
$b_{II} := 300 \ mm$	Plate width between one stiffener
$b_{III} := 288 \ mm$	Angled height of stiffener
$b_{IV} := 135 \ mm$	Width of stiffener parallell to plate
$h := 275 \ mm$	Plate thickness
$t := 12 \ mm$	Vetical height of stiffener
$t_{sl} := 6 \ mm$	Stiffener thickness

Material data:

$a := 375 \ mm$

$f_y := 355 \ MPa$

$a_1 := \dfrac{b_{II}}{2} = 150 \ mm$

$E := 210000 \ MPa$

$a_2 := \dfrac{b_{IV}}{2} = 67.5 \ mm$

$\nu := 0.3$

$a_3 := b_{III} = 288 \ mm$

$\varepsilon := \sqrt{\dfrac{235 \ MPa}{f_y}} = 0.814$

$a_4 := \dfrac{b_I}{2} = 225 \ mm$

$\gamma_{M0} := 1.00$
$\gamma_{M1} := 1.05$
$\psi := 1$
$k_\sigma := 4$

Second moment of area:

$$\theta := \mathrm{acos}\left(\frac{h}{b_{III}}\right) = 17.281 \; \boldsymbol{deg}$$

$$z_{c.1} := \frac{\left(b_{IV} \cdot t_{sl} \cdot \left(h + \frac{t}{2}\right) + 2 \cdot b_{III} \cdot t_{sl} \cdot \left(\frac{h}{2} + \frac{t}{2}\right)\right) + \left(b_{II} + 2 \; \frac{b_I}{2}\right) \cdot t \cdot \frac{t}{2} + \frac{b_I}{5} \cdot t \cdot \frac{t}{2}}{b_{IV} \cdot t_{sl} + 2 \cdot b_{III} \cdot t_{sl} + \left(b_{II} + 2 \cdot \frac{b_I}{2}\right) \cdot t + \frac{b_I}{5} \cdot t} = 54.651 \; \boldsymbol{mm}$$

$$I_{I.II} := \frac{\left(\left(b_{II} + 2 \cdot \frac{b_I}{2}\right) \cdot t^3\right)}{12} + \left(b_{II} + 2 \cdot \frac{b_I}{2}\right) \cdot t \cdot \left(z_{c.1} - \frac{t}{2}\right)^2 = \left(2.141 \cdot 10^7\right) \; \boldsymbol{mm}^4$$

$$I_{IV} := \frac{\left(b_{IV} \cdot t_{sl}{}^3\right)}{12} + b_{IV} \cdot t_{sl} \cdot \left(h + \frac{t}{2} - z_{c.1}\right)^2 = \left(4.15 \cdot 10^7\right) \; \boldsymbol{mm}^4$$

$$I_{2.III} := \frac{\left(t_{sl} \cdot b_{III}{}^3\right)}{12} \cdot \cos(\theta)^2 + b_{III} \cdot t_{sl} \cdot \left(\frac{h}{2} + \frac{t}{2} - z_{c.1}\right)^2 = \left(2.453 \cdot 10^7\right) \; \boldsymbol{mm}^4$$

$$I_{sideplate} := \frac{\left(\left(\frac{b_I}{2}\right) \cdot t^3\right)}{12} + \frac{b_I}{2} \cdot t \cdot \left(z_{c.1} - \frac{t}{2}\right)^2 = \left(6.423 \cdot 10^6\right) \; \boldsymbol{mm}^4$$

$$I_{sl} := I_{I.II} + I_{IV} + 2 \cdot I_{2.III} = \left(1.12 \cdot 10^8\right) \; \boldsymbol{mm}^4 \qquad \text{Second moment of area of one stiffener and adjacent plating}$$

$$I_{tot} := 5 \cdot \left(I_{I.II} + I_{IV} + 2 \cdot I_{2.III}\right) + 2 \cdot I_{sideplate} = \left(5.727 \cdot 10^8\right) \; \boldsymbol{mm}^4$$

$$A := b_I \cdot t \cdot 6 + b_{II} \cdot t \cdot 5 + b_{III} \cdot t_{sl} \cdot 10 + b_{IV} \cdot t_{sl} \cdot 5 = \left(7.173 \cdot 10^4\right) \; \boldsymbol{mm}^2 \qquad \text{Total area}$$

Moments in x and y direction:

$$\alpha_1 := \frac{2\,a_1}{E \cdot t^3} = \left(8.267 \cdot 10^{-7}\right) \frac{1}{N} \qquad\qquad (8.125)$$

$$\alpha_2 := \frac{2\,a_2}{E \cdot t_{sl}^{\ 3}} = \left(2.976 \cdot 10^{-6}\right) \frac{1}{N}$$

$$\alpha_3 := \frac{a_3}{E \cdot t_{sl}^{\ 3}} = \left(6.349 \cdot 10^{-6}\right) \frac{1}{N}$$

$$f := 1 + \frac{\left(a_1 - a_2\right)\,a_3}{h \cdot a_2} = 2.28$$

$$\varphi_{plt} := \frac{2\,a_4^{\ 2}}{a \cdot E \cdot t^3}\left(a_4 + \frac{a_1 \cdot \left(3 \cdot \alpha_3 + 4 \cdot \alpha_2\right)}{3 \cdot \alpha_3 + 4 \cdot \alpha_2 + 4 \cdot \alpha_1 + \dfrac{4 \cdot \alpha_1 \cdot \alpha_2}{\alpha_3}}\right) = \left(2.639 \cdot 10^{-7}\right) \frac{s^2}{kg} \qquad (8.122)$$

$$\varphi_{dis} := \frac{h \cdot a_2 \cdot \left(3 \cdot \alpha_3^{\ 2} + 4 \cdot \alpha_1 \cdot \alpha_2 + 4 \cdot \alpha_1 \cdot \alpha_3 + 4 \cdot \alpha_2 \cdot \alpha_3\right)}{2\,a_2 \cdot \alpha_2 + f \cdot 2 \cdot a_1 \cdot \alpha_1 + \left(2 + f\right)\,a_2 \cdot \alpha_3 + \left(1 + 2\,f\right)\,a_1 \cdot \alpha_3} = \left(5.212 \cdot 10^{-7}\right) \frac{s^2}{kg} \quad (8.123)$$

$$I_t := \frac{4 \cdot \left(h \cdot \dfrac{\left(b_{II} + b_{IV}\right)}{2}\right)^2}{2 \cdot \dfrac{b_{III}}{t_{sl}} + \dfrac{b_{IV}}{t_{sl}} + \dfrac{b_{II}}{t}} = \left(9.972 \cdot 10^7\right)\,mm^4 \qquad G := \frac{E}{2 \cdot \left(1 + \nu\right)} = \left(8.077 \cdot 10^4\right)\,MPa$$

$$B := \frac{E \cdot t^3}{12\,\left(1 - \nu^2\right)} = \left(3.323 \cdot 10^7\right)\,N \cdot mm \qquad\qquad (8.124)$$

$$H := 2\,B + \frac{G \cdot I_t}{2\,a} \cdot \frac{1}{2 + \dfrac{G \cdot I_t}{L \cdot a \cdot b}\,\left(\varphi_{plt} + \varphi_{dis}\right)} = \left(3.7 \cdot 10^6\right)\,J \qquad\qquad (8.121)$$

$$B_x := \frac{E \cdot I_{sl}}{2\,a} = \left(3.135 \cdot 10^{10}\right)\,N \cdot mm \qquad\qquad \text{Table 8.9 EN 1999-1-1}$$

$$B_y := \frac{2\,B \cdot a}{2\,a_4 + \dfrac{2\,a_1 \cdot a_3 \cdot t^3\,\left(4 \cdot a_2 \cdot t_{sl}^{\ 3} + 4\,a_3 \cdot t_{sl}^{\ 3}\right)}{a_3 \cdot t^3\,\left(4\,a_2 \cdot t_{sl}^{\ 3} + a_3 \cdot t_{sl}^{\ 3}\right) + a_1 \cdot t_{sl}^{\ 3}\,\left(12\,a_2 \cdot t_{sl}^{\ 3} + 4\,a_3 \cdot t_{sl}^{\ 3}\right)}} = \left(2.325 \cdot 10^7\right)\,N \cdot mm \quad (8.120)$$

$$m := 1,3..5 \qquad x := 2100 \ mm$$
$$n := 1,3..5 \qquad y := 2100 \ mm$$

$$q_{Ed} := 0.1419 \cdot \frac{N}{mm^2}$$

$$m_{x.Ed} := B_x \cdot \frac{16 \cdot q_{Ed}}{\pi^6} \cdot \left(\left(\frac{\left(\frac{1 \cdot \pi}{L}\right)^2 \cdot \sin\left(\frac{1 \cdot \pi \cdot x}{L}\right) \sin\left(\frac{1 \cdot \pi \cdot y}{b}\right)}{1 \cdot 1 \cdot \left(\frac{1^4}{L^4} \cdot B_x + \frac{2 \cdot 1^2 \cdot 1^2}{L^2 \cdot b^2} \cdot H + \frac{1^4}{b^4} \cdot B_y\right)} \right) + \left(\frac{\left(\frac{1 \cdot \pi}{L}\right)^2 \cdot \sin\left(\frac{1 \cdot \pi \cdot x}{L}\right) \sin\left(\frac{3 \cdot \pi \cdot y}{b}\right)}{1 \cdot 3 \cdot \left(\frac{1^4}{L^4} \cdot B_x + \frac{2 \cdot 1^2 \cdot 3^2}{L^2 \cdot b^2} \cdot H + \frac{3^4}{b^4} \cdot B_y\right)} \right) + \left(\frac{\left(\frac{1 \cdot}{L}\right.}{1 \cdot 5 \cdot \left(\right.} \right.$$

$$m_{x.Ed} := 290.785 \ \left(\frac{1}{m} \cdot kN \cdot m\right) \qquad\qquad (8.135)$$

$$m_{y.Ed} := B_y \cdot \frac{16 \cdot q_{Ed}}{\pi^6} \cdot \left(\left(\frac{\left(\frac{1 \cdot \pi}{b}\right)^2 \cdot \sin\left(\frac{1 \cdot \pi \cdot x}{L}\right) \sin\left(\frac{1 \cdot \pi \cdot y}{b}\right)}{1 \cdot 1 \cdot \left(\frac{1^4}{L^4} \cdot B_x + \frac{2 \cdot 1^2 \cdot 1^2}{L^2 \cdot b^2} \cdot H + \frac{1^4}{b^4} \cdot B_y\right)} \right) + \left(\frac{\left(\frac{3 \cdot \pi}{b}\right)^2 \cdot \sin\left(\frac{1 \cdot \pi \cdot x}{L}\right) \sin\left(\frac{3 \cdot \pi \cdot y}{b}\right)}{1 \cdot 3 \cdot \left(\frac{1^4}{L^4} \cdot B_x + \frac{2 \cdot 1^2 \cdot 3^2}{L^2 \cdot b^2} \cdot H + \frac{3^4}{b^4} \cdot B_y\right)} \right) +$$

$$m_{y.Ed} := 0.165 \ \left(\frac{1}{m} \cdot kN \cdot m\right) \qquad\qquad (8.136)$$

$$z_p := \frac{b_{IV} \cdot t_{sl} + 2 \cdot b_{III} \cdot t_{sl} + \left(b_I + b_{II}\right) \cdot t}{2 \cdot \left(b_I + b_{II}\right)} - \frac{t}{2} = 2.844 \; \boldsymbol{mm}$$

$$W_d := 5 \cdot \left(\left(b_I + b_{II}\right) \cdot t \cdot z_p + 2 \cdot \left(b_{III} \cdot t_{sl} \cdot \left(\frac{h}{2} - z_p\right)\right) + b_{IV} \cdot t_{sl} \cdot \left(h - z_p\right)\right) = \left(3.557 \cdot 10^6\right) \; \boldsymbol{mm}^3$$

$$m_{y.Rd} := \frac{\left(t^2 \cdot f_y\right)}{4} = 12.78 \; \boldsymbol{kN} \qquad (8.134) \qquad\qquad m_{x.Rd} := \frac{\left(W_d \cdot f_y\right)}{b} = 300.657 \; \boldsymbol{kN}$$

$$\eta_m := \sqrt{\left(\frac{m_{x.Ed}}{m_{x.Rd}}\right)^2 + \left(\frac{m_{y.Ed}}{m_{y.Rd}}\right)^2 - \left(\frac{m_{x.Ed}}{m_{x.Rd}}\right) \cdot \left(\frac{m_{y.Ed}}{m_{y.Rd}}\right)} = 0.961 \qquad\qquad (8.139)$$

Axial loads:

$$N_{y.Ed} := 150.6 \; \frac{\boldsymbol{N}}{\boldsymbol{mm}} \qquad\qquad\qquad N_{x.Ed} := 2.46 \cdot 10^6 \cdot \boldsymbol{N}$$

$$\chi_x := 0.968$$
$$\chi_y := 0.3535$$

$$N_{x.b.Rd} := \chi_x \cdot A \cdot f_y = \left(2.465 \cdot 10^7\right) \; \boldsymbol{N}$$
$$N_{y.b.Rd} := \frac{\chi_y \cdot \left(b \cdot t \cdot f_y\right)}{b} = \left(1.506 \cdot 10^3\right) \; \frac{\boldsymbol{N}}{\boldsymbol{mm}}$$

$$k_{xy} := 2 \cdot \chi_x \cdot \chi_y - 1 = -0.316 \qquad\qquad (8.143)$$

$$k_{Nm} := -1 \qquad\qquad (8.144)$$

$$\eta_N := \sqrt{\left(\frac{N_{x.Ed}}{N_{x.b.Rd}}\right)^2 + \left(\frac{N_{y.Ed}}{N_{y.b.Rd}}\right)^2 - k_{xy} \cdot \left(\frac{N_{x.Ed}}{N_{x.b.Rd}}\right) \cdot \left(\frac{N_{y.Ed}}{N_{y.b.Rd}}\right)} = 0.152 \qquad (8.141)$$

$$\boxed{U := \sqrt{\eta_N^2 + 0.9 \cdot \eta_m^2 - k_{Nm} \cdot \eta_N \cdot \eta_m} = 1} \qquad\qquad (8.140)$$

Abulfazl Masumi / Kristian Thor Gendron

NTNU
Kunnskap for en bedre verden